UNIVERSIDADE FEDERAL DO CEARÁ (UFC)

DEPARTAMENTO DE ENGENHARIA DE TRANSPORTES (DET)

PROGRAMA DE PÓS-GRADUAÇÃO EM ENGENHARIA DE TRANSPORTES (PETRAN)

LUCAS FEITOSA DE ALBUQUERQUE LIMA BABADOPULOS

A CONTRIBUTION TO COUPLE AGING TO HOT MIX ASPHALT (HMA) MECHANICAL CHARACTERIZATION UNDER LOAD-INDUCED DAMAGE

FORTALEZA

2014

LUCAS FEITOSA DE ALBUQUERQUE LIMA BABADOPULOS

A CONTRIBUTION TO COUPLE AGING TO HOT MIX ASPHALT (HMA) MECHANICAL CHARACTERIZATION UNDER LOAD-INDUCED DAMAGE

A Thesis submitted as partial fulfillment of the requirements for the Master's Degree in Transportation Engineering at *Universidade Federal do Ceará*.

Area within the Graduate Program: Transportation Infrastructure

Advisor: Jorge Barbosa Soares, Ph.D.

FORTALEZA

2014

LUCAS FEITOSA DE ALBUQUERQUE LIMA BABADOPULOS

A CONTRIBUTION TO COUPLE AGING TO HOT MIX ASPHALT (HMA)
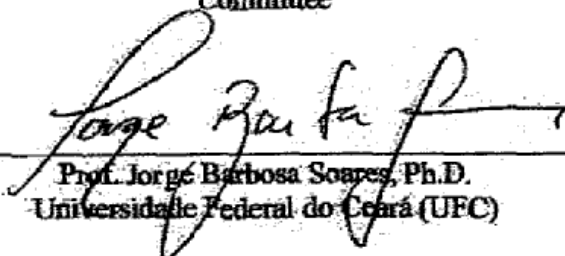MECHANICAL CHARACTERIZATION UNDER LOAD-INDUCED DAMAGE

A Thesis submitted as partial fulfillment
of the requirements for the Master's
Degree in Transportation Engineering at
Universidade Federal do Ceará.

Area within the Graduate Program:
Transportation Infrastructure

Advisor: Jorge Barbosa Soares, Ph.D.

Approved in: Jun/20/2014.

Committee
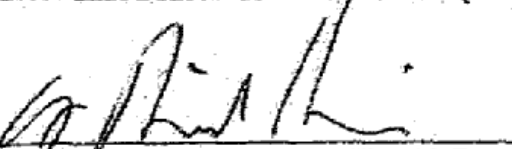
_____
Prof. Jorge Barbosa Soares, Ph.D.
Universidade Federal do Ceará (UFC)

_____
Prof². Verônica Teixeira Franco Castelo Branco, Ph.D.
Universidade Federal do Ceará (UFC)

_____
Prof. Francisco Thiago do Sacramento Aragão, Ph.D.
Universidade Federal do Rio de Janeiro (UFRJ)

_____
Prof. Youngsoo Richard Kim, Ph.D.
North Carolina State University (NCSU)

À FAMÍLIA, esse modelo fantástico para a transformação do mundo que começo a redescobrir.

ACKNOWLEDGEMENTS

As this paragraph typically deals with the emotion behind the work that was done, I think it is necessary to write it in the author's mother language. I will write it in Portuguese.

Antes de começar, gostaria de dizer que eu adoro essa seção. Só ela tenta traduzir a emoção por trás de cada trabalho e o justifica, sem precisar argumentar. É aqui que ficam impressas, ainda que como pano de fundo, as razões-emoções que estão afastadas do plano intelectual, mas que acompanham diretamente **o autor** do trabalho científico. Ainda que o estilo de todo autor apareça veladamente no texto científico, a própria escrita científica faz de tudo para esconder o que o autor **é**, para que sobressaia o que **foi feito** por ele, impessoalmente. Ademais, pensar sobre as participações dos outros nessa etapa marcante da minha vida me traz bem estar gratuitamente: mais um motivo pelo qual adoro essa seção.

Primeiro, devo dizer que foi durante o mestrado no Petran que decidi me casar com **a Priscilla** e partir para o doutorado em Lyon. Sendo assim, de certa forma, o estabelecimento desses passos como parte dos meus planos contribuiu positivamente para minha atitude em terminar bem o mestrado, mas muito mais importante que isso, mudou tudo. Obrigado, Minha Vida, por ter me movido para frente, espero que possamos mover um ao outro para sempre.

Fico muito feliz de lembrar que estar no mestrado contribuiu na minha vida trazendo novos momentos filosóficos com meu orientador-amigo, **Prof. Jorge**. Fico me perguntando se não foi a vontade de termos essas discussões que fez o trabalho incluir temas que no início não incluiria. Pouco importa, o fato é que as tivemos. Tenho certeza de que daremos um jeito de termos muitas mais... Os temas incluídos (principalmente o envelhecimento de misturas) trouxeram um sofrimento intelectual que me "envelheceu" um pouco, me permitindo o trocadilho, mas aprendi que envelhecer pode sempre ser pra melhor. Acho que fiquei alguns anos mais "velho" academicamente, apesar dos rápidos 15 meses no mestrado, e gosto de acreditar nisso. Quero estender esse parágrafo de agradecimento **à Vê**, que já faz um tempo fica nesse negócio de não ser parte oficial da minha orientação acadêmica, ainda que sendo. Quem sabe não vou ter a sorte de encontrar ela aqui por Lyon... Aliás, eu "gostaria de agradecer ao universo pela oportunidade ímpar de te conhecer [...] que sorte a minha!!!". Obrigado por tudo.

sido um companheiro na caminhada da minha formação: um enorme Obrigado. Você é *incrívis*. Que bom que ainda deu certo você aparecer via internet para as discussões do trabalho na defesa!

Um grande agradecimento aos avaliadores externos do trabalho, **Prof. Y. Richard Kim** da NCSU/Raleigh e **Prof. Thiago Aragão** da Coppe/UFRJ. O primeiro é simplesmente uma das referências internacionais na nossa área de pesquisa, enquanto o segundo é um exemplo especial de "onde podemos chegar" para os alunos do LMP que buscam a carreira acadêmica. É um privilégio e uma grande honra ter de seus ídolos lhe avaliando. Tenho muita sorte! Espero que meu trabalho tenha contribuído para as relações e trabalhos futuros do LMP, cuja camisa visto com tanto gosto desde 2007.

Agradeço também aos financiadores de pesquisa no Brasil, em especial ao que tocou diretamente esse trabalho, **o CNPq**, através da minha bolsa de mestrado e do Projeto Universal/CNPq do Prof. Jorge, que lida com caracterização viscoelastoplástica de misturas asfálticas, no qual estou inserido. Sem esse tipo de financiamento, pesquisas com teor mais fundamental dificilmente poderiam ser conduzidas e a ciência no Brasil veria seus próprios problemas ficarem "atrasados" ao longo do tempo, imagine suas soluções. Ainda bem que isso existe.

Deixei o maior agradecimento para o final e ele acaba estando na origem de tudo: **os Pais**. Esse agradecimento é estendido **aos pais dos pais e aos pais deles**, e no fundo, à razão de tudo: **a Família** (a que dedico este trabalho). Assim, ainda que eu esteja pensando muito forte nos meus, **o Marco Aurélio e a Silvia, assim como a Biba**, que criaram seis pessoas fantásticas e incrivelmente distintas entre si, no fundo estou pensando nesse modelo para mudar o mundo: fazer tudo por seus filhos. Rezo para que eu tenha a mesma sabedoria quando chegar a minha vez, enquanto agradeço pela imensa bênção que recebi de ter sido sorteado na vez deles. Amo vocês, **Familhão Baba**.

ABSTRACT

Although aging simulation in binder is performed through RTFO and PAV tests, no considerations of asphalt mixture aging are made in regular laboratory characterization. The present work is focused in incorporating aging to the modeling of the mechanical behavior of hot mix asphalt (HMA) during load-induced damage. This is accomplished by combining existing models and the adaptation of mixture aging procedures. The aging model used is based on the evolution of an internal state variable, associated to oxygen availability, aging temperature and four material parameters. These parameters are related to aging susceptibility, reaction kinetics and dependency on aging history and on aging temperature. The model allows to establish relationships between different aging processes. Results at four aging states (using two different temperatures) were analyzed and the aging model parameters were estimated. Capturing aging dependency on temperature constitutes a contribution of the present work with respect to previous results reported in the literature. The aging model is coupled to viscoplasticity and damage, comparing the behavior observed at the different aging states. Concerning the damage models, this thesis used mechanical models derived from Schapery's work potential theory to model fatigue behavior. The Simplified Viscoelastic Continuum Damage (S-VECD) model was selected. Unconfined dynamic creep tests were used to evaluate the effect of aging in the mixture resistance to permanent deformation. In addition to the state-of-the-art modeling of HMA, the characterization methods currently in use in Brazil (tensile strength, resilient modulus and controlled force indirect tensile fatigue tests) were also conducted. The possibility to simulate the material behavior for various loading conditions constitutes an advantage of the state-of-the-art model over the state-of-the practice method for fatigue characterization, used primarily to rank mixtures. It was concluded that, depending on pavement conditions and layer geometry, aging not necessarily affects negatively the fatigue behavior, while certainly improving the permanent deformation characteristics. That happens despite the fact that aging produces less damage tolerant materials, i.e., materials that fail for less evolved damage states. The framework (testing and analysis) for damage characterization of asphalt mixtures was implemented and it is expected to contribute to further developments in aging modeling of asphalt mixtures.

Keywords: Asphalt Mixtures, Aging, Fatigue, Permanent Deformation, Modeling.

RESUMO

Apesar de simulação de envelhecimento ser realizada em ligantes asfálticos através dos ensaios de RTFOT e PAV, nenhuma consideração sobre envelhecimento de misturas é feita na caracterização laboratorial comum. O presente trabalho se concentra na incorporação do envelhecimento na modelagem do comportamento mecânico de concretos asfálticos (CA) para carregamentos que induzem dano. Isto é feito através da combinação de modelos e da adaptação de procedimentos de envelhecimento existentes. O modelo de envelhecimento utilizado se baseia na evolução de uma variável interna de estado e é associado à disponibilidade de oxigênio, à temperatura e a quatro parâmetros materiais. Estes parâmetros são relacionados à susceptibilidade ao envelhecimento, à cinética de reação e à dependência sobre o histórico e sobre a temperatura de envelhecimento. O modelo permite estabelecer relações entre diferentes processos de envelhecimento. Resultados em quatro estados de envelhecimento (em duas temperaturas diferentes) foram analisados, e os parâmetros do modelo estimados. Capturar a dependência do processo quanto à temperatura constitui uma contribuição do trabalho quanto a resultados da literatura. O modelo de envelhecimento é acoplado à resposta viscoplástica e ao dano, comparando-se o comportamento nos diferentes estados. Quanto aos modelos de dano, esta dissertação trata dos derivados da teoria do potencial de trabalho de Schapery para análise da fadiga. O modelo simplificado de dano contínuo em meio viscoelástico (S-VECD) foi selecionado. Ensaios de *Creep* Dinâmico não confinado foram utilizados para avaliar o efeito do envelhecimento na resistência à deformação permanente. Além da modelagem mecânica do comportamento do CA usando modelos do Estado da Arte, também foram executados métodos de caracterização em uso no Brasil (resistência à tração, módulo de resiliência e ensaios de fadiga por compressão diametral). A possibilidade de se simular a resposta do material em várias condições de carga constitui uma vantagem do método do Estado da Arte sobre o do Estado da Prática, usado principalmente para comparar misturas. Concluiu-se que, dependendo das condições do pavimento e da geometria das camadas, o envelhecimento não necessariamente diminui a resistência à fadiga, embora certamente melhore a resistência à deformação permanente. Isso acontece apesar de o envelhecimento produzir materiais menos tolerantes ao dano, i.e., materiais que rompem para estados de dano menos evoluídos. O procedimento para a caracterização do dano em misturas asfálticas foi implementado e espera-se ter contribuído para um maior desenvolvimento da modelagem de misturas quanto ao envelhecimento.

Palavras-chave: Misturas asfálticas, Envelhecimento, Fadiga, Deformação Permanente, Modelagem.

TABLE OF CONTENTS

1   INTRODUCTION

Asphalt mixture mechanical characterization in Brazil is today primarily based on resilient modulus and indirect tensile strength tests. There is still no national standard for fatigue or permanent deformation mixture characterization. In some specific situations, especially in road concessions to the private industry, controlled force indirect tensile test at room temperature is used for the former, and laboratory traffic simulators or unconfined dynamic creep (flow number) test is used for the latter. Brazil is currently undergoing a national effort to develop its own mechanistic-empirical asphalt pavement design method, based on a national pavement material database and on the performance of test sections monitored throughout the country. A first version of the design guide is planned for 2016.

When it comes to mixture characterization in Brazil, the use of complex modulus is still restricted to academia and research centers. Therefore, it should not be considered in this first phase of the design method, which is being planned in such a way to be systematically updated. For that very reason, it is recognized the importance of leveling the country's research with international state-of-the-art developments. In this context, the present work deals with the improvement of test and analysis procedures for the characterization of asphalt mixtures considering the dependency of their properties on aging evolution. The research associated with this thesis is focused on aging and on how it relates to mechanical characterization of asphalt mixtures. Stiffness measurements at different aging conditions are used to fit the aging model. Although resistance to permanent deformation is evaluated from an experimental point of view, most of the modeling efforts in this thesis concentrate on fatigue modeling. Therefore, it deals with the coupling of viscoelasticity, viscoplasticity and damage responses to the aging of HMA. More modeling efforts are expended for the fatigue characterization. It is believed that viscoplastic behavior of asphalt materials is affected by aging in such a way that materials become more resistant to the related distress, i.e., permanent deformation. Nevertheless, this work is concerned by the change in the material properties occurring due to aging, that may impact pavements analysis and design.

Concerning damage characterization, it is important to know that there is no worldwide consensus on a procedure for the characterization of fatigue in asphalt mixtures, although it is considered a major pavement distress. In addition, there is also no widely accepted aging model or experimental procedure to take into account this phenomenon in

fatigue characterization, despite extensive literature comments on its influence. Therefore, this work will contemplate the incorporation of aging to the modeling of the mechanical behavior of hot mix asphalt (HMA) during load-induced damage. Although permanent deformation characterization is considered to be a secondary concern in comparison to fatigue when it comes to the consequences of aging, the impacts of aging on HMA resistance to permanent deformation is also presently studied. Stiffness modeling is the input used to calibrate the aging model. Then, it is possible to couple the aging model to viscoplastic and damage models presented in the literature. As previously mentioned, this research is part of a broader project related to the development of the new Brazilian mechanistic-empirical asphalt pavement design method. For this M.Sc. thesis, data for four aging states were available: unaged mixture (Age Zero), aged mixture for 2 days at 85ºC (Age 2, 85ºC), aged mixture for 2 days at 135ºC (Age 2, 135ºC), and aged mixture for 45 days at 85ºC (Age 45, 85ºC). Aging was induced to the loose asphalt mixture, in a procedure adapted from a RILEM protocol, presented in Partl et al. (2012).

Concerning the aging considerations in stiffness characterization of bituminous materials, previous works have presented viscoelastic models which included aging time as a variable (Daniel et al., 1998; Michalica et al., 2008) in addition to loading time (or frequency). However, these models are not conceived to allow easy coupling of aging to other mechanical characteristics of the asphalt mixture, such as viscoplasticity (which deals with intrinsic material properties linked to permanent deformation distress) or damage (which deals with intrinsic material properties linked to fatigue distress). This has motivated the use of the aging phenomenological model proposed by Al-Rub et al. (2013) in the present research. The referred approach couples aging to linear viscoelastic, viscoplastic and damage responses of asphalt mixtures.

The aging model utilizes an internal state variable, whose evolution depends on oxygen availability, temperature, and four material parameters. Those parameters are related to aging susceptibility, reaction kinetics, and dependency on aging history and temperature. It allows establishing a relation between the difference of aging time and the difference of temperature in two different aging processes under the same oxygen availability. The material constants are obtained by minimizing model prediction square errors with respect to experimental results.

Complex modulus results can be used to fit linear viscoelastic models at different aging states. The comparison between the linear viscoelastic parameters obtained at the different aging states allows the identification of the aging model parameters along with the linear viscoelastic parameters' aging sensitivity. With the fitted aging model parameters, viscoplastic model parameters and damage model parameters sensitivity can be estimated comparing experimental results obtained at different aging states, as shown by Al-Rub et al. (2013).

The present document contains aging modeling results obtained by comparing linear viscoelastic models from different aging states. Then, an attempt to couple these models to permanent deformation and to fatigue characterization is made. An aging experimental procedure is also proposed for asphalt mixtures herein as a contribution of the referred research under development.

1.1   Problem Statement

Asphalt pavement analysis in design guides around the globe adopts mixture properties obtained from specimens fabricated without considering long term aging processes. Nevertheless, asphalt mixtures are known to age as time passes, i.e., to change their chemical and mechanical properties with time. This is due to the chemical composition of the binder, which gives this material an aging susceptibility. Therefore, asphalt mixture properties (stiffness, resistance to permanent deformation and to fatigue) are most likely to significantly change with aging and, thus, to change the stress-strain behavior and the failure criteria of the asphalt mixture. Consequently, the problem that has motivated this research is the lack of consensus on a modeling protocol for asphalt mixtures capable of taking into account the aging process occurring in them and changing their mechanical properties, i.e., stiffness, resistance to permanent deformation and to fatigue. Changes in stiffness are the most direct effect of aging in asphalt mixtures. Resistance to permanent deformation is believed to be affected by mixture aging in a positive way. For that reason, it is a secondary concern in this work, although it is desirable to investigate its evolution with aging. Fatigue resistance is the main concern of this thesis, because it is most likely to be negatively affected by aging, reducing pavements service life, and there is still no protocol for taking this distress into account in pavement design in Brazil. Regarding these problems, some research questions are directly posed:

- How can pavement analysts model fatigue damage in asphalt mixtures in a more realistic way?
- How should asphalt mixture aging be considered when performing laboratory HMA mechanical characterization (stiffness, resistance to permanent deformation and to fatigue)?
- Is asphalt mixture resistance to permanent deformation positively affected by aging?
- What is the impact of aging temperature in the consequences (change in mechanical properties) of the aging process?
- How such considerations change the predicted service life of a typical asphalt mixture within a pavement system?

1.2   Research Objectives

The main objective of this work is to contribute to aging modeling incorporation into hot mix asphalt (HMA) models (stiffness, resistance to permanent deformation and to fatigue). As specific objectives, the following can be listed:

- To establish in the Pavement Mechanics Laboratory of *Universidade Federal do Ceará* a fatigue modeling framework based on solid concepts from continuum damage theory which is still narrowly studied in Brazil;
- To explain stiffness changes due to different aging processes based on an aging phenomenological model, and to couple the aging model to a damage model;
- To investigate changes on HMA resistance to permanent deformation due to aging;
- To evaluate the impact of the aging temperature in the HMA mechanical properties;
- To investigate the impact of aging considerations on the estimated service life of a typical asphalt mixture.

For the fatigue modeling of HMA, which is a main concern of this thesis, a Viscoelastic Continuum Damage (VECD) model based on Schapery's work potential theory was chosen. It is observed that, despite the fact that these models are well established in the literature, the approach to include aging considerations into the modeling of asphalt mixtures is intended to be a main contribution of the present work to the existing body of knowledge. Although Al-Rub et al. (2013) presented how to couple the aging model to specific

viscoplastic and damage models, the coupling to the models based on Schapery's work potential theory rests undone. The estimation of the aging dependency on temperature was also not studied by Al-Rub et al. (2013).

2   LITERATURE REVIEW

The materials available in nature have the ability to store or to dissipate mechanical energy received through loading when subjected to stress and strain. Equations relating stress and strain (and possibly its derivatives) are known as constitutive equations (or models) and the parameters (or model constants) are usually considered as material properties. For purely elastic materials, it is assumed that all mechanical energy supplied to the system is stored, both for linear and nonlinear elasticity. For the first, stress and strain correlate following a linear proportionality law, represented by the Young's Modulus E, given in stress dimensions, while for the latter, this linear proportionality does not occur. For both cases, stress (σ) depends only on the instantaneous specific deformation, or strain (ε). Consequently, the stress path during loading is always superimposed by the path during unloading (arrows in both senses indicated in Figure 1).

Figure 1 – Generic Stress versus Strain diagram (Babadopulos, 2013)
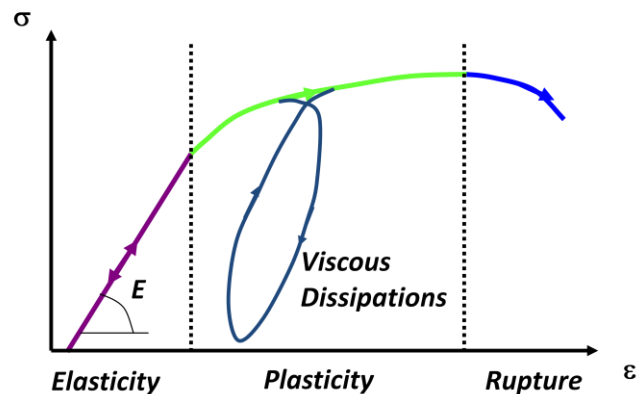
In the elastic zone, all energy introduced in the system is stored, a spring being an appropriate mechanical analog to represent this behavior. In the case of a linear viscous behavior (case of Newtonian fluids), stress is linked to the strain rate by a linear proportionality law where the proportionality constant is known as the coefficient of viscosity η, whose dimension is stress multiplied by time. In the case where the proportionality law is not linear, the fluid is said to be non-Newtonian. In both cases, all mechanical energy given to the system is dissipated (in the form of heat) and an appropriate mechanical analog is a dashpot.

Some materials, however, do not store nor dissipate entirely the mechanical energy absorbed during loading. In such cases other models may be a better representation than elastic or viscous models. Those are known as viscoelastic models. When viscoelastic materials are subjected to fast loading (high frequencies), they exhibit a behavior close to the one of elastic solids (total storage of mechanical energy). On the other hand, when slow loading is applied (low frequencies), viscoelastic materials exhibit slow deformations, flowing with time, close to viscous fluids behavior (total dissipation of mechanical energy). This is the case of asphaltic materials, which are the object of this thesis.

Usually, associations of springs and dashpots are a good choice for modeling viscoelastic behavior in a first approximation. However, in viscoelastic materials, energy can be dissipated in many ways, such as heat and volumetric damage. These material mechanical responses can either present linear or nonlinear behavior with respect to solicitation (stress or strain). Such nonlinearity can be either reversible or irreversible. If it is irreversible, it can be considered as damage, because it permanently changes the material properties. If it is reversible, it means that it did not change the material properties and it is not desirable to account for it as damage, but as a material intrinsic nonlinearity or possibly as a geometric nonlinearity. In principle, for both cases (recoverable nonlinearity and damage), the phenomenon needs to be taken into account in the constitutive equations in order to maintain a powerful predictive model. In addition, with time and despite the possible inexistence of loading, materials can change their properties. In the literature, this phenomenon is known as aging and in bituminous materials it occurs mostly for two reasons: volatilization of light fractions and oxidation. Some attempts for the consideration of all aforementioned phenomena (linear viscoelasticity, recoverable nonlinearities, damage and aging) are discussed in this Literature Review. The phenomenon of healing (closing of crack openings and consequent recovery of material integrity) is not a subject of the present work although it is widely accepted that it plays an important role in providing extra service life for asphalt pavements.

2.1 Linear Viscoelastic Models

One way to model the mechanical behavior of linear viscoelastic materials is to use mathematical functions with constants to be determined, minimizing the error between model prediction and experimental results. This process is known as curve fitting. Two kinds

of mathematical functions are extensively used in the literature to represent viscoelastic properties: (i) those based in generic functions (such as power law series or sigmoidal functions), and (ii) those based in mechanical analogs (analogical solution for the mechanical response of an association of springs and dashpots to loading). Despite the fact that good fittings are generally obtained when using generic functions to represent bituminous materials behavior, the results (material constants) are usually difficult to interpret from a physical point of view and not handy to be mathematically and computationally manipulated. For such reasons, the fitting of viscoelastic properties using those functions will not be object of this study. The works by Williams (1964) and by Park et al. (1996), relative to power laws, by Witczak and Fonseca (1996), Christensen et al. (2003) and by Bari and Witczak (2006), relative to sigmoidal functions, are recommended for the reader. On the other hand, models based on mechanical analogs, using an association of springs, dashpots and sometimes stick-slip components, allow a more simple physical interpretation. In the present work, plasticity modeling through mechanical analogs is not evaluated, then stick-slip elements will not be presented. Models using those kind of analogs applied to bituminous materials may be found in Di Benedetto et al. (2007a).

In the case where the partial energy storage depends only on the format of the stress (or strain) history and not on their magnitudes (at a given temperature), the behavior is linear (with respect to the solicitation) and an adequate mechanical analog is the association of springs and dashpots. Associations in series, in parallel, or a composition of both define linear viscoelastic models. The generalized Maxwell model (or Wiechert model) consists in an association in parallel of spring-dashpot pairs linked in series (Figure 2a). The generalized Voigt model (or Kelvin model) consists in an association in series of spring-dashpot pairs linked in parallel (Figure 2b).

Figure 2 – Linear Viscoelastic Models

(a) Maxwell-Wiechert model (above)   (b) Kelvin-Voigt model (below)
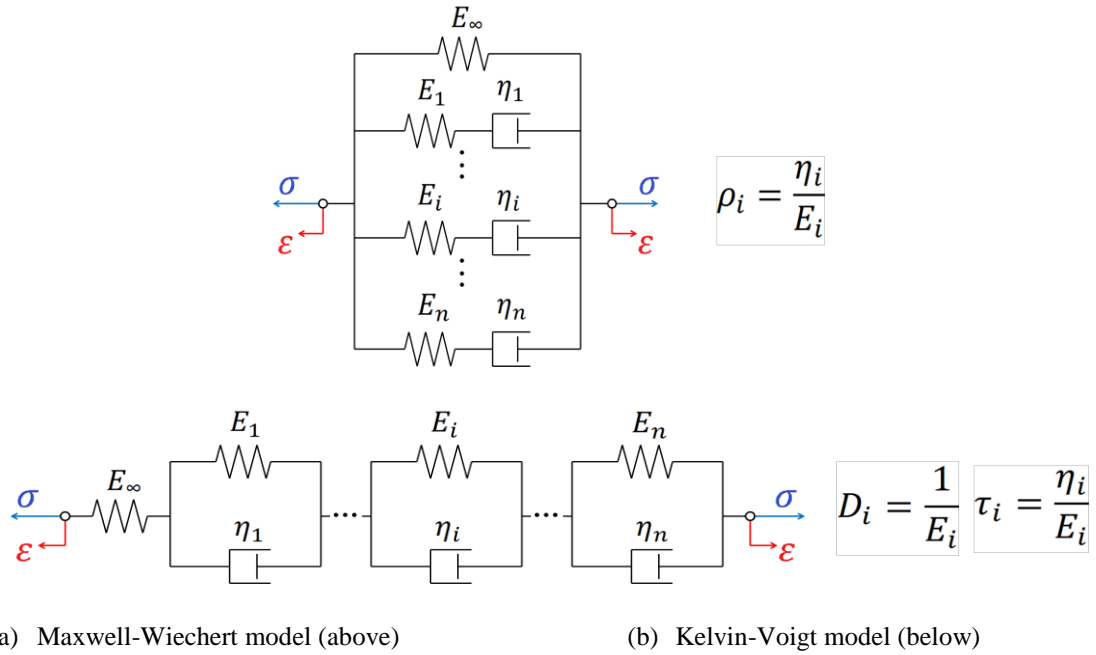
For each viscoelastic element (spring-dashpot), a time constant is defined. The variable $\rho = \frac{\eta}{E}$ (given in time dimensions) is known as relaxation time in the Maxwell-Wiechert model, and $\tau = \frac{\eta}{E}$ (also in time dimensions) is known as retardation time in Kelvin-Voigt model. In addition, E_∞ is known as the long-term modulus. The elastic compliance of an element D_i is defined as the inverse of its elastic constant E_i.

The analytical functions (relating stress and strain) obtained for these models based in linear mechanical analogs are known as Prony (or Dirichlet) series. Prony series is the most common and convenient way to represent the linear viscoelastic behavior of solid continuum media, especially bituminous materials (Soares e Souza, 2003).

For a constant strain (ε), stress decreases with time ($\sigma(t)$) (relaxation phenomenon) at a given temperature. For that temperature, the uniaxial tension-compression relaxation modulus ($E(t)$) is written as the ratio between the necessary stress and the imposed constant deformation. The Prony series which represents the relaxation modulus for the generalized Maxwell model is indicated in Equation 1.

$$E(t) = \frac{\sigma(t)}{\varepsilon} = E_\infty + \sum_{i=1}^{n} E_i . e^{(-t/\rho_i)} \qquad (1)$$

The parameters E_∞, E_i and ρ_i define a Prony series composed by n elements which represents the linear viscoelastic properties of the studied material.

For the case of a solicitation with constant stress (static creep), strain grows with time (viscoelastic flow). A Prony series for the creep compliance ($D(t)$) is analytically obtained for the generalized Voigt model and is represented by Equation 2.

$$
D(t) = \frac{\varepsilon(t)}{\sigma} = \frac{\frac{\sigma}{E_\infty} + \sum_{j=1}^{n} \frac{\sigma}{E_j}(1 - e^{-t/\tau_j})}{\sigma} = \frac{1}{E_\infty} + \sum_{j=1}^{n} \frac{1}{E_j}(1 - e^{-t/\tau_j})
$$

$$
= D_g + \sum_{j=1}^{n} D_j(1 - e^{-t/\tau_j})
$$

(2)

The parameters D_g, D_j and τ_j also define a Prony series composed by n elements which represent the linear viscoelastic properties of the studied material. The set of relaxation times $\{\rho_i\}$ associated to its respective relaxation magnitudes E_i is known as discrete viscoelastic relaxation spectrum. Similarly, the set of retardation times $\{\tau_j\}$ associated to its respective compliance magnitudes D_j is known as discrete viscoelastic retardation spectrum (Ferry, 1980). Those spectra can be generalized when the number of elements tends to infinity. The resulting continuous function relating modulus (or compliance) and time is known as relaxation (or retardation) spectrum. According to Silva et al. (2008), from eight to fifteen viscoelastic elements are necessary in order to have a good fit to experimental data. This depends on the time scale length of available data, generally one order of magnitude in the time domain being covered by one viscoelastic element.

While Prony series represents a discrete relaxation or retardation spectrum, other models can represent continuous spectra. In these models, some mechanical elements present a parabolic viscous response with respect to time (it is still linear with respect to the magnitude of the solicitation), instead of a linear one, as in the common damper. It can be said that such an element uses a power law for the description of its behavior (Christensen, 1982), but it is necessary to note that the definition of the parabolic law for these elements is based on the concept of fractional derivatives and allow pertinent physical interpretation of the results. Although these models allow a better explanation for the continuous relaxation and

retardation spectra of viscoelastic materials, Prony series is easier to manipulate for the purpose of this work, which includes integration in the time domain.

As complementary information, some models based on parabolic elements can be cited: Huet (Huet, 1963), Huet-Sayegh (Sayegh, 1965) and 2S2P1D (*two springs, two parabolic dashpots and one dashpot*) (Di Benedetto et al., 2004, 2007b) models. These models represent a gradual evolution from Huet's to 2S2P1D model by the inclusion of other mechanical analogs, which generate new constants to determine. Huet (1963) used only one spring (one constant) and two parabolic dampers (each one with two constants, resulting in five constants). Huet-Sayegh's model used one more spring associated in parallel with the Huet's model (total of six constants). Finally, 2S2P1D introduces, in addition to the past model, a linear damper in series with the Huet's element (total of seven constants). More information about those kinds of models can be found in Pronk (2003, 2006), Woldekidan (2011) and Babadopulos (2013).

Viscoelastic materials present strain response in a given instant depending not only on the stress in that instant but also on all stress history (Christensen, 1982). With the application of the Boltzmann superposition principle (Boltzmann, 1874) to a set of infinitesimal unit step functions applied as solicitation, the so-called convolution integral is obtained, representing the generic linear viscoelastic constitutive model in its integral form. This integral represents linear viscoelastic behavior independently of the chosen mathematical functions to represent the material response (Power laws, Prony series, etc). The convolution integral can be written either representing stress as a function of strain history (Equation 3) or strain as a function of stress history (Equation 4). Strain (ε) and stress (σ) must be continuous and differentiable (smooth) with respect to time, in such a way that both derivatives exist.

$$\sigma(t) = \int_0^t E(t-u)\frac{\partial \varepsilon}{\partial u}du \qquad\qquad ; t > 0 \qquad\qquad (3)$$

$$\text{or} \qquad \varepsilon(t) = \int_0^t D(t-u)\frac{\partial \sigma}{\partial u}du \qquad ; t > 0 \qquad\qquad (4)$$

Sometimes, these integrals are referred to as the convolution product between the material property (relaxation modulus in Equation 3 and creep compliance in Equation 4) and the time derivative of the solicitation (strain in Equation 3 and stress in Equation 4). They are presented herein for the one-dimensional case. It is important to observe that the theory of

linear viscoelasticity is restricted to conditions of small strains, which are satisfied in many theoretical problems, but cannot be assumed in some real cases (Soares e Souza, 2002). Souza (2012) presents a model which considers large strains (inducing nonlinearity) applied to the behavior of asphalt binders.

The relaxation modulus and the creep compliance are fundamental material properties representing the same characteristics of a given material, i.e., linear viscoelastic behavior. Consequently, they are not independent. Therefore, for the experimental characterization of the linear viscoelastic properties of a material, only one of them is necessary. However, differently from purely elastic materials, modulus and compliance are not simply reciprocal quantities ($E \times D \neq 1$). In fact, starting from the convolution integrals, it can be shown in Equations 3 and 4 that one property can be deduced from the other through Equations 5 and 6, i.e., those properties are interconvertible. This kind of procedure by which a property is obtained from the other is known as interconversion.

$$\int_0^t E(t-u)D(u)du = t \qquad\qquad ; t > 0 \tag{5}$$

$$\text{or} \qquad \int_0^t E(t)D(t-u)du = t \qquad ; t > 0 \tag{6}$$

The aforementioned properties (relaxation modulus and creep compliance) are given in the time domain, being functions of time, so they are said to be transient. Park and Schapery (1999) presented mathematical methods to obtain the relaxation spectra from the retardation spectra and vice-versa.

Similarly, in the frequency domain, two properties are defined: the complex modulus (E^*) and the complex compliance (D^*). The complex modulus (E^*) is more commonly used and usually it is not necessary to refer to the complex compliance, because these two properties are reciprocal quantities ($E^* \times D^* = 1$). The complex modulus is given by the ratio between stress and strain during a harmonic oscillation, written using complex numbers. For viscoelastic materials, in the steady state the strain signal is always delayed from the stress signal by a quantity known as the phase angle (φ). Using Euler's formula for complex exponentials, Equation 7 can be written.

$$E^* = \frac{\sigma^*}{\varepsilon^*} = \frac{\sigma_0 e^{i(\omega t + \varphi)}}{\varepsilon_0 e^{i\omega t}} = \frac{\sigma_0}{\varepsilon_0} e^{i\varphi} = |E^*| e^{i\varphi} = |E^*|(\cos\varphi + i\sin\varphi) = E' + iE'' \tag{7}$$

Where $i = \sqrt{-1}$.

$E' = |E^*|\cos\varphi$ is known as the storage modulus and represents the stored portion of the mechanical energy during harmonic loading. It can be mathematically represented by $Re(E^*)$ (real part of the complex modulus). $E'' = |E^*|\sin\varphi$ is known as the loss modulus and represents the dissipated portion of the mechanical energy during harmonic loading. It can also be mathematically represented by $Im(E^*)$ (imaginary part of complex modulus). It is to be observed that ω represents the pulsation (or angular frequency), generally expressed in rad/s, and it is directly related to the loading frequency f, in Hz, as $\omega = 2\pi f$.

As the relaxation modulus, the storage and the loss modulus can be represented by analytical equations deduced from exactly the same mechanical analogs used before for the deduction of the Prony series in relaxation (Equation 1). It can be shown that, assuming the generalized Maxwell model for the representation of linear viscoelasticity, the storage (E') and the loss (E'') moduli are calculated from Equations 8 and 9, respectively.

$$E' = E_\infty + \sum_{i=1}^{n} E_i \frac{\omega^2 \rho_i^2}{1 + \omega^2 \rho_i^2} \tag{8}$$

$$E'' = \sum_{i=1}^{n} E_i \frac{\omega \rho_i}{1 + \omega^2 \rho_i^2} \tag{9}$$

The absolute value (or norm) of the complex modulus ($|E^*|$) grows with the increase in loading frequency, and decreases with growing temperature. In the literature, most authors refer to this property as the dynamic modulus, although it does not deal with inertial properties. This property, along with the phase angle, describes the behavior of linear viscoelastic materials in the frequency domain. It is to be noted that the model parameters in Equations 8 and 9 (frequency domain) and in Equation 1 (time domain) are the same, in such a way that time and frequency domain properties are interconvertible.

At low temperatures, the behavior of homogeneous linear viscoelastic materials tends to elasticity, which means in terms of phase angle that $\varphi \approx 0$. On the other hand, at high temperatures, the behavior tends to pure viscosity, i.e., $\varphi \approx 90°$. Those tendencies are observed

for asphalt binders, but the presence of aggregate particles changes this trend in asphalt mixtures. The temperatures at which those behaviors are observed depend strongly on the analyzed material. In the case of asphalt mixtures, a composite material (thus, heterogeneous), the interlocking provided by the aggregates avoids the occurrence of the phase angle trend approaching 90º at high temperatures. In this case, actually, the phase angle does not present a monotonic trend. Generally, at the zone of low frequencies and high temperatures it grows with loading frequency, while at high frequencies and low temperatures the inverse occurs. This was observed by many authors in the literature (Clyne et al., 2003; Flintsch et al., 2005). The phenomenon can be explained by the fact that the elastic behavior ($\varphi = 0°$) of the aggregates influences more the material response when the asphalt binder is softer, i.e., at low frequencies and high temperatures (Flintsch et al., 2007). At those conditions, a decrease in frequency leads to a more elastic response, because the contribution of the aggregate particles to the material behavior becomes more important. Consequently, the phase angle decreases.

Generally, the value of the parameters in the Prony series are selected in order to fit linear viscoelastic experimental data. The data can be obtained from experiments conducted in the time domain, such as the relaxation modulus (Equation 1) and the creep compliance (Equation 2), or in the frequency domain, using the storage modulus (Equation 8) and the loss modulus (Equation 9). The fitting procedures are analogous. In this work, storage modulus data are used.

Schapery (1962) introduced the Collocation method for obtaining the parameters of a Prony series, using algebraic linear systems. Only a few experimental points are used in the fitting. The time constants (relaxation or retardation times, depending on the adopted model) are chosen among the experimental data points. The time constants are placed in the same location (collocated) of some of the observed experimental times. The free stiffness constant E_∞ (known as the long-term modulus) also needs a preestablished value, being typically assumed as the lowest modulus experimentally observed. As mentioned by Sousa et al. (2007), in the case of the relaxation test, for example, this constant assumes the value of the final plateau (when time tends to infinity) of the relaxation modulus curve. For the storage modulus curve, this corresponds to the initial plateau (frequency tends to zero).

With the imposed E_∞ and relaxation times, each modulus associated with each relaxation time is calculated in a way that the model (Equation 1) predicts exactly the

obtained experimental result at that collocated point. The simplicity of this method is its main advantage over others to fit Prony series. However, one can only take the collocated points into account when choosing the value of the model parameters. In addition, the same number of elements and experimental collocated points needs to be used, in such a way that only between around 2 and 15 experimental points can be used. The fact that not all experimental points are used, together with the subjectivity about the choice of these points, interferes in the model fitting and, thus, on its predictions. This makes it an obsolete procedure, although it is the basis of other procedures used to fit Prony series. Sometimes, a particular choice of time constants leads to associated stiffness constants with negative values. Such results are not desirable, because the model loses its physical meaning, due to the fact that some of the viscoelastic elements will tend to shorten when tensioned and extend when compressed. This can be avoided changing the choice in the time constants until strictly positive stiffness constants and a good fit are obtained.

In order to take into account all experimental data points, one can elaborate a least squares method. Babadopulos (2013) used Equation 8, which describes the storage modulus using a generalized Maxwell model, and assumed preestablished values for the time constants. One can write the cost function to minimize as $C(E_i) = \left[E'_{experimental} - \left(E_\infty + \sum_{i=1}^{n} E_i \frac{\omega^2 \rho_i^2}{1+\omega^2 \rho_i^2} \right) \right]^2$. It can be shown that, when the necessary condition for the minimization of the cost function is imposed (first derivatives with respect to the stiffness constants equal to zero), the optimum values of the constants are obtained through Equation 10. As in the Collocation method, the value of the long-term stiffness is assumed as the lowest obtained modulus. Equation 10 represents the algebraic linear system whose solution is the set of stiffness constants associated to the preestablished time constants in order to fit storage modulus (frequency domain) experimental results using a linear least squares method. It is capable of considering all M experimental points (ω_k, E_k). The dummy variable (index) j represents the lines of the linear system to solve and it varies from 1 to n (number of elements in the Prony series).

$$\sum_{i=1}^{n} \sum_{k=1}^{M} \left[\left(\frac{\omega_k^2 \rho_i^2}{1+\omega_k^2 \rho_i^2} \right) \cdot \left(\frac{\omega_k^2 \rho_j^2}{1+\omega_k^2 \rho_j^2} \right) \cdot E_i \right] = \sum_{k=1}^{M} \left[(E_k - E_\infty) \cdot \left(\frac{\omega_k^2 \rho_i^2}{1+\omega_k^2 \rho_i^2} \right) \right] \qquad (10)$$

Silva (2009) presented a linear equation analogous to Equation 10, used for the fitting in the time domain. The great feature of the linear least squares method is to maintain the simplicity of the Collocation method, but taking into account as many experimental points as desired. Besides, the residual square error $C_{min}(E_i)$ can be used as an indicator of the goodness of the fit (Babadopulos et al., 2010). As in the Collocation method, the time constants values are still preestablished, which can modify the prediction of the model. However, in the case where all obtained stiffness constants are positive, the prediction of the models obtained from two different choices of time constants is generally similar. Considering that the modulus and the phase angle at a given loading frequency and temperature characterize the linear viscoelastic behavior and not the isolated Prony series constants, it can be said that the results obtained using the linear least squares method are sufficient to model the linear viscoelastic behavior of materials. The time constants need to be chosen in such a way that all stiffness constants are positive. Babadopulos (2013) listed some practical rules in order to obtain them:

- One should choose a value near the lowest experimental modulus value (or the highest for the compliance) for the free stiffness constant E_∞ (or D_g);

- Following Schapery's (1962) recommendation, one should place time constants around one logarithmic decade apart (difference of around one order of magnitude between two consecutive time constants);

- It is possible to leave non collocated at most the first and the last logarithmic decades where experimental data is available;

- It is recommended to use the maximum number of elements possible which do not return negative stiffness constants;

- In case there are negative stiffness constants being obtained, the time constants can be shifted in the logarithmic scale (multiplied by an arbitrary factor) within the experimental results spectrum prior to a new trial;

- If there are still negative stiffness constants, the number of elements can be reduced;

- If none of the aforementioned recommendations leads to positive stiffness constants, probably there are problems with the data analyzed (noise or inconsistency). In the case of excessive noise, literature presents data presmoothing methods, usually based in generic mathematical functions

(such as power laws) for later fit a Prony series. Park and Kim (2001) and Sousa et al. (2007) are recommended for the reader;

- It is desirable to visually analyze the fit obtained, with plots of experimental data and model prediction. Sometimes, very good fits, with R^2 near 1, which means that the spectrum of experimental data points are very well predicted by the model, shows unrealistic extrapolations. Still, even with good model fits, it is not recommended to use extrapolations, using only information within the spectrum used for the calibration of the model.

It is to be noted that the linear viscoelastic model is restricted to certain stress and strain levels, which are material dependent. For asphalt mixtures, it is commonly said that the behavior is linear viscoelastic for strains smaller than 150με (Zhang et al., 2012). Even in this condition, for too many loading repetitions, fatigue damage can evolve. In this case, physical (not geometric) nonlinearity needs to be included in the constitutive models. This is discussed later in this work.

2.1.1 Stiffness Characterization

For the elastic analysis of asphalt pavements, the most used stiffness parameter in Brazilian state-of-practice is the resilient modulus (RM), whereas in North America and Europe, the dynamic modulus is widely used. For analysis involving viscoelasticity, RM is not suitable, and the dynamic modulus must be adopted. Unfortunately, this is still restricted to academia in Brazil. A brief review of these stiffness parameters is presented in this section.

Resilient Modulus (RM): an "elastic" parameter

This parameter is not within the subject of viscoelasticity, but the author found it suitable to present it together with the dynamic modulus, given that both are stiffness parameters. The resilient modulus (RM) test is standardized in Brazil by DNER-ME 133/94, and there is a more recent and updated standard by ABNT (NBR 16018:2011). Internationally, other standards are available, such as AASHTO TP 31 (1994); NCHRP 1-28 (1996); NCHRP 1-28A (2003). The test consists of a controlled force indirect tensile test with periods of loading intercalated by rest periods. RM test in Brazil is typically conducted with

0.1s loading and 0.9s rest periods, using the lowest force necessary to produce enough deformation for the LVDT measurements. RM is defined as the relation between the deviatoric tensile stress and the "recoverable" extension strain. The definition of "recoverable" strain varies from standard to standard, being a portion of the total strain generated in a loading cycle. The calculation of the RM is made using cycles occurring after some conditioning. Because of the assumption that recoverable strain is used in the calculation of RM, it is considered that only elastic strain is used in the calculation, although from the point of view of the theory of viscoelasticity this is not true (Soares and Souza, 2003; Theisen et al., 2007). During the conditioning cycles, the RM value changes from a cycle to the following cycle more than during the cycles after that conditioning process, because the material is viscoelastic and it flows more in the beginning of the test, before a kind of "steady state" is reached.

The RM test is most commonly conducted in pneumatic testing machines in Brazil. The loading pulse can be modeled by a haversine function, although in pneumatic machines only the load peak and the loading time are controlled by targeting a given cylinder pressure and a given opening time of the solenoid valve. Although vertical and horizontal measurements of the displacement of the samples are most indicated to estimate center point strains in the sample, it is more common to measure only horizontal displacement using two LVDTs mounted touching the surface of the sample.

Complex Modulus (E*)

The investigation of the complex modulus as a replacement for the RM by asphalt pavements analysts started in the decade of 1960 (Papazian, 1962; Huet, 1963; Sayegh, 1965). Its mathematical definition was presented before in this literature review. It relates the amplitudes (dynamic modulus) and the delay (phase angle) of stress and strain signals in a steady state for a harmonic loading. The possibility to analytically account for temperature and time dependency of the material behavior is the reason why these parameters is much closer to a material property than the RM. Therefore, the international tendency to use the complex modulus is likely to be reproduced in the future in Brazil for asphalt mixtures stiffness characterization.

The complex modulus test consists of applying harmonic compressive loading and obtaining the resulting strains using LVDTs mounted to the sample. Samples of 100mm in diameter by 150mm in height are generally used. Two standards are more frequently used: AASHTO TP 62-03 (2005) and ASTM D 3497-79 (2003). AASHTO TP 62-03 (2005) provisional standard was more recently established as AASHTO T 342 (2011), but consisting in the same procedure. Testing at different temperatures (temperature sweep) and using different loading frequencies (frequency sweep) together with the application of the Time-Temperature (or Frequency-Temperature) Superposition Principle (TTSP) allows the construction of master curves for both the dynamic modulus and the phase angle. The master curves are important tools to characterize viscoelastic materials such as asphalt mixtures (Medeiros, 2006) and some methods to obtain them are presented in the following section. Using the master curves, linear viscoelastic models can be fitted to the experimental data (Lee and Kim, 1998a; Park and Kim, 1998; Daniel and Kim, 2002; Soares and Souza, 2002; Silva, 2009; Babadopulos, 2013), prior to simulations of any kind of loading and the estimation of the corresponding response.

2.1.2   Master Curves Construction

In order to fit linear viscoelastic models to stiffness data obtained with temperature and frequency sweeps, it is necessary to arrange the data in a single smooth curve representing the linear viscoelastic behavior of the material. Such curve is known as the master curve.

Given a set of data obtained from temperature and frequency sweeps, isotherms are defined as the curves which relate the linear viscoelastic material property (dynamic modulus, phase angle, storage modulus or loss modulus) and the frequency of loading for each of the tested temperatures. For each temperature corresponds an isotherm, which is usually plotted in log-log or semi-log space. It is to be observed that instead of loading frequency and harmonic viscoelastic properties, the same definitions and procedures can be conducted for transient properties. Figure 3 presents an example of a set of isotherms for the dynamic modulus in log-log space.

Figure 3 – Example of Isotherms for the dynamic modulus
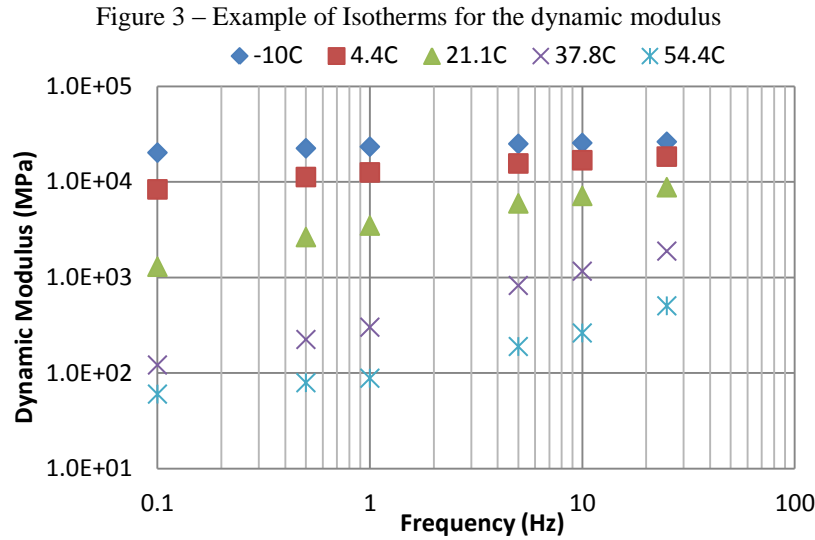
In order to gather the results in a unique curve representing all the data set, two approaches are generally applied. The first one is to eliminate the parameter frequency, representing data in ordered pairs of viscoelastic properties obtained at the same temperature and frequency. Examples of these are the Black space (φ; $\log|E^*|$) and the Cole & Cole plans (E'; E''). The second approach is the horizontal translation of the isotherms based on the TTSP Principle and this is the most common in the HMA characterization. Materials obeying the TTSP principle are said to be thermoreologically simple, as HMA is typically assumed to be. The TTSP can be understood as the existence of two different sets of temperature and loading frequency that lead to the same value of a linear viscoelastic property. This can be mathematically expressed as in Equation 11.

$$E^*(T_i, \omega_i) = E^*\big(T_0, \alpha(T_i, \omega_i)\big) \tag{11}$$

Where T is the absolute test temperature (in K) and T_0 is the adopted reference absolute temperature (in K). The function $\alpha(T_i, \omega_i)$ is usually adopted to have the form $\alpha(T_i, \omega_i) = a(T_i).\omega_i$. It is to be observed that, in a logarithmic space, $\alpha(T_i, \omega_i) = a(T_i).\omega_i$ becomes $\log[\alpha(T_i, \omega_i)] = log a(T_i) + log \omega_i$, which means that, indeed, a translation of $log a(T_i)$, that depends on the test temperature and is known as shift factor, given to the original loading pulsation in a logarithmic scale, leads to the construction of a master curve. The frequency that results from the shift is said to be the reduced frequency. Analogously, the reduced pulsation results from the shift of the physical pulsation. In addition, in the time domain, the application of the TTSP is represented by $\xi = 1/a(T).t$, where ξ represents the

reduced time and the shift factor $a(T)$ is exactly the same as for the shift in the frequency domain.

Three kinds of functions are frequently applied to relate the shift factor to the test temperature. The first one is a polynomial curve fit, the second one is the Arrhenius law, in Equation 12, and the third one is the WLF law (Williams-Landel-Ferry presented in Williams et al., 1955), in Equation 13.

$$\log a_T = 434,22 . \frac{\Delta H}{R} \left(\frac{1}{T} - \frac{1}{T_0} \right) \tag{12}$$

$$\log a_T = \frac{-C_1(T - T_0)}{C_2 + T - T_0} \tag{13}$$

In these equations, ΔH is the flux activation energy of the material (in kJ/mol.K), R is the gas constant ($R = 8,314 \text{ kJ/mol. K}$), C_1 (dimensionless) and C_2 (in K) are the coefficients of the WLF law.

In the Arrhenius law (Equation 12), although the flux activation energy ΔH is frequently used for asphalt binders, usually, the factor $0.43422 . \frac{\Delta H}{R}$ is simply replaced by the constant C, in K., for asphalt mixtures The coefficients of these laws are to be selected in order to obtain a master curve as smooth as possible. Analogous procedures can be conducted for the construction of master curves for properties in the time domain. In Figure 4a, an example of master curve is presented for the same data set used in Figure 3. It was constructed using the WLF law. In Figure 4b, the experimentally determined shift factors (dots) and the fitted Arrhenius and WLF laws corresponding to the data used to construct the master curve are presented.

Figure 4 – Master Curve examples and shift factors curve fitting comparison using Arrhenius and WLF law

(a)   (b)
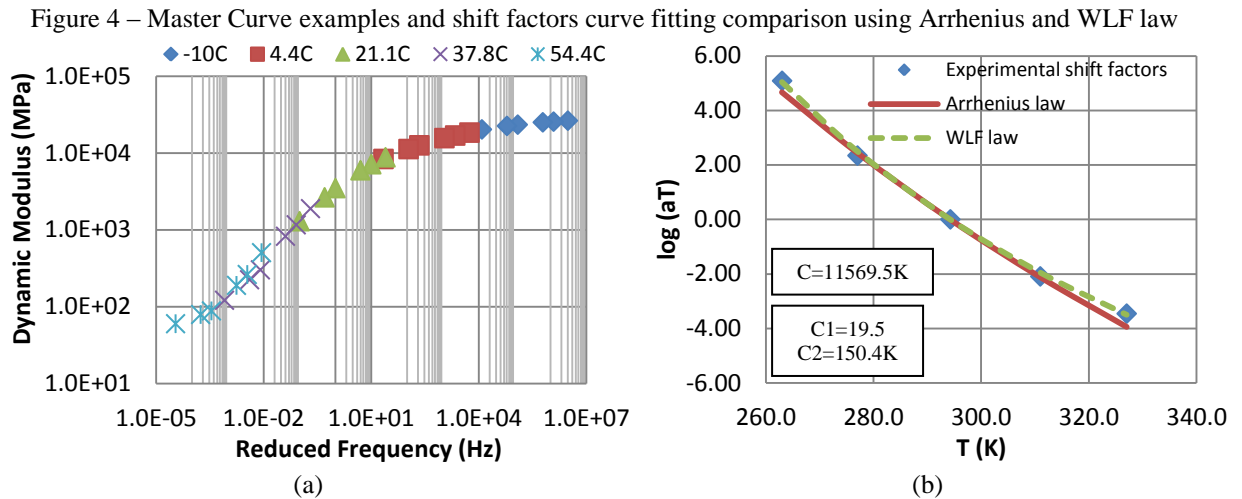
WLF law was chosen in this research because, for the available data, it provided better curve fits and thus produced smoother master curves. As it can be seen in the example in Figure 4b, fitting for the Arrhenius law is less curved, because of the use of only one curve parameter and, thus, fitting is less accurate for the highest and the lowest temperatures. For the example presented, the square error was more than 9 times lower when using WLF when compared to using the Arrhenius law. The fits were obtained using a Solver to run a least squares method, varying the curve parameters.

2.2   Viscoplasticity

Although fatigue is the main concern of the present research, viscoplastic characteristics of HMA are likely to considerably change with aging, altering HMA resistance to permanent deformation. As this occurs in such a way that HMA resistance increases, modeling efforts on the topic are secondary on this thesis. For the subject of HMA viscoplasticity, the reader is directed to the works by Di Benedetto et al. (2007a), Yun and Kim (2011), Subramanian (2011), Choi et al. (2012) and Choi (2013). At *Universidade Federal do Ceará*, Nunes (2006) applied a viscoplastic model by Tashman (2003) to asphalt mixtures containing calcinated clays as coarse aggregates, and there is ongoing research by Borges (2014) using the model developed by Choi (2013).

The most used tests for accessing viscoplastic characteristics of HMA are the so-called dynamic creep tests. These tests consist in the repetition of cycles of load and rest periods. Different load functions can be used, such as Heaviside (rectangular shaped) or haversine loading (similar to the pulse used in complex modulus tests). If the Heaviside

function is used, the test is equivalent to a creep and recovery test using high stresses (inducing nonlinearity). Different configurations of loading and rest period can be used. Temperature can also be changed and confining pressure can be used at different levels to simulate the confinement of an asphalt layer. All these test parameters change the viscoplastic response of HMA. Thus, full viscoplastic characterization can require 9 test conditions in order to generate a viscoplastic model, adopting models like the ones from Subramanian (2011) or Choi (2013), for example. When testing involves confining pressure, this kind of dynamic creep test is sometimes called triaxial repeated load permanent deformation (TRLPD) test.

For a given loading condition, permanent deformation strain is generally considered to follow three different trends. First, an initial compaction of the material occurs, followed by an approximately constant rate of deformation, and then a phase of unstable growing rate of deformation which leads to failure. These trends define three different regions for the material behavior: primary, secondary and tertiary regions. The tertiary zone is characterized by shear flow. In order to compare materials, information about how fast the material enters the tertiary zone and how fast it accumulates permanent deformation during the secondary zone can be useful. The number of cycles needed to reach the tertiary zone at a given test condition is commonly referred to as the flow number (FN). Sometimes, the dynamic creep test is called FN test for that reason. Figure 5 illustrates the behavior of a HMA during a dynamic creep test and presents an approximate division of the regions.

Figure 5 – Illustration of HMA behavior under dynamic creep tests (dashed blue line corresponding to the total permanent deformation and continuous red line corresponding to the rate of total permanent deformation
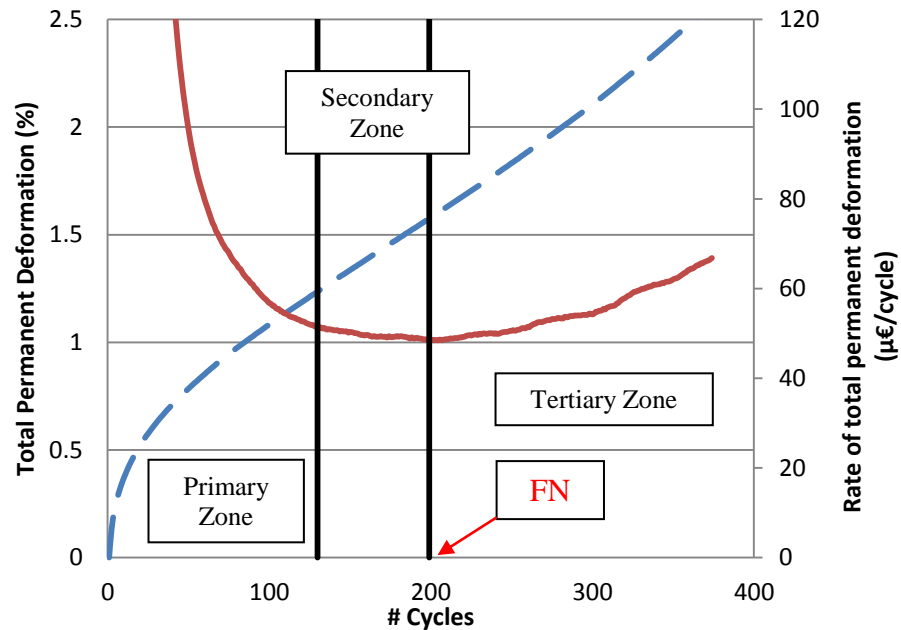
2.3 Viscoelastic Continuum Damage Models

According to Teixeira et al. (2007), the main viscoelastic continuum damage (VECD) models for HMA are based in the work by Schapery (1990a, 1990b), Park et al. (1996), and Lee and Kim (1998a, 1998b). They define evolution laws for internal state variables through strain energy and the elastic-viscoelastic correspondence principle (Schapery, 1984) to characterize the evolving damage primarily under monotonic loading (Kim and Little, 1990; Park et al., 1996; Daniel and Kim, 2002). This type of damage model, obtained from monotonic testing, is capable of capturing damage dependency on strain (or stress) history and on temperature, which is directly related to fatigue. However, monotonic tests cannot be used to define fatigue failure, because there is no cyclic loading. More recent research efforts (Underwood et al., 2010; Underwood et al., 2012) led to the simplified use of these continuum damage models for cyclic tests, and, thus, for the characterization of fatigue failure under cyclic loading of asphalt materials. This section briefly reviews the origins and the evolution of these models for asphaltic materials.

2.3.1 Thermodynamics of Irreversible Processes as Basics for Damage Modeling

The first works in the domain of continuum damage mechanics were conducted in the late 1950's. According to Lemaitre and Chaboche (1990), Kachanov (1958) was the first

to use a continuum variable to indicate the damaged state of a material, through the definition of effective stress. While Kachanov (1958) developed the analysis scope for brittle materials, Lemaitre and Chaboche (1990) worked in extending the theory to plastic materials, together with many others that intended to apply damage mechanics to their field of knowledge. All those authors highlighted the need to characterize the so-called damage tolerant materials, i.e., materials that in service will be damaged in a such way that the structure does not fail, until a certain point of damage evolution is reached. It is exactly how damage evolves and at which point this would lead to failure that the field of damage mechanics is interested in characterizing. Asphalt pavements are an example of damage tolerant structures that should be characterized following this kind of concept.

The so-called work potential models are damage models derived from Schapery's work potential theory (Schapery, 1990b), whose application to viscoelastic materials, such as asphalt mixtures, is described, for example, in Park et al. (1996) and Park and Schapery (1997). According to Krajcinovic (1989), there are three main general characteristics of continuum damage models: i) the mathematical representation of a damage variable; ii) a particular form for the strain energy density; and iii) an appropriate form for the kinetics law defining the evolution of damage. The three elements used in the particular case of work potential models are briefly described in this section.

According to Schapery (1990b), the mechanical behavior of any material can be expressed in terms of relations between generalized forces (Q_j) and generalized displacements (q_j). The existence of a strain energy density function W is assumed in a way that it respects the property represented by Equation 14, which defines the relation between generalized forces and generalized displacements.

$$Q_j = \frac{\partial W(q_j, S_m)}{\partial q_j} \tag{14}$$

In Equation 14, W is a work potential, i.e., a scalar function of the generalized displacements and of the thermodynamic state of the material (represented by the variables S_m), from which the generalized forces derive. The variables S_m are also known as internal state variables (ISV). The index subscripts (j and m) in the variables indicate the possible

existence of many of them. In this kind of formulation, Q_j and q_j are frequently referred to as conjugate pairs or conjugate variables, because of the relationship they keep through the partial derivative of the potential. The ISVs serve to account for the effects of damage and also any other microstructural changes occurring during a thermodynamic process. For an arbitrary infinitesimal process which occurs with changes in q_j and S_m, Equation 15 can be written.

$$dW = \frac{\partial W}{\partial q_j} dq_j + \frac{\partial W}{\partial S_m} dS_m \tag{15}$$

Equation 15 indicates the contributions of the generalized forces ($Q_j = \frac{\partial W(q_j, S_m)}{\partial q_j}$) and of the thermodynamic force (defined as $f_m \equiv -\frac{\partial W}{\partial S_m}$) to the work in an infinitesimal process. In order to develop an analyzing procedure for ISV evolution, an ISV law must be specified. Such a law is represented by Equation 16.

$$f_m = \frac{\partial W_S}{\partial S_m} \tag{16}$$

Where W_S is a state function of the ISVs. In that equation, the left hand side can be interpreted as the available force producing changes in microstructure (damage and others), while the right hand side can be interpreted as the required forces to do it. Park and Schapery (1997), for example, presented the analysis of a problem setting the evolution law for one ISV as $S = W_S$, or $f_m = 1$. It is to be observed that curve fitting will be needed to link mechanical properties to the ISVs (like the C *vs* S curve explained later).

In order to analyze viscoelastic problems in a simpler way, Schapery (1984) proposed the use of the elastic-viscoelastic correspondence principle, which allows the use of known classical solutions for elastic problems to produce solutions for the corresponding problems in viscoelasticity. In practice, it can be done by taking the Inverse Laplace-Carson Transform of the elastic solution. An easier way to interpret the elastic-viscoelastic correspondence principle can be represented by Equation 17.

$$\varepsilon^R = \frac{1}{E_R} \int_0^t E(t-u) \frac{\partial \varepsilon}{\partial u} du \qquad\qquad ; t > 0 \qquad\qquad\qquad (17)$$

Where ε^R is called the pseudo strain and E_R is the reference modulus, which is an arbitrary constant that has the same unit as the relaxation modulus $E(t)$. It should be noticed that if E_R value is set to 1 (unity), the pseudo strain will have the same value as the linear viscoelastic stress, predicted from the convolution integral (Equation 3). So, in linear viscoelastic conditions, the pseudo secant modulus (ratio between σ and ε^R, or $C = \sigma/\varepsilon^R$) will be equal to one. However, as the internal microstructure changes (such as the evolving damage), the stress actually required for loading may decrease, so the pseudo secant modulus decrease. In other words, the slope of σ *vs* ε^R decreases. If the changes in the internal microstructure are the only reason for the pseudo secant modulus to change, C is only a function of the ISVs, i.e., $C = C(S_m)$, and $\sigma = C(S_m).\varepsilon^R$. As the problem with viscoelasticity is being regarded through the elastic-viscoelastic correspondence principle, the stress is the conjugate pair of pseudo strain (see Equation 14), i.e., $\sigma = \frac{\partial W(\varepsilon^R, S_m)}{\partial \varepsilon^R}$. Respecting that relation, the work potential is chosen to be the pseudo strain energy density function, represented by Equation 18.

$$W^R = \frac{1}{2} C(S_m).(\varepsilon^R)^2 \qquad\qquad\qquad\qquad\qquad\qquad (18)$$

The last element that constitutes a typical work potential model for viscoelastic materials is the ISV evolution law (generically represented by Equation 16) and it depends on the particular definition chosen for the state variables. Park et al. (1996) successfully applied an ISV evolution law for asphalt concrete in direct tension-compression using only one state variable, S, and assuming that it was primarily linked to the evolution of damage. Many other authors did the same (Chehab, 2002, Daniel and Kim, 2002, Underwood et al., 2010, Underwood et al., 2012 in the United States; Lundström and Isacsson, 2003a, Lundström and Isacsson, 2003b, Lundström et al., 2003, Lundström and Isacsson, 2004, Lundström et al., 2004 in Europe; Martins, 2014; and Nascimento et al., 2014 in Brazil). Another example of the use of work potential models in Brazil is the work by Mello (2008), using four-point bending tests in beams of asphalt concrete.

The following reasoning can lead to the definition of damage evolution laws for viscoelastic materials. Materials have a certain potential to absorb energy, but that energy serves both to deform and to change internal microstructure (in the case studied here, to produce damage). One could take the pseudo strain energy density function (which is a work potential linked to the material's ability to recover from deformed state) as the indication of the absorption of the energy during loading. In this case, the damage rate could be linked to the change in pseudo strain energy, for example through $f = \frac{dS}{dt} = -\frac{\partial W^R}{\partial S}$. The time derivative is a way to explicitly make the ISV a function of time (rate-dependency). Although that equation could be an option of ISV evolution law, Park et al. (1996) stated that it is to be understood that not only the available force for growth of S (denoted by f) but also the resistance against its growth are rate-dependent for most viscoelastic materials. This observation was made regarding micromechanics crack-growth laws for viscoelastic materials available in Schapery (1975) and Schapery (1984). Therefore, as the damage state variable in a global scale should in principle be linked to micromechanical properties, evolution laws similar in form to power-law crack-growth laws for viscoelastic materials should be adopted. Most researchers nowadays use damage evolution laws described as in Equation 19.

$$\frac{dS}{dt} = \left(-\frac{\partial W^R}{\partial S} \right)^{\alpha} \tag{19}$$

In this equation, α is a material-dependent constant directly related to creep or relaxation material properties (i.e., its ability to relax stresses). If m denotes the maximum log-log derivative of the relaxation modulus of the material over all time spectrum, the expression $\alpha = 1 + 1/m$ is commonly used for displacement controlled tests, while $\alpha = 1/m$ is more frequently used for force controlled tests. According to Park et al. (1996), the choice of the expression α is linked to the micromechanical behavior of a crack tip in viscoelastic media, which is described in more details by Schapery (1975). In-depth discussion around it is not an objective of this work. It is to be observed that the chosen expression did not lead to a simple unit for the damage variable ($[stress]^{\alpha/(\alpha+1)}[time]^{1/(\alpha+1)}$). A simple way to look to the damage ISV is as a way to "count" damage, so, S can be regarded as a "damage counting".

An important contribution to damage characterization of asphalt concrete through the use of work potential models was made by Daniel and Kim (2002). The referred authors

experimentally presented $C(S)$ as a function independent of the applied loading conditions (cyclic *vs* monotonic loading, amplitude/rate, frequency) and temperature, for a given material. This is why the C *vs* S curve is commonly referred to as the damage characteristic curve and treated as a material property (as the complex modulus). Another important contribution is the one by Chehab (2002), where it was shown that the time-temperature superposition for an asphalt mixture is not only valid for the undamaged state, but also for the damage states. It is to be noticed that these are very strong assumptions, but they are also very powerful, allowing faster laboratory damage and fatigue characterization of asphaltic materials, combined with the fact that cyclic tests can be used to obtain both the C *vs* S curves and the failure criteria. The tests are shorter because of the use of higher loading amplitudes, which lead to fatigue failure more rapidly, consequently reducing laboratory time. In addition, time-temperature superposition coefficients do not need to be fit for each damage state. Together with those advantages, good agreement between prediction and test results and between prediction and real scale data (FHWA Accelerated Loading Facility) have been obtained (Underwood et al., 2009). With the presented basis of the work potential models, the final general expressions which describe the behavior of asphalt concrete under loading that induces damage can be represented by Equations 20 and 21.

$$\sigma = C(S).\varepsilon^R \tag{20}$$

$$\varepsilon_{ve} = E_R \int_0^{\xi} D(\xi - u)\frac{d\left(\frac{\sigma}{C(S)}\right)}{du}du \tag{21}$$

Where ε_{ve} indicates the strain calculated from the stress history considering the induced damage during loading, and ξ is the reduced time and it indicates the application of the time-temperature superposition principle to the analysis of the problem. For time integration (as in Equations 3 and 4) the variable u is used. In order to obtain $C(S)$ from experiments, both the material integrity C and the damage variable S must be calculated for each step in time in the test, obtaining $C(t)$ and $S(t)$. While $C(t)$ can be directly obtained from its definition $C = \sigma/\varepsilon^R$ for each time step, $S(t)$ is obtained from the application of the equation representing the damage evolution law (Equation 19 is the most widely adopted).

A simplified way to look at Schapery's work potential models is that the undamaged stress (or strain) can be used to calculate the undamaged stiffness that the material

should present for a given loading path. Comparison between the actual stiffness and the undamaged one can be used to estimate the damage in the sample. The elastic-viscoelastic correspondence principle allows the calculation of material integrity with a simple method, using the definition of reference modulus (E_R) and pseudo strain (ε^R - linear viscoelastic stress σ^{lve} divided by E_R, i.e., $\varepsilon^R = \sigma^{lve}/E_R$). The secant pseudo stiffness (S^R) is defined as the ratio between the measured maximum stress (σ) and the correspondent pseudo strain (ε^R). The normalized pseudo stiffness (C) is defined as the ratio between the actual S^R and the initial secant pseudo stiffness (I), and it accounts for sample-to-sample variation of stiffness. This is represented by Equation 22.

$$C = \frac{S^R}{I} = \frac{\sigma/\varepsilon^R}{\sigma^{lve}/\varepsilon^R} = \frac{\sigma}{\sigma^{lve}} \tag{22}$$

In other words, a comparison between the actual response (measured stress - σ) and the linear viscoelastic predicted one (pseudo strain - $\varepsilon^R = \sigma^{lve}$, assuming $E_R=1$) allows the calculation of C, which can be interpreted as the material integrity and can be directly related to Lemaitre and Chaboche's (1990) traditional damage variable (noted D in the authors' books). According to those authors, defining the concept of effective stress as $\tilde{\sigma} = \sigma/(1 - D)$ (where the tilde indicates the measure in a damaged state), the mathematical representation for the damage variable could be chosen as $D = 1 - \tilde{E}/E$ (where E is the Young's modulus of the material). The referred authors physically defined this variable as the relative (or corrected) area of cracks and cavities cut by the plane normal to the direction of loading. It is to be observed that, in this case, the loss of cross section area due to damage (microcracks) is assumed to be the reason of the modulus decrease. It is important to observe that the viscoelastic continuum damage models are most easily fit to experimental data using direct tension with constant strain rate tests. This is due to the fact that the convolution integral (Equation 3) is most easily solved in an analytical way, for calculating the pseudo strain. In other words, the convolution integral allows easy calculation of the linear viscoelastic stress σ^{lve} that should be obtained in the case where no damage propagates in the sample. Comparison of the actually measured stress σ and σ^{lve} allow one to obtain the material integrity varying with time. However, it is again to be remembered that monotonic tests hardly indicates failure criterion for fatigue modeling. In a first approximation, the values of C and S at failure could be used as prediction parameters for fatigue simulation.

Some last remarks about Schapery's work potential models need to be made. It is to be observed that, prior to the damage modeling, linear mechanical analogs need to be already obtained after stiffness characterization and that damage put aside, the model reduces to pure linear viscoelasticity. This means that no recoverable nonlinearity linked to loading amplitude dependency of the viscoelastic mechanical response is taken into account by the model. Coutinho et al. (2014) discussed the relevance of considering recoverable nonlinearities and used stress sweep tests to estimate the loading level that divided a recoverable nonlinearity zone from the damage zone. It is important to know that other authors (Di Benedetto et al., 2011; Mangiafico, 2014) used strain sweep tests to characterize amplitude dependency of asphalt mixtures and to estimate the decrease in dynamic modulus due to amplitude dependency in cyclic tests and concluded that this kind of nonlinearity can represent most of the change in mechanical response in some cases. Underwood and Kim (2013) also studied this subject, concluding that asphalt mixtures could exhibit nonlinear viscoelastic behavior. However, they combined nonlinear viscoelasticity to the S-VECD model and concluded that for fatigue simulation, it was not necessary to include nonlinearity considerations in the analysis. Following these results, the S-VECD without considerations of strain dependency of the dynamic modulus is sufficient for fatigue modeling.

Di Benedetto et al. (2011) stated that the temperature of the sample increases during cyclic tests due to the heat generated by viscous dissipation, inducing a sensible decrease in the material modulus. According to those authors, this could considerably change predictions made from material characterization from fatigue tests. Along with nonlinearities and hysteretic temperature increase, the so-called thixotropy, should also be considered. According to International Union of Pure and Applied Chemistry (IUPAC) terminology, "the application of a finite shear to a system after a long rest may result in a decrease of viscosity or the consistency. If the decrease persists when the shear is discontinued, this behavior is called work softening (or shear breakdown), whereas if the original viscosity or consistency is recovered this behavior is called thixotropy". Using that definition and 24h rest periods between multiple cyclic tests, Mangiafico (2014) estimated the effect of thixotropy in the modulus loss during "fatigue" tests in asphalt mixtures. However, it is important to observe that it is not clear whether thixotropy really occurs or if healing phenomena are taking place and sealing microcracks which had propagated within the sample. Asphalt healing is currently an active field of study in asphalt materials and it directly affects fatigue characterization, but it does not constitute an objective of this thesis. The same is true for thixotropy, as for none of

them a ready-to-use characterization technique compatible with work potential models is yet available.

To address the subject of temperature influence on results from fatigue tests obtained using viscoelastic continuum damage models derived from Schapery's work potential theory, one could refer to Lundström and Ekblad (2006). Those authors evaluated 80m diameter by 120mm height HMA samples in controlled strain fatigue tests, while monitoring its surface temperature. The measured temperature indeed increased up to 3ºC at failure for tests at 20ºC and strain amplitude of 500μ. For that test temperature, dynamic modulus varied 12% for a change in temperature of 1ºC, which justifies the concerns about taking conclusions from tests at those conditions. So, those authors decided to obtain a corrected characteristic curve, by obtaining the reduced time (TTSP) considering the different average temperatures measured at each loading cycle. It was noticed that, although visually the C vs S curves may appear similar, a simulation of the modulus decrease during the same test conditions could lead to 40% errors in estimating the number of cycles at failure, considering the failure criterion of 50% loss in dynamic modulus. These remarks are illustrated in Figures 6a and 6b.

Figure 6 – (a) C vs S curves obtained from cyclic tests using uncorrected and corrected temperature data at test temperature of 10°C; (b) Simulations of 200μ controlled strain test based on corrected and uncorrected characteristic curves at 10°C.

| (a) | (b) |
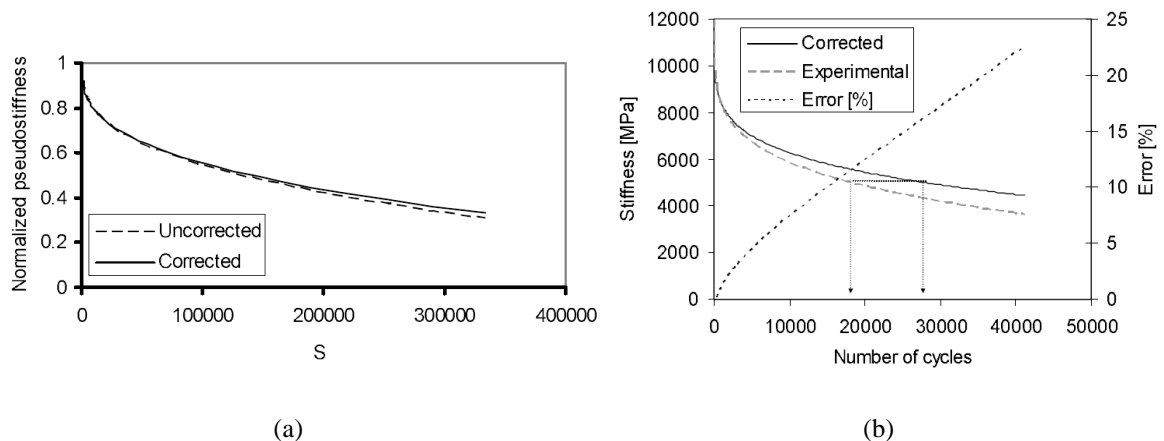
Adapted from Lundström and Ekblad (2006)

Based on those results, Lundström and Ekblad (2006) pointed out that it could be argued that this difference is of a magnitude comparable to the repeatability of fatigue tests, thus of minor importance. However, it should be noted that the difference is systematic. They concluded that work potential models are applicable to characterize fatigue-related damage

growth in asphalt concrete mixtures at different loading modes, excitation amplitudes and temperatures, but the temperature increase during the test should be taken into account. Despite these observations, the present work does not intend to implement them, but to use the approach described in AASHTO TP 107 (2014) to obtain C *vs* S characteristic curves, i.e., assuming constant temperature during the tests. This is due to the fact that, despite the errors produced by neglecting all the aforementioned effects, the model shows powerful capabilities of reasonable engineering predictions, while still being a ready-to-use method.

In the present work, the decrease in the HMA stiffness during cyclic tests is considered to be generated only by damage for simplification purposes, i.e., all stiffness loss is considered to be due to the fatigue process only. The chosen damage model was the simplified viscoelastic continuum damage (S-VECD) model as presented by Underwood et al. (2012), explained in the next section, using also a failure criterion from Sabouri and Kim (2014). A provisional standard (AASHTO TP 107, 2014) is available for the experimental determination of the damage characteristic curve.

2.3.2 The Simplified Viscoelastic Continuum Damage Model (S-VECD)

As mentioned before, in the first research efforts for conceiving damage models, monotonic tests (much simpler than cyclic tests) were used to obtain C *vs* S curves, but no fatigue criterion could be extracted from them, as no repetition of cycles occur. This means that although the main damage property (C *vs* S curves) could be extracted from monotonic tests, no fatigue failure criterion could be obtained. When considering cyclic harmonic loading, such a criterion is possible. A viscoelastic continuum damage model based on Schapery's work potential theory and further developed and simplified at North Carolina State University - NCSU (Daniel and Kim, 2002; Kim and Chehab, 2004; Underwood et al., 2012) for asphalt mixtures, using data from tests is available in the literature. It is known as the Simplified Viscoelastic Continuum Damage (S-VECD) model and it can be used to explain the evolution of C and S. In addition, as it is obtained from harmonic tension-compression loading, it is possible to link the model to failure criteria. For the S-VECD characterization, cyclic tests with controlled crosshead displacement amplitude are conducted. After sufficient evolution of damage, the sample fails due to fatigue. Phase angle drop can be used to determine the moment of failure. The S-VECD is further explained in the next topic.

The S-VECD was conceived to be used in laboratories as a time-saving damage characterization procedure for asphalt mixtures and, as cyclic tests are used to calibrate the model, fatigue criteria can be obtained. This kind of model allows asphalt mixture behavior prediction under various loading paths inducing nonlinear material behavior (Kim, 2009). Analogously to Equations 3 and 4 for linear viscoelasticity, Equations 20 and 21 are still used to represent how to obtain the stress (or strain) history from the strain (or stress) history and from the material intrinsic properties for loading path inducing damage. In principle, the basics of the models are exactly the same, but a numerical simplification was made and a systematization of test analysis was documented in the provisional standard AASHTO TP 107 (2014).

Underwood et al. (2012) provided the formulation of the S-VECD and exemplified its use for fatigue modeling, while AASHTO TP 107 (2014) presents the details for the test procedures and calculation process, which ends up with the experimental characterization of the damage curve for a given material. Derivation of the model can be found in Kim et al. (2008) and Underwood et al. (2010). Testing at different conditions allows verifying the agreement of the model with respect to the observations (indicated by the collapse of multiple damage characteristic curves obtained at different conditions with different samples). This is due to the fact that curves obtained at different conditions must collapse if fatigue is the predominant phenomenon occurring in the test and if the VECD model can explain the material behavior.

When analyzing fatigue tests, sample-to-sample variation can produce fatigue samples with different dynamic modulus when compared to the samples tested to obtain this last property. As Equation 22 showed, this needs to be taken into account in the analysis of fatigue results. This can be done by performing short dynamic modulus tests at the fatigue test frequency but using low forces, prior to the fatigue test. Such procedure is called fingerprint test. Its results can be taken into account using the definition of the dynamic modulus ratio (*DMR*), as in Equations 23 and 24.

$$DMR = \frac{|E^*|_{fingerprint}}{|E^*|_{LVE}} \tag{23}$$

$$|E^*|_{LVE} = \sqrt{\left[E_\infty + \sum_{i=1}^{N} \frac{E_i \omega_R^2 \rho_i^2}{\omega_R^2 \rho_i^2 + 1}\right]^2 + \left[\sum_{i=1}^{N} \frac{E_i \omega_R \rho_i^2}{\omega_R^2 \rho_i^2 + 1}\right]^2} \tag{24}$$

It is to be observed that $|E^*|_{LVE}$ consists in the norm of the complex modulus presented before in Equation 7. Using the definition of *DMR*, Equation 22 can be rewritten as Equation 25. It is to be observed that in this equation, the pseudo strain is obtained from the convolution integral (Equation 17) using the Prony series that represents the mean linear viscoelastic properties for the mixture of the fatigue test sample. This means that the Prony series parameters are optimal for the mixture, but not necessarily for that very sample used in the fatigue test. Also, the Prony series parameters are optimized for all tested frequency spectrum. It means that they are not necessarily optimal for the material behavior at the specific fatigue test conditions of temperature and frequency.

$$C = \frac{\sigma}{\varepsilon^R . DMR} \tag{25}$$

It is to be observed that when using the S-VECD model, the time-temperature superposition principle needs to be applied in order to consider the influence of the temperature in the material linear viscoelastic estimated response. This is accomplished by the application of the expression for the reduced time ($\xi = 1/a(T).t$), commented in topic 2.1.2. (Master Curves Construction). This expression is used for the initial data points where the steady state cannot yet be assumed (until the first peak of tension force). For the remaining of the data, where the cyclic test indeed occurs, a simplified analysis procedure, derived from the assumption of steady state of the material response, is used. For that data, Equation 26 is used to obtain a representative reduced time for the time at which each cycle occurred.

$$\xi = \frac{1}{a(T)} \left[\frac{t_{peak} + t_{valley}}{2}\right] \tag{26}$$

While the material integrity parameter can be calculated from Equation 25, the damage accumulation parameter can be calculated by applying the assumed damage evolution law (Equation 19). It can be shown that its discretization can be represented by Equations 27 and 28 for continuous data and they are used for the first data points (until the first peak

force). In those equations, the subscript k indicates the kth data point being analyzed and n the number of data points analyzed.

$$\Delta S_k = \begin{cases} \left[-\dfrac{DMR}{2}(\varepsilon^R)^2(C_k - C_{k-1}) \right]^{\alpha/(\alpha+1)} (\Delta\xi)^{1/(\alpha+1)}, & C_k \leq C_{k-1} \\ \\ 0 & C_k > C_{k-1} \end{cases} \tag{27}$$

$$S_k = \sum_{k=1}^{n} \Delta S_k \tag{28}$$

In Equation 27, the piece-wise function definition was used to avoid calculation of negative damage variations in the case where measurements indicated an increase in the value of the integrity. These fluctuations may occur within the data analyzed and negative damage is obviously not reasonable.

As commented before, the aforementioned equations are used for the very first data points, until the first force peak, when the force is always in the tension direction. This means that the direct discretization of the convolution integral is applied for those data. For the rest of the data, when the harmonic solicitation indeed occurs, steady state is assumed and the calculation of the integrals can be simplified. The analysis procedure for the cyclic data is presented next. The cyclic pseudo secant modulus is calculated as presented in Equation 29.

$$C^* = \frac{\sigma_{pp}}{\varepsilon_{pp}^R . DMR} \tag{29}$$

The subscript "pp" indicates that the quantity is taken from a peak to the following (actually, a valley) in the signal. It is equivalent to the amplitude of that signal. The peak-to-peak strain amplitude can be calculated considering the ratio between the mean LVDT displacement amplitude and the distance between LVDT measurements (the gauge length, or *GL*). The peak-to-peak stress is equivalent to the force amplitude divided by the cross section circular area of the cylindrical sample. Finally, the peak-to-peak pseudo strain can be calculated using Equation 30.

$$\varepsilon_{pp}^R = \varepsilon_{pp}.\,|E^*|_{LVE} \tag{30}$$

One of the assumptions made in the S-VECD is that only tension induces damage. So, although all strain amplitude is used to calculate the material integrity parameter, it cannot be used to calculate the value of the damage ISV. In fact, only the tension amplitude pseudo strain should be used. Therefore, it needs to be calculated. In the cyclic tests analysis, this is considered in the calculations through the use of the parameter β, known as the functional form factor and indicated by Equation 31.

$$\beta = \frac{F_{peak} + F_{valley}}{|F_{peak}| + |F_{valley}|} \tag{31}$$

The value of the functional form parameter depends on the peak and valley values of the force signal at each cycle. It can be observed that if the signal is centered in the time axis, i.e., the mean value of the force is zero, then $\beta = 0$. The resulting value for this parameter serves at estimating the tension amplitude pseudo strain (ε_{ta}^R) from the peak-to-peak pseudo strain, as indicated in Equation 32.

$$\varepsilon_{ta}^R = \frac{\beta + 1}{2}\varepsilon_{pp}^R \tag{32}$$

It is to be observed that if the signal is centered ($\beta = 0$), the tension amplitude pseudo strain is equal to half of the peak-to-peak pseudo strain. If there is only tension in the test ($\beta = 1$), then the tension amplitude pseudo strain is equal to the peak-to-peak pseudo strain. If there is only compression in the test ($\beta = -1$), then the tension amplitude pseudo strain is equal to zero. This will serve to disregard the damage that would be calculated from compressive forces, as it is assumed not to exist.

The second factor that is used to account for the period where samples are being damaged, i.e., where tension force is applied, is the form adjustment factor, K_1. It is calculated for each cycle from Equation 33.

$$K_1 = \frac{1}{t_e - t_b} \left[\left(\frac{1}{\beta + 1} \right)^{2\alpha} \int_{t_b}^{t_e} (\beta - \cos(2\pi f t))^{2\alpha} dt \right] \tag{33}$$

Where f denotes the loading frequency and for the fatigue tests it is commonly set to 10Hz. The constants (for each cycle) t_b and t_e are the times of the beginning and of the end of the tension time interval within the analyzed cycle. They can be calculated as functions of β as presented in Equations 34 and 35.

$$t_b = \frac{\cos^{-1}(\beta)}{2\pi f} \tag{34}$$

$$t_e = \frac{2\pi - \cos^{-1}(\beta)}{2\pi f} \tag{35}$$

Finally, the damage for the cyclic data can be calculated by applying the assumed damage evolution law (Equation 19). It can be shown that its discretization form is represented by Equations 36 and 37.

$$\Delta S_k = \begin{cases} \left[-\frac{DMR}{2} (\varepsilon_{ta}^R)^2 (C_k^* - C_{k-1}^*) \right]^{\alpha/(\alpha+1)} (\Delta\xi)^{1/(\alpha+1)} (K_1)^{1/(\alpha+1)}, & C_k \leq C_{k-1} \\ 0 & C_k > C_{k-1} \end{cases} \tag{36}$$

$$S_k = S_{1st\_peak} + \sum_{k=1}^{n} \Delta S_k \tag{37}$$

In Equation 37, it is to be observed that the damage that occurs in the cyclic data is summed to the accumulated damage in the first instants of loading, until the first tension force peak S_{1st_peak} in order to calculate the total damage. Again, as in Equation 27, in Equation 37 the piece-wise function definition was used to avoid calculation of negative damage variations.

AASHTO TP 107 (2014) also recommends the use of data filters in order to avoid spurious calculation of damage evolution. This provisional standard indicates a procedure to filter the data and also how to decide what filter ratio to use. Briefly, for the cyclic part of the test, data points are divided in two groups: early cycles and late cycles. The number of cycles that defines the limit between those groups is arbitrary and set to 10% of the number of cycles to failure. Then, for each group, a filter ratio is applied, i.e., groups of n cycles are averaged in all measurements (including time) and taken as representative of that group of cycles. As a rule of thumb, the provisional standard indicates the averaging of $n = 10$ cycles for early cycles and $n = 100$ for late cycles. In this work, those values of filter ratio were used for the data filter.

After all described calculation, the curves C *vs* ξ and S *vs* ξ are constructed. These curves are very sensitive to test conditions. However, if the observations made by Daniel and Kim (2002) that C *vs* S is a material property, and those by Chehab (2002) that the time-temperature superposition principle apply for both undamaged and damaged states, eliminating the time parameter ξ should allow one to obtain a unique C *vs* S, i.e., the damage curves must collapse.

Other continuum damage models are available in the literature, such as a recently proposed modeling framework developed at Texas A&M University (Darabi, 2011; Darabi et al., 2011; Darabi et al., 2012a; Darabi et al., 2012b; Al-Rub and Darabi, 2012) which accounts for viscoplasticity, damage and healing for asphalt mixtures. An approach which divides modulus decrease during cyclic tests in four parts, corresponding to its source (nonlinearity, heating, fatigue and thixotropy) is also available (Di Benedetto et al., 2011). However, the S-VECD was chosen in the present work as it is considered by the author as the most ready-to-use method for fatigue modeling available today in the literature.

2.3.3 Example of S-VECD Fitting

In this section, a brief example of the S-VECD described before is presented, using three 100mm diameter by 150mm height samples of a 12.5mm unaged unmodified mixture with 6.0% bitumen and 4.0±0.4% air voids, tested at 19±0.5ºC in three different initial strain amplitudes (ISA), targeting 200, 350 and 500μ. Controlled crosshead tests were used, as all fatigue tests in this work. It is to be noticed that this kind of test is neither a stress

controlled nor an on-specimen strain controlled test, as it can be seen in Figure 7. However, the versatility of the S-VECD model allows the use of these tests to obtain the damage characteristic curve and also failure criteria to estimate fatigue behavior of the tested material in various loading conditions.

Figure 7 – Example of evolution of stress amplitude (in blue) and mean on-specimen strain amplitude (in red) during controlled crosshead tests
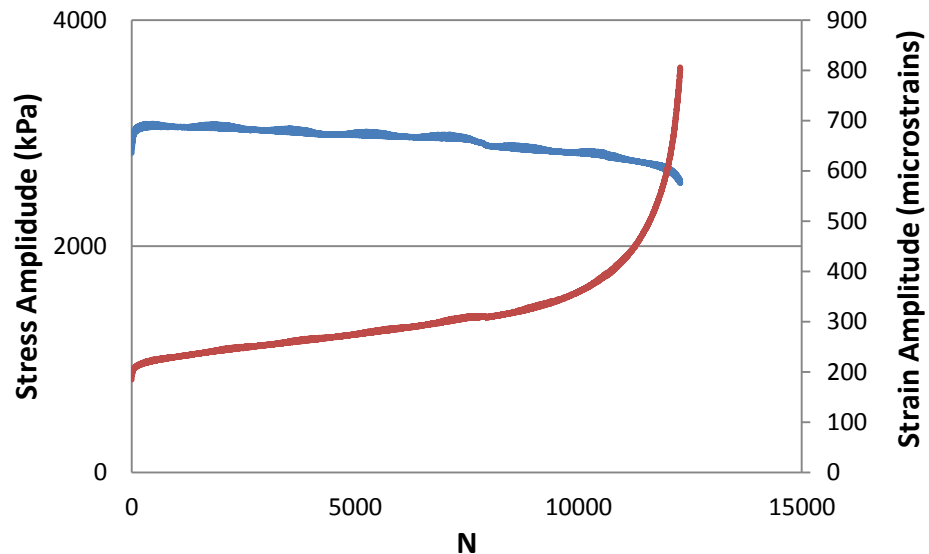
All raw data from the tests in this work were treated in a signal processing routine written in MatLab. Firstly, the peaks of the raw force signal were identified by comparing neighbor values. The times of the beginning and the end of each loading cycle were defined by the times in which force peaks occurred. The first data points (initial test time until the first force peak) were treated separately for damage calculation. After them, force and displacement signals were fitted using a Levenberg-Marquardt algorithm previously implemented by Gavin (2013) whose MatLab functions are available in internet links recommended by that author. The Levenberg-Marquardt algorithm is a frequently used technique to solve nonlinear least squares problems, as typical curve fitting problems. It can be interpreted as a combination of the gradient descent method with the Gauss-Newton method (two other optimization methods), which improves an initial guess for the solution until convergence. In the former, the sum of the squared errors is reduced by varying the parameters in the direction of the greatest reduction of the least squares objective function. In the latter, the sum of the squared errors is reduced by fitting quadratic function to the least squares objective function and finding its minimum. So, when the fitted function parameters are far from their optimal value, the Levenberg-Marquardt algorithm acts more like a gradient

descent method, while acting more like the Gauss-Newton method when the parameters are close to their optimal value. The function used to fit harmonic signals in this work is represented by Equation 38.

$$f(t) = A.\cos(\omega t) + B.\sin(\omega t) + C.t + D \qquad (38)$$

In Equation 38, $f(t)$ indicates the signal being processed and A, B, C and D are the parameters to be optimized by the least squares method solved using Levenberg-Marquardt algorithm. The harmonic pulsation for all signals was assumed to be the nominal pulsation used in the test, i.e., that the test machine executed the loading pulses with the exact requested pulsation ($\omega = 2\pi f$, with $f = 10Hz$ for the tests in this work). The function $C.t$ serves only to obtain possible slopes of the signal, which are not related to its amplitude or its phase (characteristics that the procedure intends to find). The parameter D is used to obtain the mean ordinate of the signal, which is also not directly related to the relevant material parameters. Finally, $A.\cos(\omega t) + B.\sin(\omega t)$ serves for obtaining both the amplitude and the phase of each signal, using Equations 39 and 40.

$$|f^*| = 2.\sqrt{(A^2 + B^2)} \qquad (39)$$

$$\varphi(f^*) = \arctan\left(-\frac{B}{A}\right) \qquad (40)$$

In Equations 39 and 40, $|f^*|$ denotes the amplitude of the signal and $\varphi(f^*)$ its phase with respect to the time in which the signal begins ($t = 0$). It is to be observed that $A.\cos(\omega t) + B.\sin(\omega t) = \sqrt{(A^2 + B^2)}\frac{(A.\cos\omega t + B.\sin\omega t)}{\sqrt{(A^2 + B^2)}}$, and the development of this expression leads to $A.\cos(\omega t) + B.\sin(\omega t) = \sqrt{(A^2 + B^2)}(\cos\varphi\cos\omega t - \sin\varphi\sin\omega t)$, which justifies the use of Equations 39 and 40. The absence of an optimization parameter (φ) inside the harmonic functions cosine and sine makes the optimization procedure simpler and less dependent of the initial guess of the fitting parameters.

After processing the signals of force (measured in the load cell) and displacement (measured in three on-specimen LVDTs and also in the actuator) following that logic,

material properties such as the dynamic modulus and the phase angle can be obtained by comparing the values of $|f^*|$ and $\varphi(f^*)$ of each signal and considering the test geometry. The dynamic modulus is obtained by taking the ratio between the amplitudes of force and displacement and multiplying the result by a geometry constant, related to the force distribution (by the section area of the sample) and to the gauge length where LVDT measures were taken. The phase angle is the phase difference between the signal of force and the signal of displacement. An example of the fitting for both force and mean LVDT displacement signals is presented in Figure 8. The raw data is represented by F_dat and u_dat, while the fitted data by F_fit and u_fit, for force and displacement signals, respectively. It is to be observed that sometimes the sign convention of the load cell and the testing machine may be different from the sign convention for the displacements. For example, the testing machine available for this research considers the compressive force positive, while the calculated displacement from LVDT measurements of position is positive for extension. In order to deal with this difference in the analysis, the force signal was inverted, indicating positive force for extension.

Figure 8 – Example of evolution of nominal stress and mean on-specimen strain during controlled crosshead tests
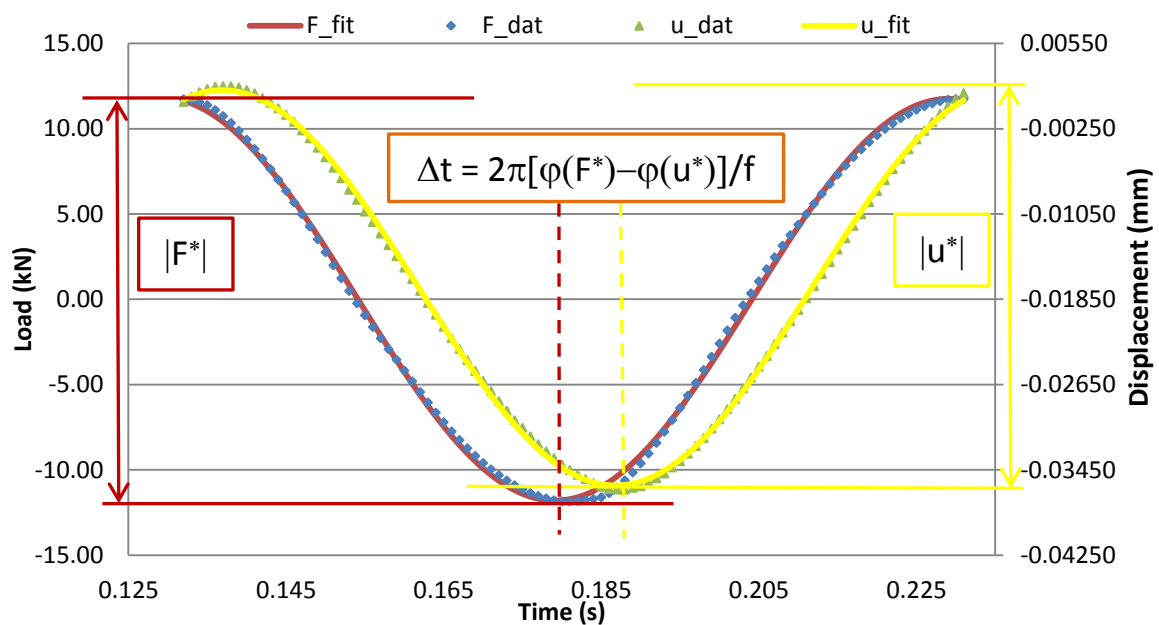

In Figure 8, the amplitudes of the signals of force and mean displacement are illustrated, together with the time lag between them. The time lag is proportional to the phase difference between the signals.

After all signals are processed, Figure 9 can be plotted and the number of cycles to failure can be defined. It is indicated by the user after appreciation of the evolution of the phase angle. The phase lag between force and actuator displacement is used only as an additional information if the microcracks coalesced in a macrocrack within the LVDT measurements. However, if the macrocrack appears out of the LVDT measurements, it is helpful to appreciate both phase angle evolutions (on-specimen LVDT and actuator position measurements), as the phase angle drop is usually unclear for the mean on-specimen LVDT displacement.

Figure 9 – Example of Dynamic Modulus and Phase Angle results in fatigue tests with controlled crosshead
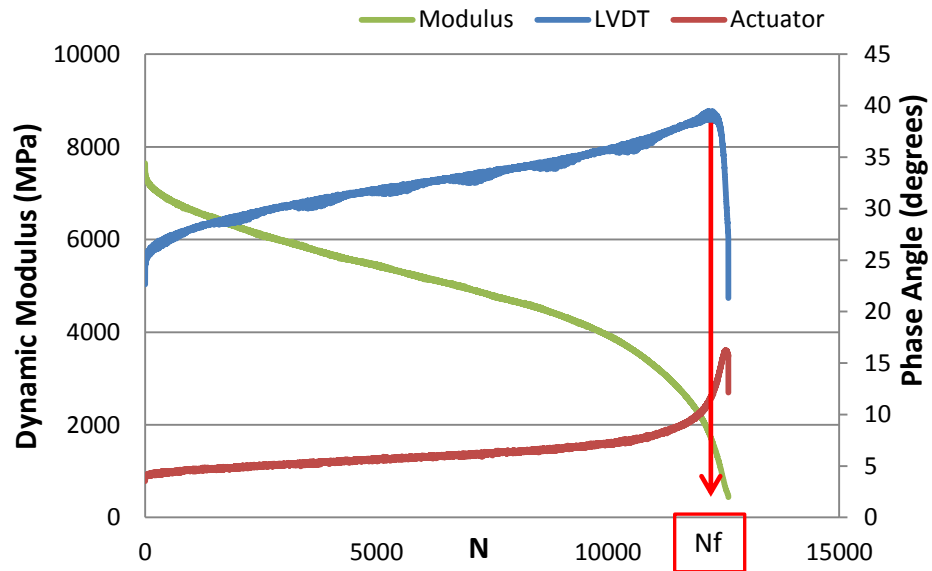

Using the results from the signal processing, the damage calculation routine is executed as described before, in order to obtain the evolution of the material integrity and the damage accumulation. Figures 10a and 10b result from the damage calculation routine, where the evolution of material integrity and damage accumulation with time were calculated.

Figure 10 – Example of the evolution of (a) material integrity and (b) damage accumulation with time in controlled crosshead fatigue tests

(a)

(b)
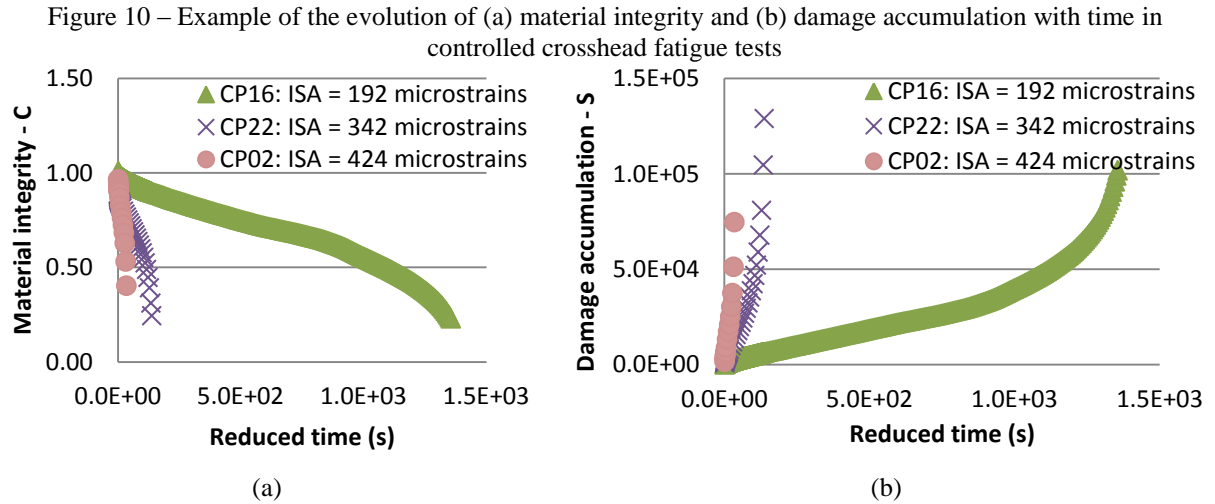
It is to be observed that the results presented in Figures 10a and 10b were obtained at different loading amplitudes, indicated by the initial strain amplitude (ISA) measured with the LVDTs. Also, the evolution of the material integrity and that of the damage accumulation with respect to reduced time (after application of the time-temperature superposition principle) are very different for the three tests. If the assumption that the C *vs* S curve is a material property independent of the loading conditions and the temperature for a given material, as shown by Daniel and Kim (2002) for asphalt mixtures, the curves obtained for each sample should collapse. Figure 11 presents the plot of the three C *vs* S curves and a fit of a power law for the damage characteristic curve of the material obtained from tests in other samples, constructed under the assumption of a unique C *vs* S.

Figure 11 – Example of the evolution of material integrity with damage accumulation in fatigue tests with controlled crosshead

$$C = 1 - C_{11}S^{C_{12}}$$
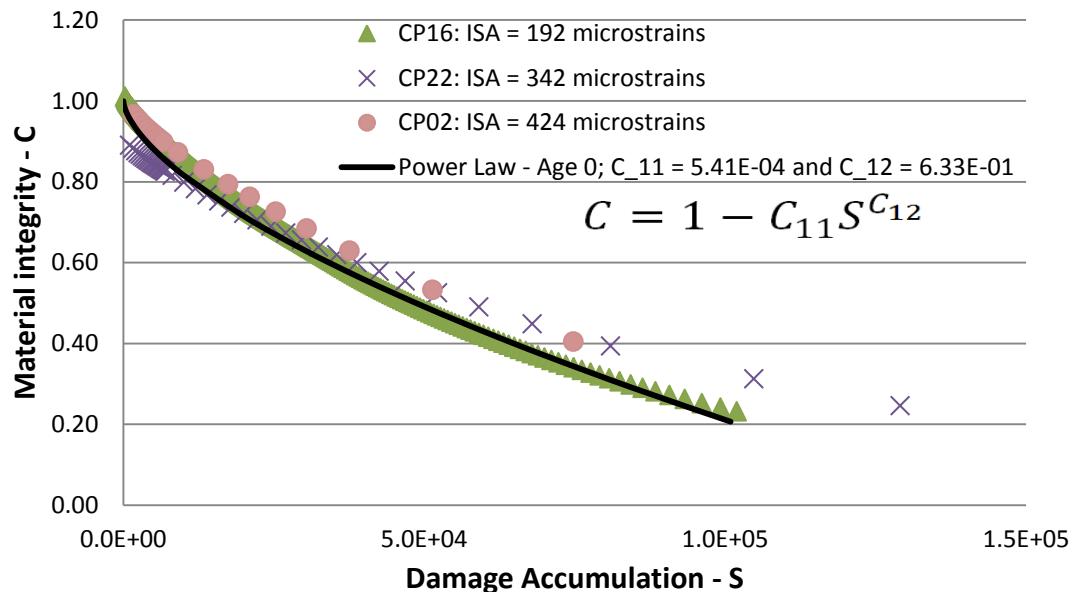
From Figure 11, it can be seen that the damage curves obtained from tests at different amplitudes and using different samples are approximately the same. This encourages the use of a fitted damage characteristic curve as a material property for the damage modeling of the asphalt mixtures. It also reinforces the hypothesis made and verified by Daniel and Kim (2002) and Chehab (2002), i.e., unique C *vs* S and time-temperature superposition coefficients for damaged and undamaged states. Exponential or power models are commonly used to fit the damage characteristic curves. The use of a particular one is a choice of the analyst which changes only the final equation used to estimate the number of cycles to failure (N_f) at given conditions. Two laws of evolution are typically used to fit the damage characteristic curves: the power law and the exponential law. They are represented by Equations 41 and 42, respectively.

$$C = 1 - C_{11}S^{C_{12}} \tag{41}$$

$$C = e^{aS^b} \tag{42}$$

In Equation 41, C_{11} and C_{12} are material constants to be determined for the power law model. Analogously, in Equation 42, a and b are material constants to be determined for the exponential model. For the S-VECD using the power law, the final equation used to estimate N_f for different loading (at constant strain amplitude) conditions is represented by Equation 43, while Equation 44 is used for the exponential law. In the case of constant stress amplitude, Equations 45 and 46 are used for fatigue simulation, for the power law and the exponential law damage characteristic curve, respectively. These equations were presented by Underwood et al. (2012), and according to those authors, the integrals can be numerically solved with sufficient accuracy using the trapezoidal method and 200 discretized steps within the integration limits. All equations are obtained when assuming that the initial value of the damage accumulation is substantially less than its value at failure and that the number of cycles to failure is substantially greater than 1.

$$N_f = \frac{(f_{red})(2^\alpha)S_{failure}^{\alpha - \alpha C_{12} + 1}}{(\alpha - \alpha C_{12} + 1)(C_{11}C_{12})^\alpha \left[(\beta + 1)(\varepsilon_{0,pp})(|E^*|_{LVE})\right]^{2\alpha}K_1} \tag{43}$$

$$N_f = \frac{(-1)^\alpha (f_{red})(2^{3\alpha})}{[(\beta + 1)(\varepsilon_{0,pp})(|E^*|_{LVE})]^{2\alpha} K_1} \int_0^{S_{failure}} \left(abS^{b-1}e^{aS^b}\right)^{-\alpha} (dS) \qquad (44)$$

$$N_f = \frac{(f_{red})(2^{3\alpha})(|E^*|_{LVE})^{2\alpha}}{[(\beta + 1)(\sigma_{0,pp})]^{2\alpha} K_1} \int_0^{\hat{S}_{failure}} \left(\frac{(1 - \hat{C}_{11}\hat{S}^{C_{12}})^2}{\hat{C}_{11}C_{12}\hat{S}^{C_{12}-1}}\right)^\alpha (d\hat{S}) \qquad (45)$$

$$N_f = \frac{(f_{red})(2^{3\alpha})(|E^*|_{LVE})^{2\alpha}}{[(\beta + 1)(\sigma_{0,pp})]^{2\alpha} K_1} \int_0^{\hat{S}_{failure}} \left(-\hat{a}b\hat{S}^{b-1}e^{-\hat{a}\hat{S}^b}\right)^{-\alpha} (d\hat{S}) \qquad (46)$$

In Equations 45 and 46 the quantities marked with a hat (^) are defined by Equations 47 to 49. It is to be observed that they are new constants composed from the combination of the original material constants.

$$\hat{S}_{failure} = \frac{S_{failure}}{|E^*|^{\frac{2\alpha}{\alpha+1}}} \qquad (47)$$

$$\hat{C}_{11} = C_{11}\left(|E^*|^{\frac{2\alpha}{\alpha+1}}\right)^{C_{12}} \qquad (48)$$

$$\hat{a} = a\left(|E^*|^{\frac{2\alpha}{\alpha+1}}\right)^b \qquad (49)$$

2.3.4 Fatigue Failure Criteria

Many fatigue failure criteria for asphalt mixtures have already been presented in the literature. Some of them are as simple as defining a percentage loss in the material modulus, usually 50% (AASHTO T321-03), which does not consider possible differences between the capabilities of undergoing damage of different materials and also at different temperatures and loading frequencies. It is reasonable to assume that different materials fail with different loss in modulus. Also, a given material can bear damage differently at different temperatures and loading frequencies. If the objective of characterizing damage properties of damage tolerant materials is to model until what point they can bear loading without failure,

another criterion should be used. Other criteria are based on energy dissipation (Pronk and Hopman 1990; Pronk 1997; Ghuzlan, 2001), considering that failure occurs when most of the energy given to the material is used to propagate cracks. However, in tests, usually these models are observed to be mode-dependent, thus, not accessing material properties. Finally, another criterion for failure of a sample in a laboratory fatigue test is the change in trend in the phase angle evolution during the test. This latter was adopted in this work as mentioned before (see Figure 9). According to Reese (1997), during a fatigue test, the asphalt mix accumulates distress in the form of microcracks, so the elasticity (which can be understood here as the storage modulus) should be going down (phase angle numerically increasing). When the phase angle versus number of cycles curve reverses direction (phase angle decreases), this is generally associated with the coalescence of microcracks into macrocracks, resulting in failure of the sample. This criterion may also be mode-dependent, if used without other considerations. However, recent contributions made by Sabouri and Kim (2014) allowed its combination with a new energy-based criterion, producing a mode-independent failure criterion for fatigue life of asphalt materials. Because of the potential to use it for modeling fatigue behavior of asphalt materials in different loading conditions, this criterion was chosen for the present work and it is briefly described in this section.

In cyclic loading, the maximum pseudo strain energy absorbed by the material is accumulated when maximum tension amplitude is reached. This energy can be expressed by Equation 50.

$$W_{max}^R = \frac{1}{2} C^* \left(\varepsilon_{0,ta}^R \right)^2 \tag{50}$$

The energy parameter in the left-hand side of the equation represents the material's ability to absorb energy, which decreases as damage occurs. This is indicated by the fact that the cyclic pseudo secant modulus reduces, reducing the value of W_{max}^R. If the change in pseudo strain energy is assumed to be caused by damage evolution, the total released pseudo strain energy (W_C^R) can be used as an indication of the energy loss due to damage propagation. According to Zhang et al. (2013), the total released pseudo strain energy (W_C^R) is defined as the triangular area between the straight lines $\sigma = \varepsilon^R$, $\sigma = C^* \varepsilon^R$ and $\varepsilon^R = \varepsilon_{max}^R$ (maximum value of pseudo strain within a cycle). This area is illustrated in Figure 12.

Figure 12 – Illustration of the area corresponding to the total released pseudo strain energy in the σ vs ε^R plane
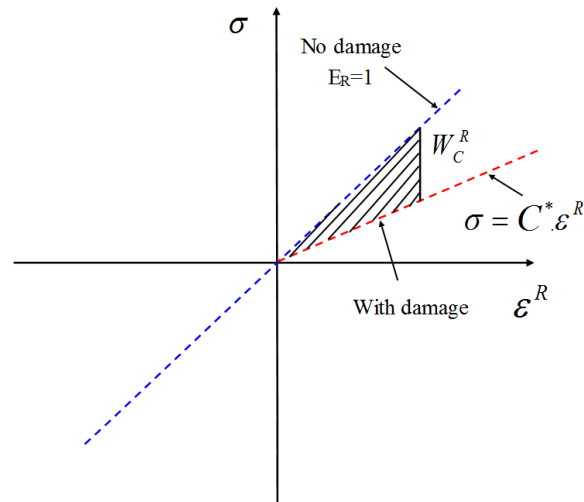
Adapted from Zhang et al. (2013)

Zhang et al. (2013) presented an energy-based failure criterion which consists of the minimum rate of W_C^R during the loading cycles. That failure criterion presented very good correlations with N_f for a given asphalt mixture, but that correlation was mode-dependent. The mode dependency does not encourage the use of the relation between the minimum rate of W_C^R and N_f for fatigue modeling, due to the fact that in field the mixture does not experience loading exactly as in any laboratory tests. This is why it is so important to look for mode-independent material properties that could be used for simulations.

In order to improve this energy-based failure criterion, Sabouri and Kim (2014) proposed the use of a new energy-based criterion which could be mode-independent. Those authors observed the evolution of W_C^R in different tests with different modes of loading, but with similar values of N_f. It was noticed that in controlled crosshead tests, more energy was released at the end of the loading history, when the material was losing its integrity rapidly. In controlled on-specimen strain, that happened at the beginning of the test, because the specimen is forced through a constant and higher on-specimen strain at the start of the test. So, as the energy in the different tests evolves differently, the new criteria should take into account the whole loading history. Sabouri and Kim (2014) defined G^R as the rate of change of the averaged released pseudo strain energy (per cycle) throughout the entire history of the test, being represented by Equation 51.

$$G^R = \frac{\overline{W_C^R}}{N_f} = \frac{\int_0^{N_f} W_C^R}{\left(N_f\right)^2} \tag{51}$$

For the tests performed by Sabouri and Kim (2014), G^R has proven to have a unique relation with N_f regardless of the mode of loading. The encouragement to use this criterion for fatigue modeling is the fact that, if it is indeed mode-independent, it can be used to predict the fatigue behavior under other loading conditions. This is done in combination with the S-VECD model. As a test is simulated, for each cycle increment, the energy (Equation 50) and the averaged released pseudo strain energy (Equation 51) can be calculated. When the simulated G^R *vs* N curve crosses the G^R *vs* N_f curve, the number of cycles of intersection is an estimate for the simulated number of cycles. The G^R criterion was chosen for the purpose of this research and its calculation was implemented in a MatLab routine along with the damage calculation. An example of the relation between G^R and N_f obtained in this work for controlled crosshead tests is presented in Figure 13. The groups of results were separated by target strain amplitude (200, 350 and 500μ).

Figure 13 – Example of relation between G^R and N_f obtained in this work for eight samples tested at three target strain amplitudes (200, 350 and 500 microstrains) and 19ºC
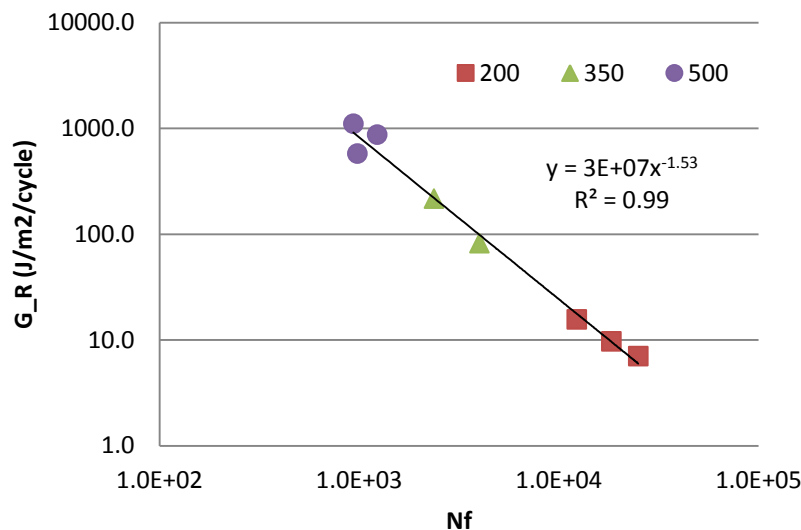
2.4 Aging

Aging is generally referred in the literature as a change occurring in time in chemical and mechanical properties of materials not related to loading. Since the production

phase, asphalt binders are subjected to conditions which induce a change in their chemical and mechanical properties, i.e., aging, which can be of different types. Volatilization of light fractions, for example, produces physical aging, which is characterized by the reversibility of the process. The oxidative aging, on the other hand, is induced by irreversible chemical reactions of the binder with diffused oxygen in its volume. It is the main type of aging occurring in the asphalt layer in its service life, because of the temperatures it is subjected to, i.e., lower temperatures than in short-term aging. Oxidative aging is also temperature-dependent. Ultraviolet radiation and moisture are considered by some authors as sources of aging of asphalt binders (Wright, 1965), although they are not studied in this research. This research is focused in oxidative aging of asphalt mixtures and its consequences in the mechanical properties of aged materials. The aging of asphalt binder is usually divided into two phases: the short-term aging, occurring during mixing and compaction, and the long-term aging, occurring during the pavement service life. Most authors consider that the first one is predominantly characterized by the loss of light fractions, whereas in the second one oxidative aging is the predominant mechanism.

Binder aging is largely reported in the open literature, with relevant contributions made four decades ago (Lee and Huang, 1973), among other publications (Lau et al., 1992; Petersen et al., 1993). On the other hand, constitutive modeling of asphalt mixture aging is a relatively undeveloped subject. In Brazil, an attempt to include aging in constitutive modeling of asphalt mixtures is undergoing at *Universidade Federal do Ceará*. This thesis is a part of that attempt, focusing in the relation of aging with the mechanical behavior of asphalt mixtures, through constitutive modeling. Different laboratory mixture aging methods are being considered, and mixture properties are subsequently obtained. For the purpose of the present research, a brief literature review for asphalt binder aging, HMA aging and aging models for HMA is presented in this section.

There are two ways of accessing aging properties of asphalt materials for practical applications. The first and easiest one is to test unaged and aged binders in the laboratory and compare the results. Testing different binders allows the choice of the less aging susceptible. This is what has been done for asphalt pavement applications in the past years, through the Rolling Thin Film Oven (RTFO) test, used to simulate short-term (construction, mix and lay-down) aging, and the Pressure Aging Vessel (PAV) test, used to simulate in-service long-term aging. To describe those tests and associated results in detail is not an objective of the present

research, since no constitutive properties for aged asphalt mixtures can be obtained from those procedures. The tests are limited to comparing aging susceptibility of binders, not taking into account the aggregates or the mix volumetrics influence in the process. However, they are the only ready-to-use aging methods for practical applications in asphalt paving.

The second way to access aging properties of asphalt materials is to prepare directly the asphalt mixtures and wait them to age. This can be done waiting field aging, that occurs in a long time scale (years), or increasing temperature and/or oxygen availability (pressure, in practice) in laboratory aging tests. Although for binder aging procedures, pressure can be more easily increased due to the small quantity of the material to test, this can be rather difficult for asphalt mixtures. On the other hand, ovens can be used to increase temperature and accelerate aging in asphalt mixtures. Studies reported in the literature present two ways of doing that: with compacted samples (used by Walubita, 2006, for example, and also the AASHTO R 30, 2002 - or SHRP - protocol) and with loose samples, prior to compaction (used by Partl et al., 2012, the RILEM TC206 procedure). Both present advantages and disadvantages. The main advantage of aging compacted samples is that compaction problems will not exist after aging, given the fact that wire nets can be used to maintain the shape of the samples (Baek et al., 2012). However, this procedure leads to heterogeneous aging of the sample and, if the goal is to obtain material properties of the aged mixture, this certainly negatively affects the results. The main advantage in aging loose mixture is exactly the more homogeneous aged mixture obtained. However, this benefit comes with the cost that compaction will be influenced by the aging state of the material. As an additional information, for the continuum damage test to access material fatigue properties used in this work, more material fragility at the top and at the bottom of the samples (most exposed to air contact than the core of the sample) would conduct to failure outside the LVDT measurements and, thus, would negatively impact the results. Finally, to laboratory age asphalt mixtures, loose samples were chosen in a procedure presented next in the section of HMA aging. Comparing results from both laboratory aging procedures is a subject addressed by undergoing research at *Universidade Federal do Ceará*.

2.4.1 Asphalt Binder Aging

Works reported in the literature established chemical pressure- and temperature-dependent aging models for asphalt binders, which predict the basic carbonyl reaction rate. This rate, generally called the binder oxidation rate, is measured based on the rate of change of the Carbonyl Area (CA) which is the area under the absorption curve from infrared spectroscopy within the range of 1650 to 1820 cm^{-1} of wave number (Liu et al., 1998). Carbonyl presents its peak of absorbance for the wave number around 1700 cm^{-1}. The CA reaction rate was found to be approximately constant for asphalt binders after an initial jump (Glover et al., 2008), where CA increases faster. Also, it is pointed out in the literature that CA and the norm of the complex viscosity correlate linearly for asphalt binders. According to Liu et al. (1996) and Liu et al. (1998) both the rate of change of the norm of the complex viscosity (r_η) and of the CA (r_{CA}), after the initial jump, follow Arrhenius-type laws, as indicated by Equation 52.

$$r_{CA} = \frac{\partial(CA)}{\partial t} = A.P^\alpha.exp\left(-\frac{E_a}{RT}\right) \quad \text{and} \quad r_\eta = HS.r_{CA} \tag{52}$$

Where A is a pre-exponential factor, P is the pressure and α is the reaction order with respect to pressure, E_a is the activation energy, R is the gas constant, T is the temperature, and HS is the hardening susceptibility. The hardening susceptibility is an example of coupling mechanical behavior (viscosity, in this case) to aging (using CA change as an indicator). It is to be observed from Equation 52 that CA is considered to grow linearly for constant pressure and temperature.

Alavi et al. (2013) used the kind of model presented in Equation 52 to represent the carbonyl growth in six asphalt mixtures (two binders - modified by SBS and unmodified - and three different aggregate mineralogical sources) subjected to an oven aging procedure. The aging process included short-term and long-term stage. The short-term aging was induced to the mixtures following AASHTO R 30 (2002) (loose samples in a 135°C oven for 4 h before compaction). The long-term aging was simulated in the compacted asphalt mixture samples with air voids content of 7% ± 0.5% using the Superpave gyratory compactor. Oven aging was induced at 60°C for periods of 3, 6, and 9 months. After the planned aging times, the samples were let to cool at room temperature and, after, cut to 100mm diameter by

150mm height prior to complex modulus (E*) tests. Asphalt binder recovered from the aged samples was tested for spectroscopy. CA was obtained for the different aging states. Continuum spectra models (2S2P1D) were fit to experimental complex modulus data and coupling between the linear viscoelastic parameters for the 2S2P1D model were obtained from curve fitting, where those parameters were considered as functions of the CA.

Qin et al. (2014) also present coupling between chemical and rheological properties of asphalt binders from field aging at various aging conditions. They were searching to find a model capable of predicting field binder rheology under varying aging severities and different pavement depths. The referred authors studied asphalt binders from three different origins (Bachaquero PG 70-22, rocky mountain blend crude oil source PG 76-16, and another Venezuelan crude oil source PG 76-22) aged in field conditions (in Virginia and Arizona) for approximately 8 years and also laboratory aged binders. For some field samples, accelerated field aging conditions were provided by surface heating to 74ºC for 8 weeks. Binders were extracted and recovered prior to testing for mechanical properties (DSR - Dynamic Shear Rheometer) and chemical properties (SARA - saturates, aromatics, resins and asphaltenes - fractions and FTIR - Fourier Transform Infrared Spectroscopy). Firstly, from test results, the authors concluded that field aging can be far more severe at the pavement surface than standard binder aging laboratory tests (RTFO and PAV). Secondly, absorbance related to carbonyl (peak for wave number around 1,700 cm^{-1} as mentioned before) and sulfoxide (which presents its peak of absorbance for the wave number around 1,030 cm^{-1}) functional groups were used as indication of chemical aging in order to relate to rheological properties (same idea as the CA rate model). Good agreements (R^2 between 0.937 and 0.997 depending on the analyzed property) of the presented model with observations were obtained, independently on the aging process (field or laboratory) used, aging severity or pavement depth. This represents a great contribution with respect to other results presented in literature (for example Herrington and Ball, 1996), because it encourages the use of aging models that take into account the aging time and the aging conditions in order to predict rheology from chemical properties.

The example of the work by Herrington and Ball (1996) was chosen here to illustrate that some authors believe that although aging processes may give rise to asphalt binders with similar rheological properties for different aging periods, different gel permeation chromatography (gpc) and infrared spectroscopy profiles can be observed. This

indicates that different oxidation temperatures may lead to different oxidation products. So, Herrington and Ball (1996) suggested that not only the rate of oxidation should be considered temperature-dependent, but also the oxidation mechanism itself. This would imply that high-temperature oxidation test procedures may not realistically model in-situ oxidation product composition, therefore not accurately predicting rheological changes in the field.

Although Herrington and Ball (1996) concerns are in fact valid, modeling aging, which is a phenomenon that occurs in a large time scale (years), would be prohibitive in laboratory. Thus, at the present state of knowledge of asphalt oxidation the best chance for accessing aging properties is to evaluate them in an accelerated way by the increase in temperature and/or oxygen availability (increasing pressure in tests, for example), being the first of those the easiest. The need for simplification in aging modeling and also results like those in Qin et al. (2014) encourage the use of chemical-rheological models for practical applications in aging results (change in mechanical properties) prediction.

2.4.2   HMA Aging

The SHRP protocol previously mentioned consists in a laboratory aging procedure for compacted samples. Originally only one long-term aging time was used, but this can be changed in a simple way, i.e., waiting for longer periods in order to access more severe aging states. Baek et al. (2012), for example, used the SHRP protocol for the following conditions:

- Short-term aging (STA). The loose, uncompacted mixture is conditioned at 135°C for 4 h and then compacted. Specimens are cored and cut for testing.
- Long-term aging, Level 1 (LTA1). The aging procedure is the same as for STA, except the specimens are conditioned at 85°C for 2 days before testing after coring and cutting.
- Long-term aging, Level 2 (LTA2). The aging procedure is the same as for STA, except the specimens are conditioned at 85°C for 4 days before testing after coring and cutting.
- Long-term aging, Level 3 (LTA3). The aging procedure is the same as for STA, except the specimens are conditioned at 85°C for 8 days before testing after coring and cutting.

Other laboratory aging protocol was used by Walubita (2006) and data from that work were used by Al-Rub et al. (2013) for calibrating for the first time the aging model proposed in that work.

Table 1 – Description of laboratory aging procedures used by Walubita (2006) whose data were input for the paper by Al-Rub et al. (2013)

Laboratory Aging Condition	Aging Process	Description
0 months	4h AASHTO PP2 STOA of loose HMAC mix at 135 °C plus 0 months aging of compacted HMAC specimens at 60 °C in an environmental temperature-controlled room	Simulates the time period just after HMAC in situ field construction at the end of the compaction (AASHTO PP2, 1994)
3 months	4h AASHTO PP2 STOA of loose HMAC mix at 135 °C plus 3 months aging of compacted HMAC specimens at 60 °C in an environmental temperature-controlled room	Simulates 3 to 6 years of Texas HMAC environmental exposure (Glover et al., 2005)
6 months	4h AASHTO PP2 STOA of loose HMAC mix at 135 °C plus 6 months aging of compacted HMAC specimens at 60 °C in an environmental temperature-controlled room	Simulates 6 to 12 years of Texas HMAC environmental exposure (Glover et al., 2005)

Adapted from Walibuta (2006)

On the other hand, an example of loose mixture aging is presented by Partl et al. (2012), which is known as the RILEM protocol. It consists of aging a loose mixture in 30×50×8cm cooking trays. For short-term aging the loose mixture is aged for 4h at 135ºC, as in the SHRP protocol. For the long-term aging, the loose mixture is aged for up to 9 days at 85ºC. According to the results from Partl et al. (2012), recovered binder from aged mixture samples of 3 days presented equivalent properties to RTFO and PAV aged binders.

It is to be observed that the temperatures and aging times used in the referred research works are arbitrary, and much research effort is still needed to really understand the aging process. It is also to be noticed that the need to wait for 3 to 9 days of laboratory aging time does not encourage this method for practical applications. In addition, the use of only one temperature for long-term aging avoids the possibility to capture the temperature dependency of the aging process. Those are some of the reasons why in this work another (and higher) aging temperature was selected to be tested (135ºC), in addition to 85ºC, along with other long-term aging periods (0, 2, and 45 days). Of course 45 days of tests is not of practical use, but it was expected that the modeling efforts in this work could lead to the

definition of shorter aging experimental procedures capable of representing the aging phenomenon in agreement with data from longer aging procedures. Extended periods were needed for modeling the aging phenomenon under a spread range of time, as it will be seen in the next topic with the procedure proposed by Al-Rub et al. (2013). These authors used mechanical properties results for asphalt mixture obtained in the work by Walubita (2006), which presented compacted asphalt samples aged until 6 months at 85ºC. The use of two aging temperatures, instead of only one, in the present work was expected to provide new information of asphalt mixtures oxidation process from the point of view of the Al-Rub et al.'s model.

2.4.3 Aging Models for HMA

Al-Rub et al. (2013) proposed a phenomenological mechanistic-based aging model conceptually similar to the chemical model in Equation 52. Those authors established a general law for the evolution of an aging internal state variable which has many similarities to the CA in Equation 17. In the same work, the aging internal state variable is coupled to the effects of aging, i.e., change in mechanical properties such as viscoelastic, viscoplastic and damage characteristics. The general expression for the model is represented by Equation 53.

$$\dot{A} = \Gamma^\alpha \theta^{k_1} (1 - A)^{k_2} exp\left[-k_3\left(1 - \frac{T}{T_0}\right)\right] \qquad (53)$$

Where A is the aging internal state variable, $\dot{A}$ its time derivative, θ is the normalized oxygen content (between 0 and 1), T_0 the reference aging absolute temperature, and T the actual absolute temperature. The four aging model parameters are the aging dependency on normalized oxygen content k_1 (similar to the reaction order in Equation 52), the aging history dependency k_2 (which accounts for possible changes in rate of aging), the aging temperature dependency k_3, and the aging fluidity parameter Γ^α. The last one is given in s^{-1} and its inverse can be interpreted as a relaxation time for the aging process, i.e., time necessary for a fixed change in the original value of the aging variable. With respect to the Arrhenius law presented in Equation 52 for the CA growth, it is similar to the pre-exponential factor.

The aging internal state variable ranges from 0 to 1, with $A = 0$ representing an unaged material, whereas $A = 1$ represents a completely aged material, i.e., there are no remaining oxidizable fractions in the material. This variable has somewhat for aging modeling the same function as Lemaitre and Chaboche's (1990) damage variable had for the damage modeling, i.e., it is a state variable varying from 0 to 1, where 0 indicates the beginning of the process and 1 the theoretical limit for the process. It is to be observed that, although 1 indicates the theoretical limit for the evolution of the aging state variable, depending on the aging parameters, an increment on the aging variable could be reached with very long aging times, meaning that the aging process is stopping.

The generalized model can be simplified, by assuming that there is always available oxygen for the oxidation reaction ($\theta = 1$), $k_2 = 1$, and integrating it. The result is shown in Equation 54.

$$A = 1 - (1 - A_0)e^{-c_1 t} \qquad (54)$$

Where A_0 is the value of the aging state variable in the beginning of the aging process ($A_0 = A(t)_{t=0}$) and $c_1 = \Gamma^\alpha exp\left[-k_3\left(1 - \frac{T}{T_0}\right)\right]$. The product $t' = c_1 t$ can be seen as a reduced aging time, taking aging temperature into account, in an analogous manner with respect to reduced loading frequency and reduced loading time for viscoelastic characterization. That model (Equation 54) was applied by Babadopulos et al. (2014) for modeling aging and linear viscoelasticity coupling for Age Zero, Age 2, 85ºC and Age 2, 135ºC. Those data are also presented in this work. The simulation in modulus increase resulted in an exponential growth, because of the assumed value for the aging history dependency constant $k_2 = 1$. This parameter could instead be considered different from 1 and included as an optimization parameter in the analysis. Greater values of k_2 indicate more "resistance" to the growth of the value of the aging state variable. In the case k_2 is considered different from 1, it can be shown by simple integration that the model considering the aging history parameter is represented by Equation 55, which was not presented in the original paper by Al-Rub et al. (2013).

$$A = 1 - (1 - A_0).(1 - c_2.t)^{\frac{1}{1-k_2}} \qquad (55)$$

Where a new constant, c_2, is introduced and it is equivalent to $c_2 = \frac{c_1(1-k_2)}{(1-A_0)^{1-k_2}}$. Finally, it is to be observed that if $k_2 = 0$, the model reduces to an Arrhenius type model, which is characterized by a constant rate of growth in the aging variable for given pressure and temperature. Figure 14 shows a parametric analysis of the evolution of the aging state variable for different values of the aging history dependency parameter, using Equations 54 and 55. It is to be observed that time (x-axis) is in logarithmic scale. In natural scale, $k_2 = 0.01$ (value near 0) produces a curve for the aging state variable evolution which is approximately a straight line (Arrhenius type model, with constant rate).

Figure 14 – Parametric analysis of the evolution of the aging variable for varying aging history dependency with logarithmic time scale
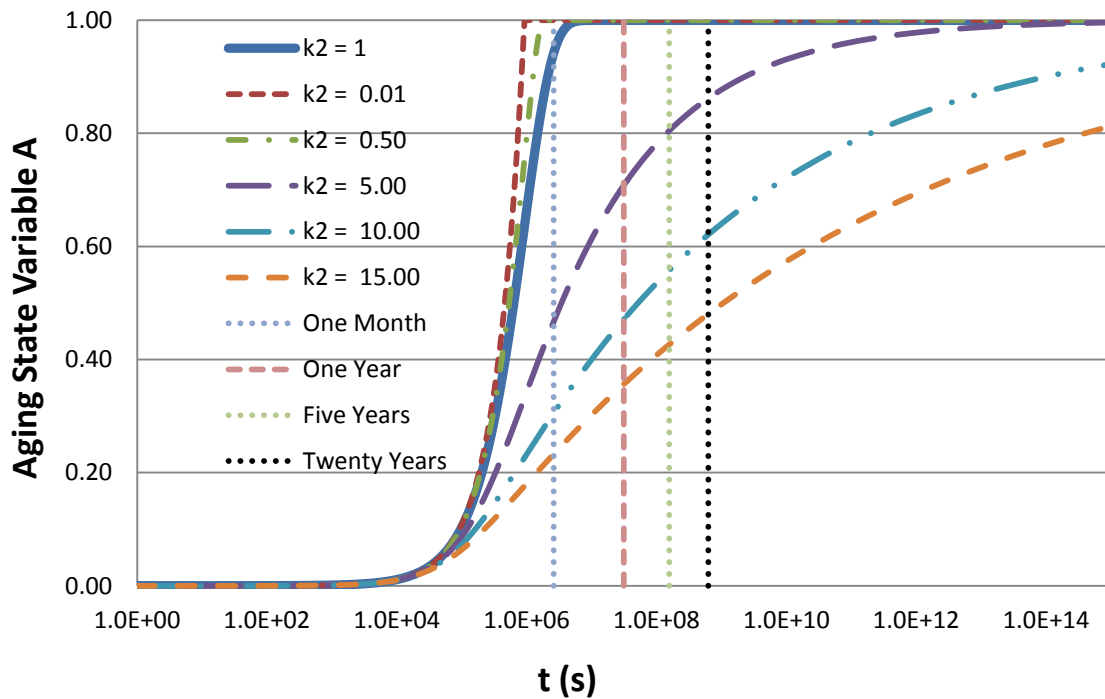
In the parametric analysis presented in Figure 14, only the aging history dependency parameter (k_2) was varied. The other parameters were set to $A_0 = 0$, $\Gamma^\alpha = 9.95 \cdot 10^{-7} s^{-1}$, $\theta = 1$, $T_0 = 21.1°C$, $k_3 = 3.03$, as obtained by Babadopulos et al. (2014). The aging temperature was set to 30°C. As $\theta = 1$, the results of the analysis do not depend on the value of k_1. The first thing to be observed is that for low values of the aging state variable, all examples of aging evolution are similar, not depending strongly on the value of the aging history parameter. This is expected, because this parameter acts as a power of the quantity $(1 - A)$, so it is not strongly changed for low values of A.

It is also to be observed that although in a first sight all aging evolution appears to be fast even for evolved aging states, it is to be remembered that time scale is logarithmic. For example, between the beginning of the process and the first month, there is more aging evolution for $k_2 = 15$ than in the next five years. Actually, in a natural scale, although not mathematically, aging evolution appears to have an asymptotic behavior, with the asymptote depending in the value of k_2. This can be observed in Figure 15 (natural time scale in the x-axis).

Figure 15 – Parametric analysis of the evolution of the aging variable for varying aging history dependency with natural time scale
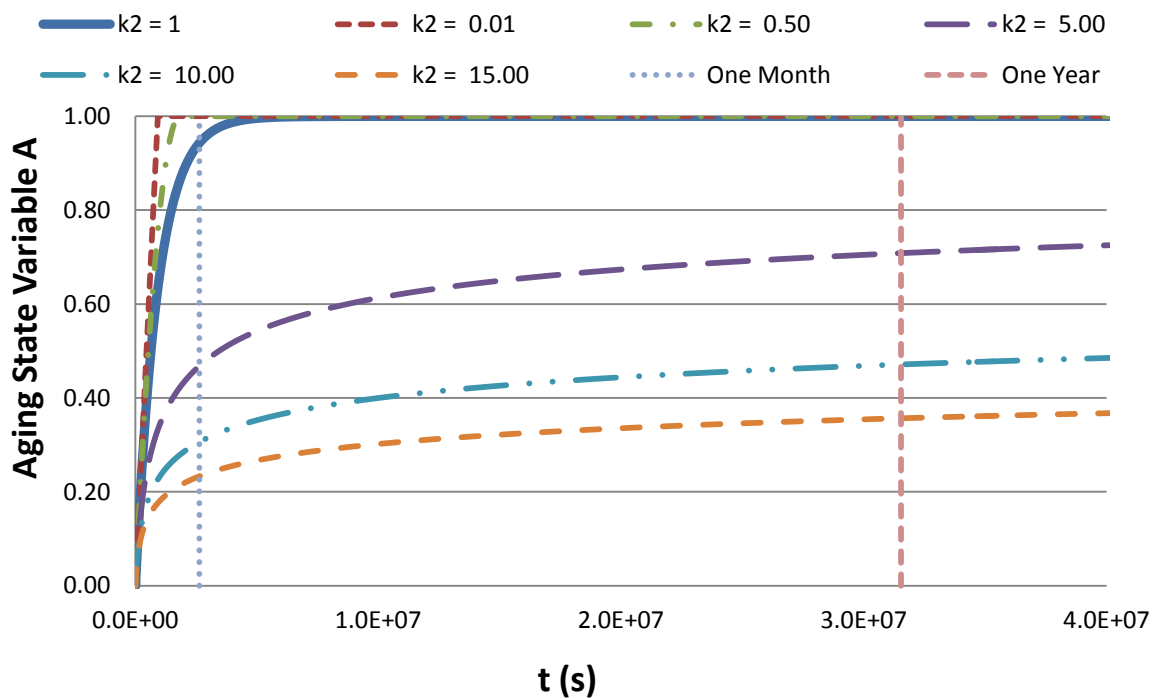
Regarding data presented in Figure 15, it can be observed that, in practice, not necessarily a value near 1 is reached in the aging process by the aging state variable. It depends on the value of the aging history parameter. Moreover, it is to be noticed that although the aging state variable serves as an "aging counting", it is related to mechanical behavior through aging susceptibility parameters, presented in the next paragraph. So, it is not possible to evaluate the impact of aging without taking into consideration the value of the susceptibility parameters, i.e., $A = 0.3$, for example, does not mean a change in 30% in any mechanical property. It will only be possible to estimate mechanical behavior changes after coupling the aging model to the mechanical models.

The aging model can be coupled in the constitutive modeling of asphalt mixtures as shown by Al-Rub et al. (2013). For the coupling to linear viscoelasticity, the referred authors used the creep compliance discrete spectra at different aging states. In the present work, the relaxation modulus discrete spectra were used. Both properties represent the linear viscoelastic behavior equivalently. As in this work modulus values are obtained from optimization, they were directly used for the aging model calibration. Equations 56, 57 and 58 represent the coupling between the linear viscoelasticity and the aging of the material.

$$(E_\infty)_A = (1 - A)^{-\alpha_1} . E_\infty \tag{56}$$

$$(E_i)_A = (1 - A)^{-\alpha_2} . E_i \tag{57}$$

$$(\rho_i)_A = (1 - A)^{-\alpha_3} . \rho_i \tag{58}$$

The subscript A indicates the aged state. The model parameters represent the relaxation spectrum susceptibility with respect to aging (α_1 for the elastic modulus, α_2 for the transient modulus, and α_3 for the relaxation times). It is to be observed that they all derive from the same reasoning to couple aging to the linear viscoelastic properties of the material, i.e., that the change in a linear viscoelastic parameter can be represented by a power of $(1 - A)$, where A represents the "aging counting". That power, α, is a material parameter for the aging coupling and represents that parameter's aging susceptibility. That reasoning can be represented by Equation 59.

$$(Viscoelastic\ parameter)_{Aged} = (1 - A)^{-\alpha} . (Viscoelastic\ parameter)_{Unaged} \tag{59}$$

2.5 Mechanical Models with Coupled Aging

Baek et al. (2012) studied the influence of oxidative aging on mixture properties, aiming at reporting effects of lab induced aging on linear viscoelastic and damage properties of asphalt mixtures. According to those authors, this is a necessary effort towards the incorporation of aging effects considerations into a more comprehensive analytical framework to predict performance of asphalt mixtures in pavements. The research herein represents a similar effort, characterizing linear viscoelasticity, viscoplasticity and damage of asphalt mixtures, using a protocol for aging different from the one used by Baek et al. (2012). These

authors used a modified SHRP protocol, as previously mentioned, aging compacted mixtures until 8 days at 85ºC. They concluded that stiffness increases with aging time over the entire frequency spectrum, but that a clearer trend is observed at low reduced frequencies (slow loading at warm temperatures), which can be due to the fact that a large difference between binder and aggregates stiffness exists at those conditions.

For the damage properties, it was observed by Baek et al. (2012) that aging clearly differentiates the damage characteristic curves of the aged mixtures. Also, the S-VECD model was successfully applied to characterize the damage properties of aged asphalt mixtures. Fatigue failure in the aged asphalt mixture was found to be a function of both fatigue test temperature and aging level. However, it is observed that the aging process used in the tests (SHRP protocol for compacted mixtures), may have produced more heterogeneous samples for the fatigue test, leading to failure with more dispersed material integrity due to local fragilities. Baek et al. (2012) also implemented simulations of structure behavior considering aging using the VECD-FEP++, a finite element program used in NCSU for the modeling of asphalt pavement structures. The results of the simulation showed that aging significantly affects the fatigue behavior of the structure, most importantly at the pavement surface, and that it is more significant under warm climate conditions. In the present work, the same damage model is used, but the aging procedures and consequently the aging states are different. As loose mixtures were aged in the laboratory up to 45 days at 85ºC, more evolved aging states were covered in the present research.

Al-Rub et al. (2013) used other kind of mechanical model for characterizing damage, which was presented by Darabi et al. (2011). The models used by those authors are mathematically similar to the model that describes the aging state variable evolution (Equation 53). In the case of damage, its evolution depends on effective total strain, a function of the stress invariants (damage driving force), temperature and damage history. Analogously as the aging fluidity parameter for the aging model, it is noticed that the damage model results are mainly driven by a pre-exponential factor called damage fluidity parameter. Its inverse can be understood as the "damage relaxation time". For the modeling of coupled aging and damage in Al-Rub et al. (2013), only that parameter was made a function of the aging.

3 MATERIALS AND METHODS

3.1 Investigated Asphalt Mixtures

The asphalt mixture investigated in the present research is a dense asphalt concrete with 12.5mm nominal maximum aggregate size. The binder is classified by penetration as a 50/70. From the perspective of the performance grading system it is classified as a PG 64-22. For the designed air void content (4.0%), the required binder content was 6.0% (by weight of the total mixture). The resulting maximum theoretical (measured) specific gravity (G_{mm}) determined by the Rice test was 2.392 (average results from three samples).

The materials tested in this research are the reference unaged mixture (Age Zero), and that very mixture subjected to different aging procedures, becoming the so-called aged mixtures. Results covered two different temperatures for the aging period of two days (Age 2, 85ºC and Age 2, 135ºC) and only one temperature for the aging period of 45 days (Age 45, 85ºC). The mixture aged for 45 days at 135ºC was also prepared, but there was not sufficient cohesion and the loose mixture was too stiff and "dry", so that it was impossible to compact using the Superpave gyratory compactor. Testing different temperatures allowed the identification of the mixture aging sensitivity with respect to aging temperature, which constitutes a contribution with respect to the results originally presented by Al-Rub et al. (2013), where aging temperature dependency was not evaluated. The data used by Al-Rub et al. (2013), as previously mentioned in the Literature Review, were obtained by Walubita (2006), and the procedures used were already described in Table 1.

From the data obtained in the present work, it was observed that the G_{mm} considerably changes with aging, given the fact that variations in the third decimal place of its value impact directly the value of the estimated air voids content. The results were 2.403 for Age 2, 85ºC, 2.402 for Age 2, 135ºC and 2.412 for Age 45, 85ºC. Figure 16 illustrates the cooking trays used for the laboratory aging procedure. It is to be observed that although the trays present a height of 8cm, the loose mixture occupied less than 6cm, in order to facilitate oxygen penetration.

Figure 16 – Cooking trays used for the laboratory aging experimental procedure
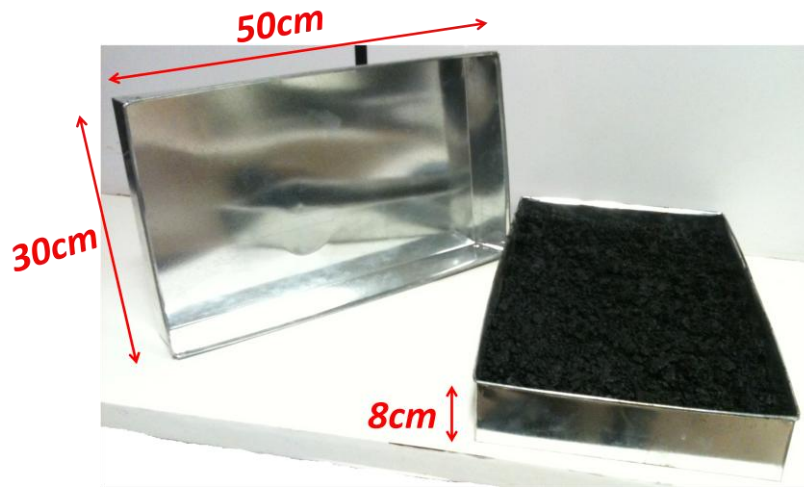
In this research, samples were always prepared targeting 4.0% air void content. This way, samples from complex modulus tests could be reused for dynamic creep tests, reducing laboratory efforts. The time spent (of the order of 3h) at the high temperature of the complex modulus test (54.4ºC) was considered not to change the aging state of the tested mixture. That time is much shorter than the one spent in the oven (from 2 to 45 days) and also, the aging temperatures studied in this research (85 and 135ºC) are much higher than the highest test temperature. Also, the small strains associated with complex modulus tests were considered not to change finite deformation responses, e.g., those in the dynamic creep tests. Therefore, samples already tested for dynamic modulus could be reused for dynamic creep tests. It is to be observed that usually samples presenting 7% air voids are tested for the dynamic creep.

For the state-of-the-art characterization procedures in this research, sample preparation in the Superpave gyratory compactor was set to stop at a fixed height, targeting 150mm, as the number of gyrations necessary to produce samples with 4.0% air voids could change due to the bitumen viscosity variation induced by aging. The diameter of the mould was 100mm. Final heights near 150mm were obtained, using approximately 2,630kg of mixture to prepare each sample. Because all required equipment is not available for cutting and coring, samples were not cored or cut, but used directly from gyratory compaction in the mechanical tests. The main concern which encourages the use of cored and cut samples is to obtain the maximum homogeneity in the sample and that less voids are concentrated near the bottom and the top of the samples. In direct tension-compression fatigue tests, fragility in

those regions lead to more frequent top and bottom failures, which is not desirable because it can change results from mechanical characterization. For each aging condition (Age Zero; Age 2, 85ºC; Age 2, 135ºC; Age 45, 85ºC), 15 samples were prepared following the described procedure. The obtained mean air void contents were 4.3, 4.5, 4.7 and 6.0%, respectively.

For the state-of-the-practice in Brazil characterization procedures, the final target height for the samples was 63.5mm. The diameter of the mould was 100mm. Samples were also prepared in the Superpave gyratory compactor.

3.2   Testing Procedures

Both the state-of-the-practice in Brazil and the state-of-the-art tests for asphalt mixture stiffness, permanent deformation and fatigue characterization are presented in this section.

3.2.1   Stiffness Characterization

Resilient Modulus (RM)

In this work, ABNT NBR 16018:2011 protocol was used to obtain the value of the RM for the mixture at each aging state. Two LVDTs placed in the horizontal diameter of Marshall (100mm diameter by 63.5mm height) specimens (perpendicular to the compression load) are used.

Complex Modulus (E*)

AASHTO T 342 (2011) (equivalent to the former provisional standard AASHTO TP 62-03, 2005) was the test protocol adopted for HMA stiffness characterization. The results are typically shown in master curves for both $|E^*|$ and φ. Mean results were obtained from tests in four Superpave samples of 100mm diameter by 150mm height, using three axial LVDTs mounted 120º apart on the surface of the sample, around its circumference. Fingerprint tests (short-time complex modulus tests, at very small strain amplitudes) were conducted in order to select the load pulse to be tested. A strain amplitude of 67.5µ was the target, expecting to reach strain amplitudes in the interval between 60 and 75µ. At such strain

levels, linearity conditions should be respected and negligible strain dependency (nonlinearity) observed. The master curves for each aging state were obtained after horizontally shifting the isotherms, using the WLF Law (Williams et al., 1955).

3.2.2 Permanent Deformation Characterization

The test chosen to evaluate resistance to permanent deformation was the unconfined dynamic creep test. Before starting the test, a period of 60s of conditioning loading was imposed to the materials. The load pulse was controlled in order to produce haversine stress during 0.1s reaching a peak of 204kPa. A seating stress equivalent to 5% of the peak stress, i.e., 10.2kPa, was adopted for the 0.9s long rest period. Tests were conducted at 60 ± 0.5ºC. Total permanent deformation was evaluated along with its rate with respect to the number of cycles. When the rate reached a minimum, it was considered that flow number (FN) was reached. FN is defined as the number of cycles in which the material behavior initiates a region of unstable shear flow (tertiary zone). Before that, two zones characterize HMA behavior: an accommodation region (primary zone) and a constant rate of deformation region (secondary zone). The minimum rate of deformation with respect to the number of cycles was also evaluated. Mean and coefficient of variation were taken from test results for 6 specimens per aging state. Figure 17a illustrates the two pairs of membranes used to avoid friction and consequent generation of shear stresses at the bottom and the top of the samples. Grease is used in between the membranes to reduce friction and allow the Poisson's effect during compression of the samples. Figure 17b illustrates the change in geometry of the sample, which reduces in height after the test due to the accumulation of plastic deformation.

Figure 17 – (a) Example of tested Superpave sample in the dynamic creep test and the used membranes; (b) Comparison between a non-tested and a tested Superpave sample in the dynamic creep test

(a)   (b)
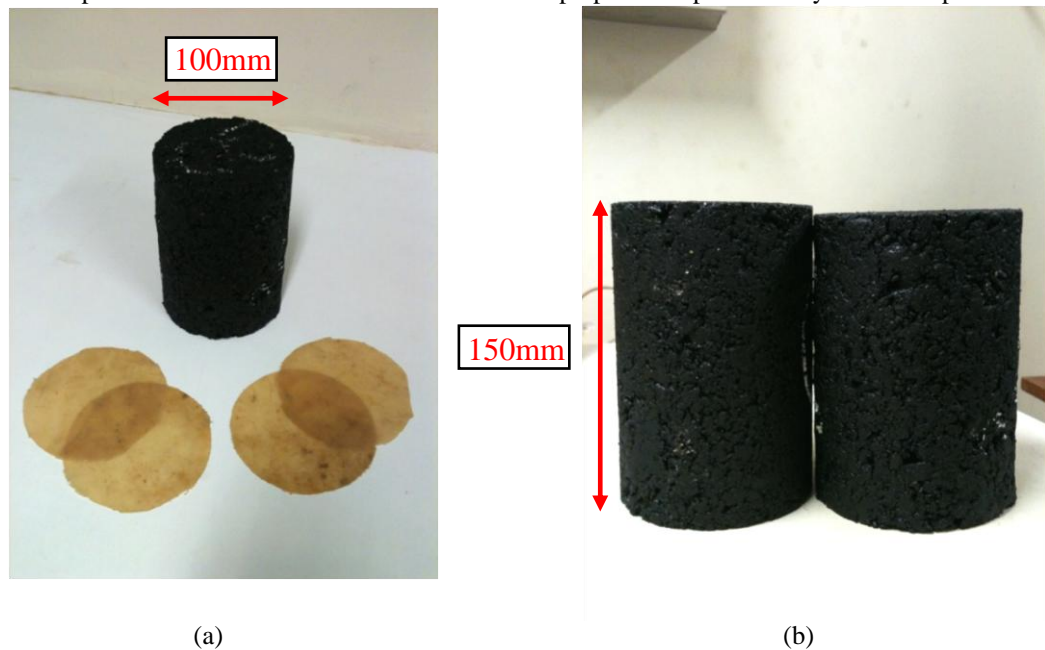
3.2.3   Fatigue Characterization

Controlled Crosshead Tension Compression Fatigue Tests

In the research herein, controlled crosshead harmonic fatigue tests were conducted using 9 HMA samples per aging condition. The results were used to fit the Simplified Viscoelastic Continuum Damage model. As previously mentioned, the *C vs S* is meant to be a material characteristic curve. The tests were conducted at different conditions, varying the strain amplitude. Three samples were used for testing at each one of the three different target strain levels (around 200, 350 and 500μ). Before every fatigue test, a short-time tension-compression complex modulus test (fingerprint test) was conducted in order to capture sample-to-sample variation. These tests consist of complex modulus tests at very small strains conducted to capture sample-to-sample variations.

LVDT geometry for these tests was exactly the same as in the complex modulus tests. For each tested strain amplitude, three specimens were used. Prior to testing, samples were glued to top and bottom endplates. The endplates were connected to the testing machine using screw connections. The gluing process takes around 16h (depending on the curing time of the glue) and a mounting jig is necessary to align the axis of the endplates and the samples. However, after 4h, the used glue (a low plasticity epoxy glue for metals and concrete) was

cured enough in order to take the sample out of the mounting jig to begin the next gluing process. Figure 18 illustrates the sample preparation process (a) and the mounted fatigue test (b).

Figure 18 – (a) Illustration of the gluing process of the endplates to the HMA sample; (b) Illustration of mounted fatigue test

(a)   (b)
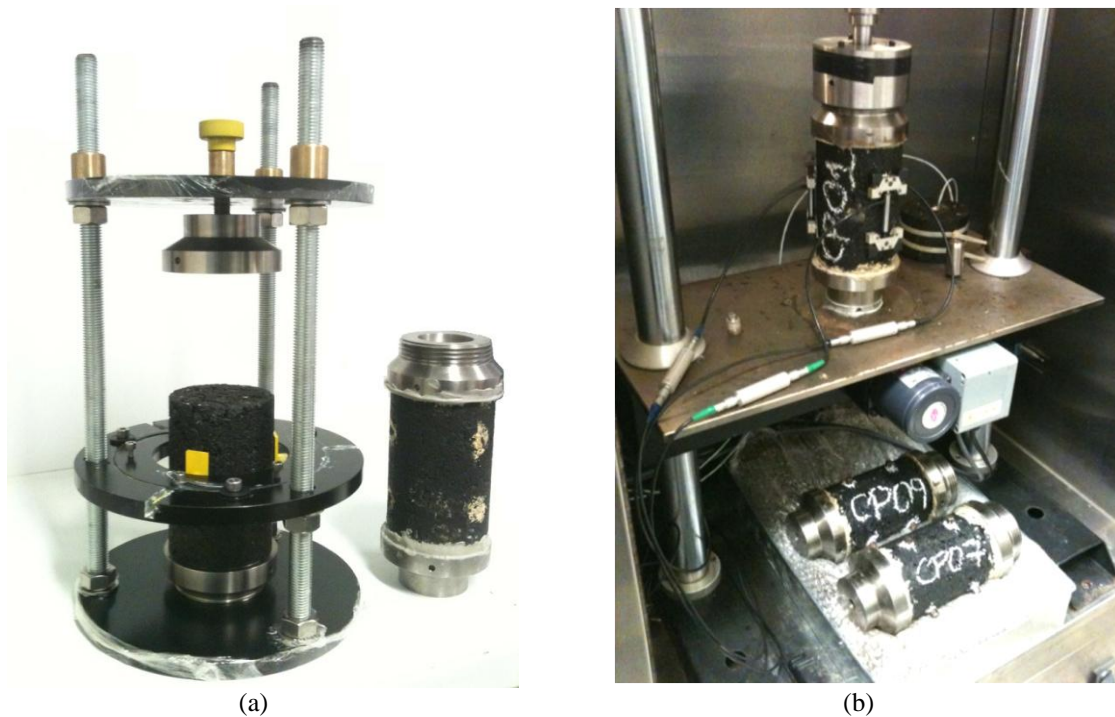
Controlled Force Indirect Tensile Fatigue Tests

The most used fatigue test in Brazil is the controlled force indirect tensile test. Percentages (generally 30, 40 and 50%) of the tensile strength of the material are used as the reference stresses in the test, i.e., the corresponding loads are applied to the specimen to generate those stress values in the mid center of the cylinder. Typically three samples per stress amplitude are used, and a log-log graph is produced with the number of cycles to failure against the difference between compressive stress and tensile stress in the midpoint of the cylinder specimen (Wöhler curves). Although it appears to be a controlled stress test, only the stress at the first cycle corresponds to the intended "controlled stress", because damage evolves in the material and the force applied to the sample is distributed in smaller cross sectional areas as the load cycles progress, until failure in the material. In addition, as loading is always imposed in the same direction (compression for the vertical diametral line and tension for the horizontal diametral line), failure is not assured to be caused by fatigue. The

loading can be interpreted as the sum of a constant creep loading and a deviatoric loading. Both excessive flow and deviatoric loading may induce damage to the sample. Thus, it is very difficult to extract information only about fatigue failure from this test. This may explain why a laboratory to field shift factor of 10^4 has been used in Brazil to "estimate" fatigue life of asphalt mixtures.

3.2.4 Experimental Campaign

Figure 19 presents the flow chart summarizing the tests planned for each aging state investigated. Although results from characterization of mixture at Age 45, 135ºC were planned to be available for this research, there was not sufficient cohesion in the aged mixture and it was too stiff and "dry", therefore impossible to compact using the Superpave gyratory compactor. Consequently, no mechanical characterization results are available for that aging state. Nevertheless, the author believes that identifying that it was impossible to obtain compacted mixture samples for that aging state also constitutes a result of the present research. In addition, controlled force indirect tensile fatigue test results for aged materials above Age 2, 85ºC with Marshall samples were difficult to obtain, because of the increase in stiffness of the material and the consequent longer test durations (more than a day for a single sample) in force controlled mode.

Figure 19 – Flow Chart for the Laboratory Activities to Characterize Each Aging State
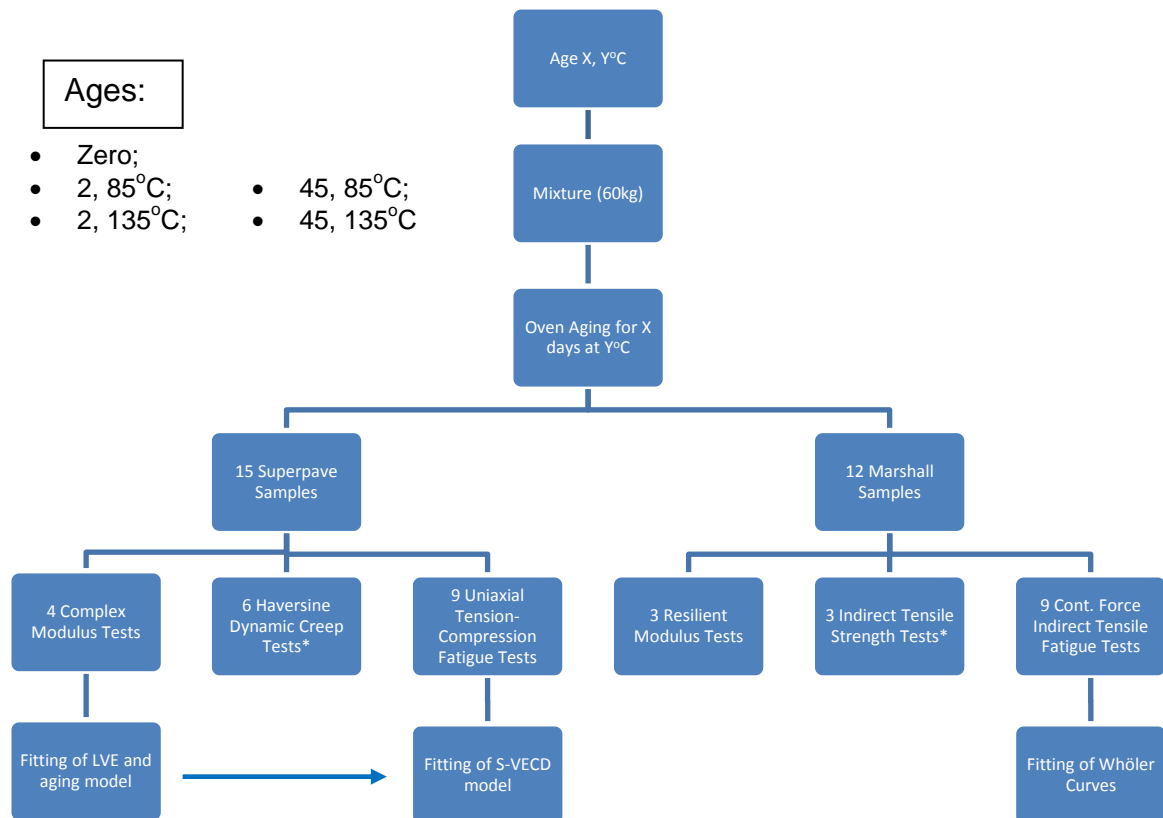
In Figure 19, the Haversine Dynamic Creep and the Resilient Modulus tests were marked with a star, in order to indicate that they were conducted with samples which have been already tested for other mechanical property. Dynamic Creep tests used the 4 samples tested for complex modulus. No relation between the measured properties and the fact the sample has or has not been tested for complex modulus was observed. Tensile Strength test samples were the same used for Resilient Modulus testing. Indicated TS for calculating 5%TS for the choice of the load in RM test was 1MPa.

A word regarding the time consumed at each experimental step is given as additional information to this work. Mixture (60kg) can be prepared in 1 day, while compaction (27 samples) needs typically 2 days to be completed. For the mixture aged for 2 days, all samples were compacted in the same day, in order to avoid differences in the samples due to re-heating of the mixtures prior to compaction. For the mechanical tests, 1 day (~12h) is enough to complete the 4 complex modulus tests after the overnight period for temperature stabilization in the test chamber for test at -10ºC. Approximately the same time is used for the dynamic creep tests (depending on the permanent deformation resistance of the

mixture). Although for the fatigue tests 1 day would be sufficient for testing, the sample preparation takes 1 day per group of three samples, because only one mounting jig is available at the Pavement Mechanics Laboratory (LMP/UFC). For resilient modulus and tensile strength tests, half a day is necessary, while diametral compression fatigue can take more than 1 day (depending on mixture's resistance to fatigue and aging state) per sample to finish. It is important to observe that more than one-day-consuming tests can be performed in the same day if they require different equipments, and that tests in Superpave samples are conducted in a UTM-25, while Marshall samples are tested in a pneumatic machine.

4   **RESULTS AND DISCUSSION**

In this chapter, the experimental results (dynamic modulus, phase angle, dynamic creep and fatigue test results), for Age Zero, Age 2, 85ºC, Age 2, 135ºC and Age 45, 85ºC are described and compared. Some results of state-of-the-practice asphalt mixture characterization in Brazil are also presented and compared.

The procedure to fit the adopted linear viscoelastic and aging models is also described, and the resulting parameters are presented. The first results obtained for early ages (Age Zero, Age 2, 85ºC and Age 2, 135ºC) were presented in Babadopulos et al. (2014), which also contains the first estimates of the aging model parameters. At that point of the research, the simplified model presented in Equation 54 was used instead of Equation 55, i.e., the aging history dependency was considered to present the value of $k_2 = 1$ (simplified aging model). However, when Age 45, 85ºC was included in the analysis, it was foreseen that the optimization of the aging history dependency parameter would be needed. This was confirmed in the overall results presented in this thesis, which includes the aging history dependency parameter in the optimization. A comparison is made between model prediction and experimental results. Also, the model obtained with the overall results of the thesis is compared with the model obtained in Babadopulos et al. (2014), which only contained mixtures aged at earlier ages. At the end, a brief aging simulation is performed, showing the estimated change of the mixture stiffness, according to the fitted aging model.

Besides investigating stiffness dependency on aging, unconfined dynamic creep results (viscoplastic characterization) and tension-compression fatigue (continuum damage characterization) are also presented in this chapter. The results of these two main distresses in asphalt mixtures for different aging states are presented. Behavior observed at the different aging states is then compared. Using the fitted aging model, the author has tried to contribute to the understanding of the coupling between results from dynamic creep tests and aging, as well as coupling between damage and aging.

4.1   Linear Viscoelastic Characterization and Aging

The stiffness characterization results are shown in master curves obtained at 21.1ºC for both $|E^*|$ and φ, as indicated in Figures 20a and 20b, respectively. The master

curves for each aging state were obtained after horizontally shifting the isotherms, using the WLF Law (Williams et al., 1955).

Figure 20 – Dynamic Modulus (a) and Phase Angle (b) Master Curves for the Three Tested Aging States

(a)   (b)
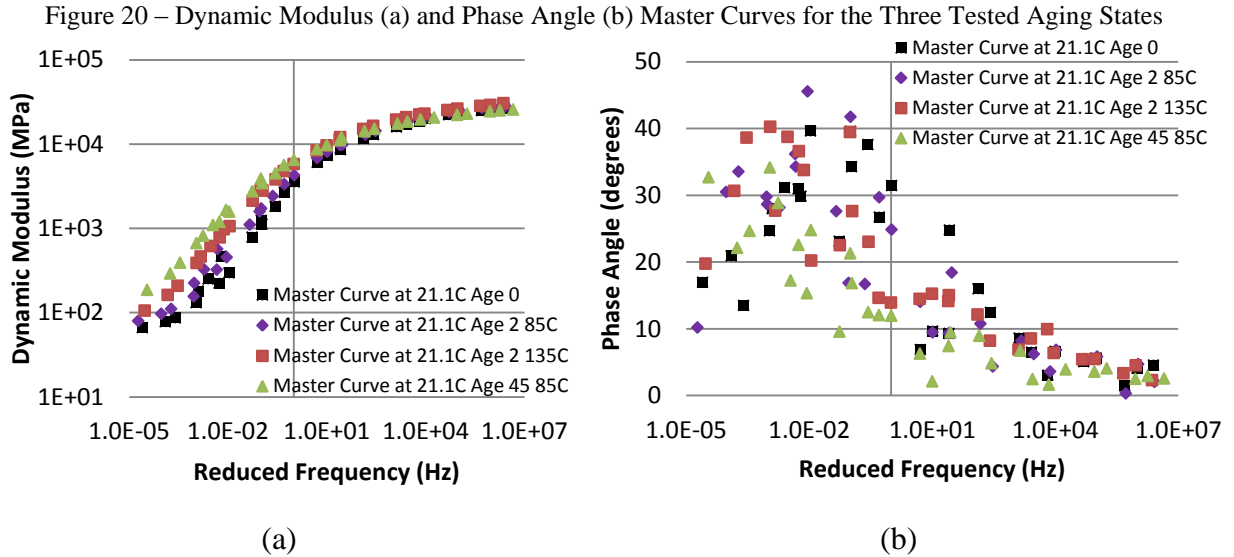
With respect to the stiffness characterization in Figure 20a, it can be seen that $|E^*|$ gradually increases as aging evolves. In logarithmic scale (Figure 20a), the dynamic modulus at low reduced frequencies (or high temperatures) seems to be much more affected by aging then at high reduced frequencies, as observed by other authors (Glover et al., 2008). This means that the percentage change in dynamic modulus is higher at low reduced frequencies. That can be due to the fact that in the region of low reduced frequencies the binder properties influence more the bulk response of the mixture. As aging affects directly the binder, the master curve at low reduced frequencies is more influenced by aging. The scatter of φ results may not present a clear trend for the phase angle as aging evolves, as seen in Figure 20b. However, there is an indication that the peak value of the phase angle tends to occur at lower reduced frequencies as aging evolves. The peak phase angle seems to occur around 2.10^{-2}Hz for Age Zero; 9.10^{-3}Hz for Age 2, 85ºC; 1.10^{-3}Hz for Age 2, 135ºC; and below 1.10^{-4}Hz for Age 45, 85ºC. Although the peak values of phase angle seem not to change in the first three aging states, being between 40º and 45º, at the last aging state it is approximately equal to 35º. For higher reduced frequencies (above the peak phase angle), the phase angle value is slightly lower for increasing aged states, i.e., the mixture appears to be more elastic as aging progresses for those loading frequencies. That decrease in the phase angle is dependent on the loading frequency. For example, it decreases from approximately 18º for Age Zero to 12º for Age 45, 85ºC at 10Hz, and from around 5º to 3º at 10^5Hz. It is observed that the frequencies above the phase angle peak (approximate to 10^{-2}Hz at 21.1ºC) represent low speed traffic, so,

for almost all practical loading applications the phase angle after aging will present slightly reduced values for the studied mixture. Baek et al. (2012) made the same observation, but analyzing less scattered data, associated with aging states not as distinct as the ones considered in the present research. The referred authors used the SHRP protocol for aging in compacted mixtures up to 8 days of aging at 85ºC.

Linear Viscoelasticity Modeling

The discrete relaxation and retardation spectra obtained for the studied asphalt mixture at the four tested aging conditions are summarized in Tables 2a and 2b, respectively. These parameters describe the linear viscoelastic behavior of the asphalt mixture and can be used to simulate any loading path that does not cause material nonlinearities, e.g., plasticity or damage.

Table 2a – Relaxation Spectra for the Four Evaluated Aging States

	Age Zero	Age 2, 85ºC	Age 2, 135ºC	Age 45, 85ºC
E_∞ (MPa) =	60	75	90	85
ρ_i (s)	E_i (MPa)	E_i (MPa)	E_i (MPa)	E_i (MPa)
1.00E-07	1.62E+03	1.90E+03	3.29E+03	1.90E+03
1.00E-06	2.65E+03	2.78E+03	2.88E+03	2.39E+03
1.00E-05	3.87E+03	4.20E+03	3.66E+03	2.35E+03
1.00E-04	4.67E+03	4.66E+03	4.09E+03	3.38E+03
1.00E-03	4.82E+03	4.89E+03	5.17E+03	3.61E+03
1.00E-02	2.84E+03	3.48E+03	4.50E+03	3.61E+03
1.00E-01	4.42E+03	4.11E+03	3.70E+03	3.41E+03
1.00E+00	1.32E+03	1.81E+03	2.87E+03	2.74E+03
1.00E+01	3.02E+02	6.35E+02	9.51E+02	1.52E+03
1.00E+02	1.45E+02	1.54E+02	4.52E+02	7.21E+02
1.00E+03	3.02E+01	6.05E+01	7.08E+01	2.64E+02

Table 2b — Retardation Spectra for the Four Evaluated Aging States

	Age Zero	Age 2, 85ºC	Age 2, 135ºC	Age 45, 85ºC
D_0 (MPa^{-1}) =	3.74E-05	3.48E-05	3.15E-05	3.85E-05
τ_j (s)	D_j (MPa^{-1})	D_j (MPa^{-1})	D_j (MPa^{-1})	Dj (MPa-1)
1.00E-07	2.21E-06	2.25E-06	3.24E-06	2.77E-06
1.00E-06	4.34E-06	4.01E-06	4.11E-06	4.52E-06
1.00E-05	8.00E-06	7.58E-06	5.69E-06	5.25E-06
1.00E-04	1.47E-05	1.32E-05	9.53E-06	9.60E-06
1.00E-03	3.01E-05	2.47E-05	1.75E-05	1.61E-05
1.00E-02	4.27E-05	3.92E-05	3.45E-05	2.67E-05
1.00E-01	7.79E-05	8.00E-05	6.18E-05	5.11E-05
1.00E+00	4.44E-04	2.88E-04	1.50E-04	1.08E-04
1.00E+01	1.59E-03	8.50E-04	5.44E-04	3.06E-04
1.00E+02	3.63E-03	3.10E-03	9.95E-04	3.83E-04
1.00E+03	1.04E-02	7.34E-03	7.64E-03	4.82E-03

The linear viscoelastic models (Prony series for the relaxation modulus) summarized in Table 2a presented a satisfactory fitting to the experimental data. Those presented in Table 2b (Prony series for the creep compliance) were obtained by the interconversion presented by Park and Schapery (1999). The good fitting was observed both for the storage modulus E' (fitting input) and the loss modulus E'' (not the fitting input), as seen in Figure 21. This indicates that linearity limits were respected during laboratory tests.

Figure 21 – Measured and Modeled (Prony series) Storage and Loss Moduli for
(a) Age Zero, (b) Age 2, 85ºC, (c) Age 2, 135ºC and (d) Age 45, 85ºC

(a)

(b)

(c)

(d)
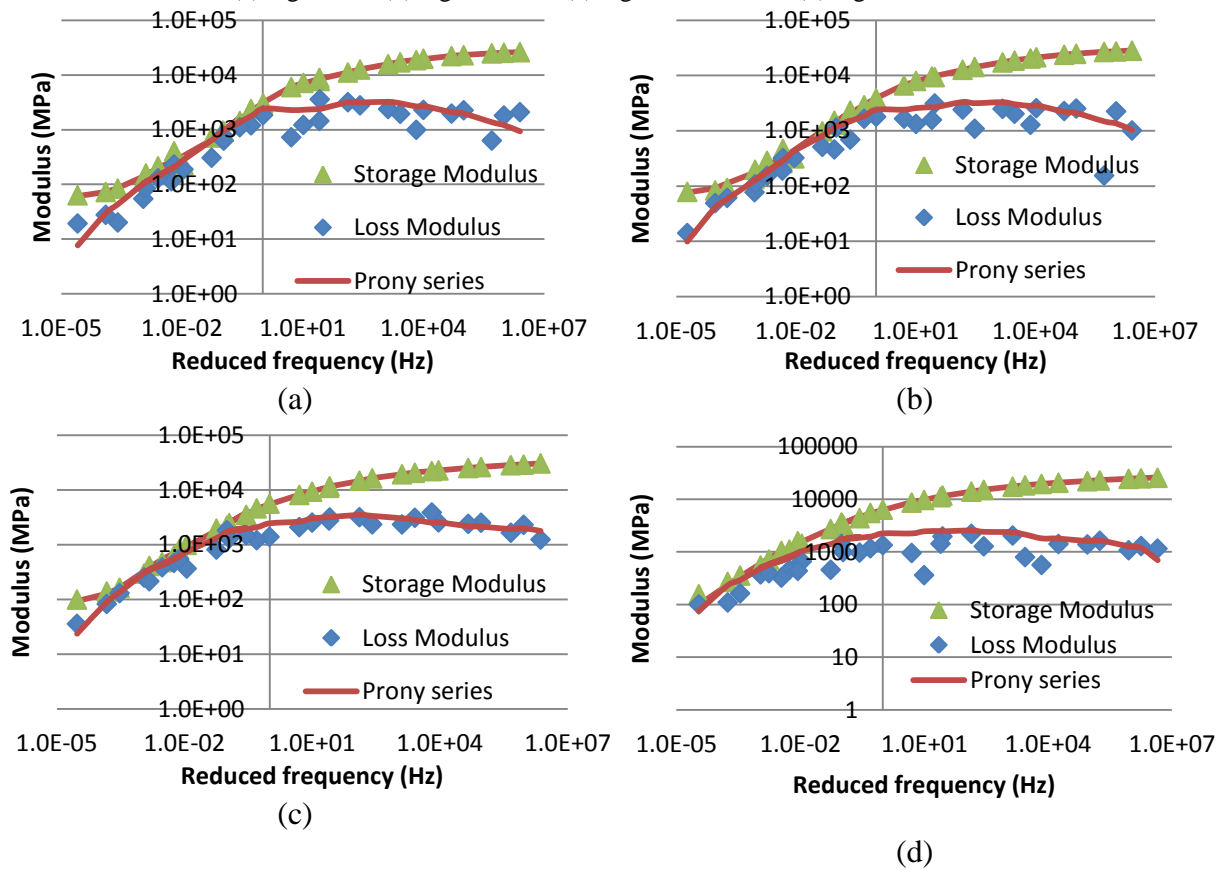
Aging Modeling

In this section, the previously obtained viscoelastic models are considered as inputs for the aging modeling. Henceforth, aging modeling consists in determining the best set of parameters, with respect to the experimental data, for the simplified model presented in the Literature Review: the reference temperature (T_0), the aging fluidity parameter (Γ^α), the initial aging state (A_0), the aging temperature dependency (k_3), and the relaxation spectra susceptibility with respect to aging (α_1 for the elastic modulus, α_2 for the transient modulus components, and α_3 for the relaxation times). The optimization of the aging oxygen availability dependency (k_1) was not pursued for this work, because no experimental data obtained with different oxygen availabilities is available. So, the value of that particular parameter was assumed to be equal to 0.15 (as in Al-Rub et al., 2013). Babadopulos et al. (2014) did not need the aging history dependency (k_2) to fit the data because only early ages (Ages Zero, 2, 85ºC and 2, 135ºC) were taken into account at that stage of the research work. When including the results of Age 45, 85ºC in the optimization process, k_2 needs to be taken

into account in order to obtain an acceptable fitting. A reference temperature (T_0) of 21.1°C was considered.

The first step for fitting the aging model is the estimation of the values of the aging state variable (A). Those values provide an indication of the material aging state that corresponds to the aging condition caused by the laboratory procedure applied to the loose mixture. The initial aging state (A_0) was assumed to be zero, as Age Zero was taken as the beginning of the aging process. However, A_0 can be assumed to have a value different from zero, accounting for short-term aging (Al-Rub et al., 2013). Such assumption simply means that the initial aging state would have occurred before the one referred in this work as Age Zero. Data from earlier aging states than short-term aged mixture were not planned for this research. It is to be observed that the selected aging model deals most with oxidative aging, therefore mainly after short-term aging.

The parameter α_3, which accounts for the aging susceptibility of the relaxation time, was assumed to be zero ($\alpha_3 = 0$), as the magnitudes of the discrete relaxation spectra were obtained at exactly the same relaxation times, in such a way that they did not vary with respect to the aging state. As the elastic (E_∞) and the transient components (E_i's) magnitudes did vary with respect to the aging state (A), the ratios between aged and unaged magnitudes were used as indicators of the change in aging state. In addition, the aging susceptibility of the elastic and the transient relaxation modulus components magnitudes are given by α_1 and α_2, respectively.

Therefore, if the relaxation magnitudes are to be modeled using a combination of the unaged relaxation spectra and the aging model, the least squares method can be applied to minimize the error in the model prediction. This is done varying the values of the aging state variable ($A_{2,85°C}$, $A_{2,135°C}$ and $A_{45,85°C}$), and the elastic (E_∞) and transient components (E_i's) aging susceptibility, indicated by α_1 and α_2. The procedure was carried out using Excel Solver and the results were $\alpha_1 = 0.00$, $\alpha_2 = 1.19$, $A_{2,85°C} = 0.132$, $A_{2,135°C} = 0.264$, and $A_{45,85°C} = 0.364$. With the obtained aging state variable values, the aging model could be fitted by the determination of optimal $\Gamma^\alpha = 9.64 \times 10^{-7} \text{s}^{-1}$, $k_2 = 11.30$, and $k_3 = 5.28$. The summary of the results is presented in Table 3.

Table 3 – Results for the Fitted Aging Model to the Studied Mixture

Γ^α (1/s)	A_0 ( )	k_1 ( )	k_2 ( )	k_3 ( )	α_1 ( )	α_2 ( )	α_3 ( )	T_0 (ºC)
9.64×10^{-7}	0.00	0.15	11.30	5.28	0.00	1.19	0.00	21.1

Combining the aging model, whose parameters are presented in Table 3, with the linear viscoelastic model, whose parameters are presented in Table 2, one can represent all data of this work. Figure 22 presents the comparison between experimental storage and loss moduli results at the three investigated aging states, along with the corresponding fitting lines predicted by the combination of the viscoelastic Prony series and the aging model.

It can be seen that the aging model, combined with the unaged discrete relaxation spectrum, can fit stiffness experimental data for asphalt mixtures, at least for early ages (Figures 22a and 22b). However, when examining the experimental data of the most evolved aging state (Figure 22c), it is possible to identify that the aging model is underestimating the storage modulus for reduced frequencies below 10Hz, while it overestimates results for reduced frequencies above 10Hz. The reason is that the relaxation discrete spectra obtained in this work changed with aging in a more pronounced way for relaxation times above 10^{-1}s, i.e., exactly corresponding to the frequency of 10Hz. This can be better observed in Figure 23. In that figure, the ratio between aged and unaged transient modulus components (somewhat related to Equation 57) is plotted against their corresponding relaxation times. Those values were obtained using results from the linear viscoelastic fitting without coupling to aging.

2222222222222222

Figure 22 – Measured and Modeled (Prony series combined to aging model) Storage and Loss Moduli for (a) Age 2, 85ºC, (b) Age 2, 135ºC and (c) Age 45, 85ºC
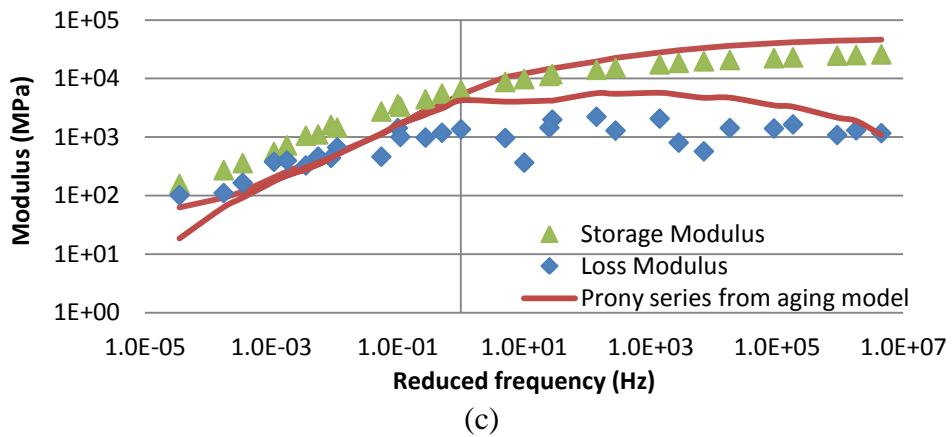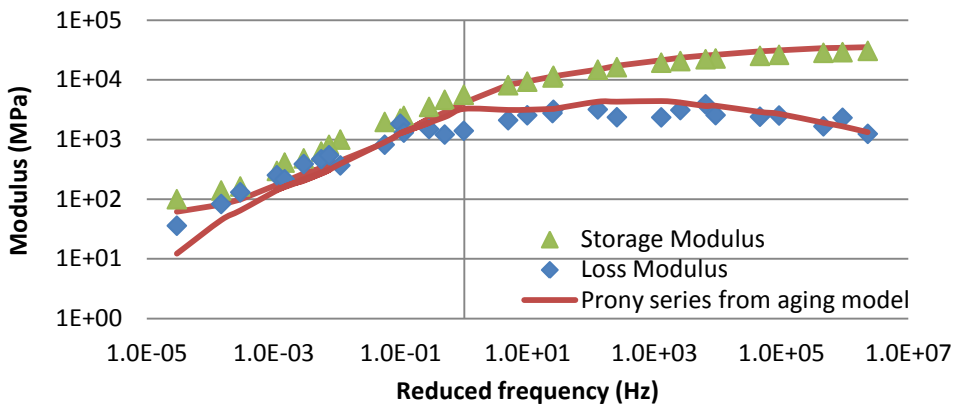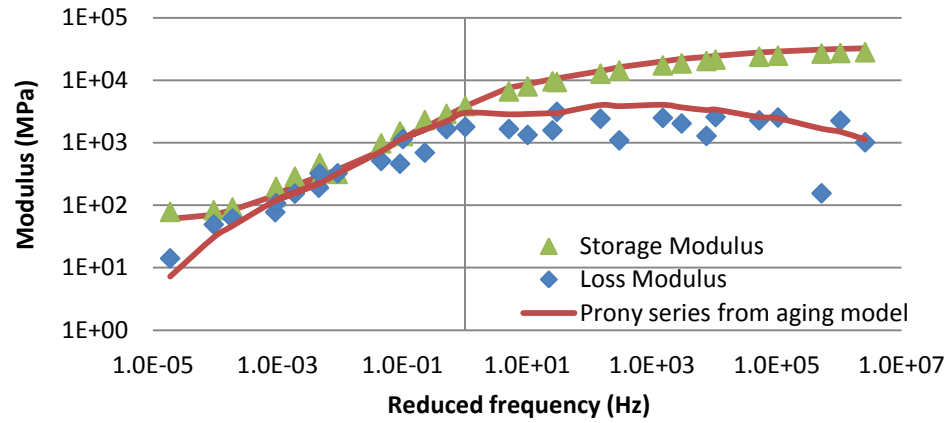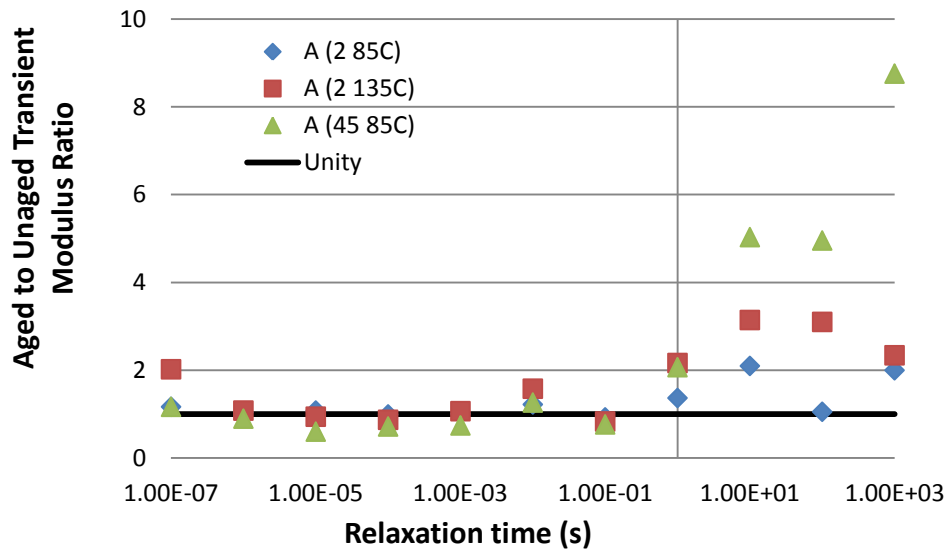
Figure 23 – Ratio between aged and unaged transient modulus components for each collocated relaxation time

Results presented in Figure 22c and complemented by Figure 23 suggest that a single value for α_2 is not sufficient to represent the dynamic modulus master curve variation induced by aging. As pointed out by Al-Rub et al. (2013), the model with only one value of α_2 for all transient modulus components corresponds mathematically to a vertical shift in the master curve of dynamic modulus. A mathematical demonstration can be found in the work by those authors.

However, experimental results from the present work lead to the conclusion that aging produces not only a vertical shift but also an inclination in the master curve. This inclination is due to the fact that transient modulus components associated to higher relaxation times suffer higher increase after aging than the transient modulus components associated to lower relaxation times. This should be expected, as it was already observed that the dynamic modulus master curve changes more with aging for low reduced frequencies, i.e., the part of the master curve more associated to the behavior of the binder, which is the component of the material that ages. As mentioned before, this is in agreement with results from the literature (Glover et al., 2008).

Al-Rub et al. (2013) used experimental data from Walubita (2006) (see Table 1) to fit the aging model for data covering up to 6 months of aging of compacted mixtures at 60ºC. Those authors evaluated two asphalt mixtures, obtaining Γ^α of 3.33×10^{-7} and $9.30 \times 10^{-7} \text{s}^{-1}$, i.e., the same order of magnitude found in the present work ($9.64 \times 10^{-7} \text{s}^{-1}$). Al-

Rub et al. (2013) stated that Γ^α can be used as an indicator of mixtures susceptibility to oxidative aging, with $1/\Gamma^\alpha$ being regarded as a "relaxation time" for aging. In this work, temperature dependency was captured, because data was generated using aging at two different temperatures. In addition, aging history dependency was captured.

4.2   Permanent Deformation Characterization

In this section, the results obtained from the unconfined repeated load permanent deformation tests are summarized. Measurements of axial deformation allowed the assessment of the total strain accumulated during the tests. Evaluation of strain evolution allows identifying the moment at which the secondary zone ends and the tertiary (shear flow) zone begins. This is done in an easy way by evaluating the rate of permanent deformation in each cycle. When this rate reaches a minimum, it is considered that the sample entered the shear flow zone, i.e., that number of cycles is considered to be the Flow Number (FN) of the tested mixture.

Figure 24 presents a comparison between results of the permanent deformation test for the three first aging states studied in this work, not yet considering aging at 45 days to facilitate the perception of the trends (overall information including the aging state 45, 85ºC is subsequently contained in Figure 25). Both total permanent deformation (%) (dashed lines) and rate of permanent deformation (µε/cycle) (continuous lines) are presented.

Figure 24 – Examples of Flow Number results for the three first aging states
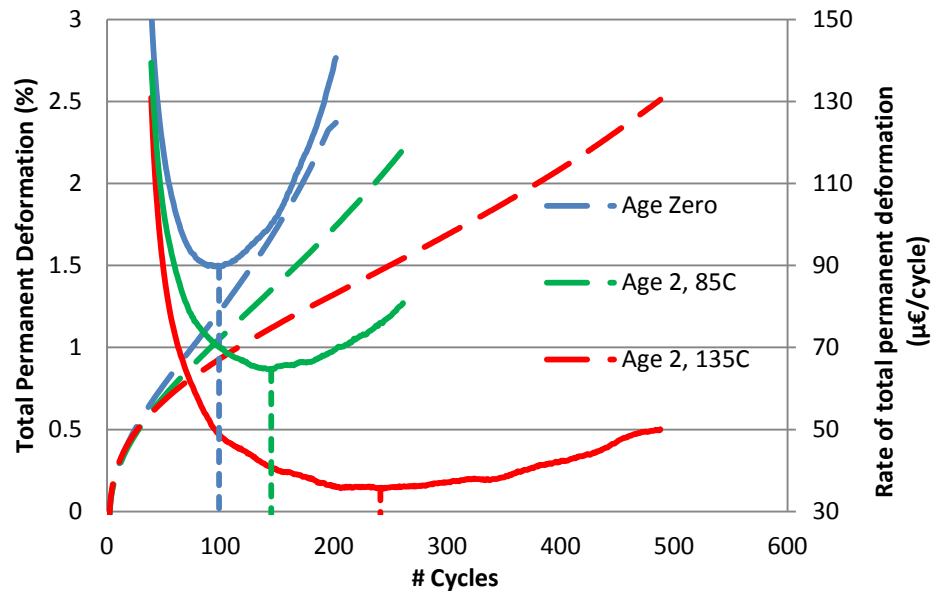
It can be seen from Figure 24 that as aging evolves, FN increases, which indicates that the resistance to permanent deformation increases with aging. It can also be noticed that the minimum rate of permanent deformation (slope of the secondary zone) decreases as aging evolves. This is in accordance with experience, which indicates that permanent deformation is a distress that shows up at early ages in asphalt mixtures if they are not well designed. As aging progresses the mixture becomes more resistant to permanent deformation. Another interesting aspect is that in the primary zone (accommodation of the mixture), the mixture at all aging states presented similar results. This indicates that this zone is much less affected by the change in binder properties associated to aging than the two other zones. These findings remain true when considering the aging state 45, 85ºC, as shown in Figure 25.

Figure 25 – Examples of Flow Number results including the 45, 85ºC aged mixture
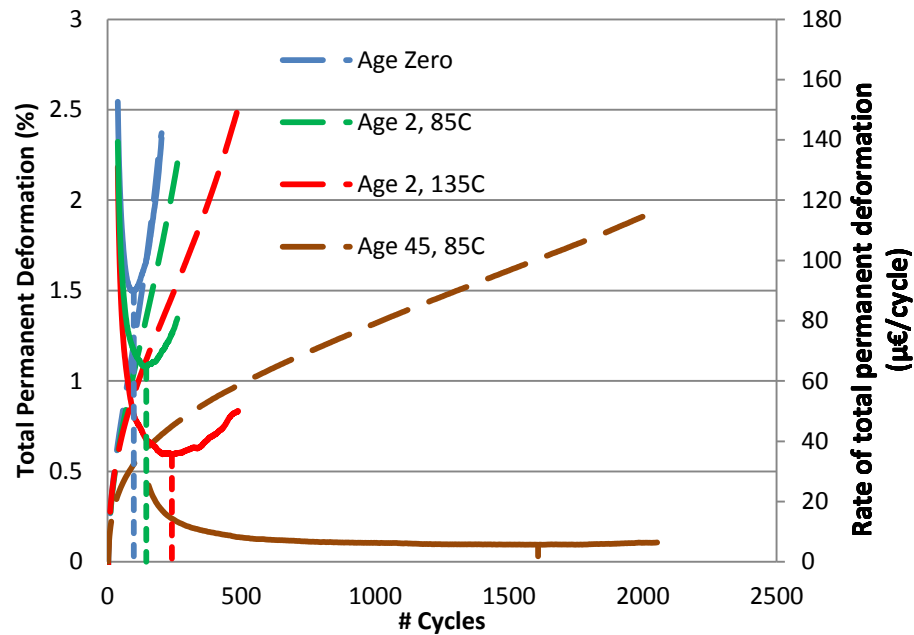
Mean and coefficient of variation results of the data from permanent deformation tests are summarized in Table 4: FN and slope of the secondary zone ($\min\frac{d\varepsilon_p}{dN}$) for all four investigated aging states.

Table 4 – Results for the Permanent Deformation Characterization

Results		Age Zero	Age 2, 85ºC	Age 2, 135ºC	Age 45, 85ºC
FN	Mean (#cycles)	110	144	258	1373
	CV (%)	21	18	21	30
$\min\frac{d\varepsilon_p}{dN}$	Mean (µε/cycle)	92	74	34	7
	CV (%)	23	28	34	44

The same comments made for Figures 24 and 25 hold when observing the results in Table 4. They confirm the expectation from the literature that as aging occurs mixture resistance to permanent deformation is significantly increased. It is to be observed the trend of an increase in the coefficient of variation of the results associated with more aged materials when compared to less aged materials. Furthermore, outliers from Age 2, 135ºC (two outliers) and Age 45, 85ºC (one outlier) were eliminated. Therefore, there are only four results considered for the former and five for the latter, instead of six results, as for the other two aging states. The results allow one to conclude that aging considerably changes viscoplasticity of asphalt mixture, increasing its resistance to permanent deformation. Flow number results

from the last aging state (45 days at 85ºC), for example, are more than 10 times greater in average than those for the unaged mixture.

4.3   Fatigue Characterization

In this section, fatigue results at the different aging states are described and compared. The S-VECD model is fitted to the results from the tension-compression cyclic tests performed with mixture samples at the four investigated aging states. The procedure used for the data processing was presented in sections 2.3.3 and 2.3.4. Individual sample results are presented in more detail in Appendix A. Only the fitted models are presented and compared herein. An example of S-VECD fitting obtained by the Petrobras Research Center (Cenpes) for a typical asphalt mixture used in Brazil is presented for comparison purposes. It consists in an asphalt concrete with nominal maximum aggregate size (NMAS) of 19mm, with 50/70 penetration grade asphalt binder, and it was represented in the legend as HMA 19mm 50/70.

Figure 26 presents the obtained damage characteristic curves, where the estimated values for the curve parameters are presented in the legend. The fitted lines for each mixture tested in this investigation were plotted until the respective mean value of the material integrity at failure was reached (these values are indicated in Table 5). For HMA 19mm 50/70, that information was not available. In Table 5, the values (mean and coefficient of variation) of material integrity (C_f) and damage accumulation (S_f) at failure for the different aging states are presented.

Figure 26 – Damage characteristic curves for the investigated aging states
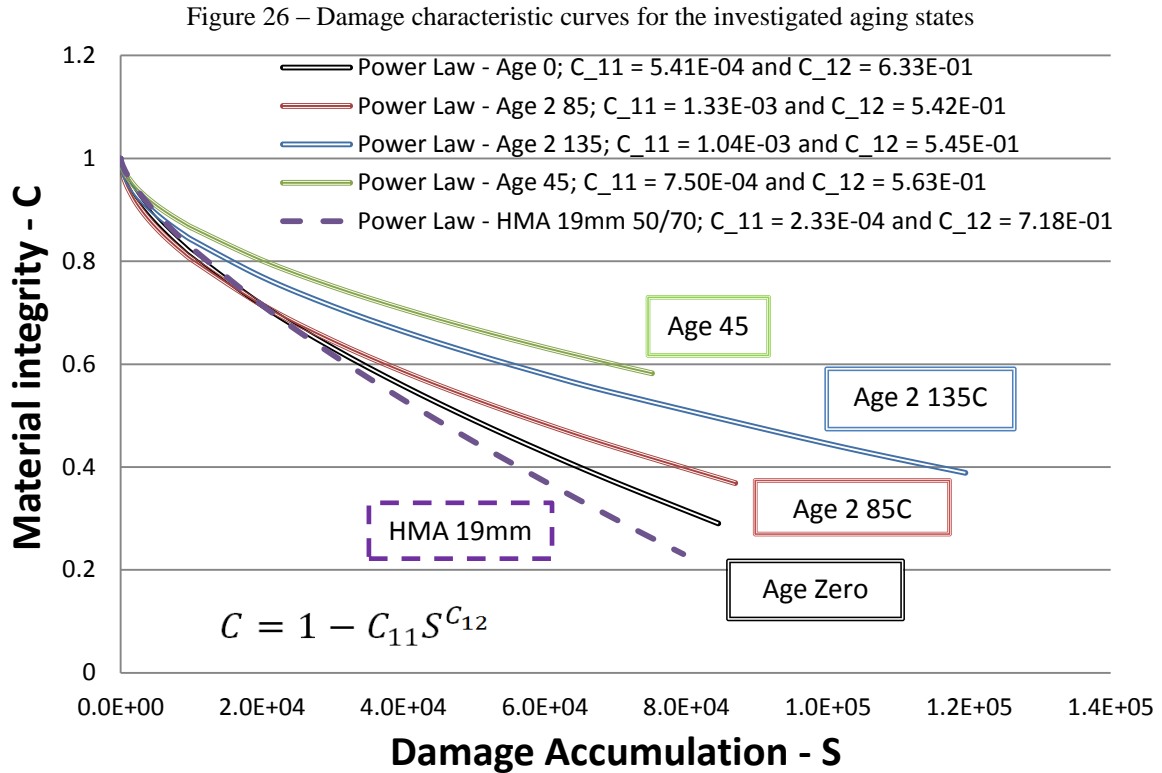
Table 5 – Mean and CV of material integrity (C_f) and damage accumulation (S_f) values at failure

	Age Zero	Age 2, 85ºC	Age 2, 135ºC	Age 45, 85ºC
Mean C_f	0.29	0.37	0.39	0.57
CV (%)	21	38	27	35
Mean S_f	100,897	100,387	122,072	83,249
CV (%)	21	42	33	72

Comparing the unaged damage characteristic curve obtained in this thesis with the curve obtained by the mixture tested at Cenpes, one may note that the mixtures present relatively similar results. This was expected because of the similarities between both mixtures, specifically binder classification (50/70 penetration grade), binder content (5.5% and 6.0%) and NMAS (12.5mm and 19mm).

The first clear trend with respect to aging observed from the results is that the damage characteristic curve tends to present higher values of material integrity (C) for the same values of damage accumulation (S). It is to be observed that, as all mixtures present different stiffness and damage curves, higher values of material integrity for a given value of damage accumulation do not mean more resistant materials. This will be confirmed later, with simulations of constant strain amplitude fatigue tests.

Another trend observed in Figure 26 and Table 5 is the increase in the material integrity at failure as aging progresses. This means that the material is failing for less evolved damaged conditions (with less damage tolerance), i.e., with lower loss in undamaged cross sectional area from the point of view of Lemaitre and Chaboche's (1990) damage variable (described in the Literature Review as $D = \frac{S_D}{S} = (1 - C)$). However, high coefficients of variation in measures of material integrity at failure were obtained for the aged states (between 27 and 38%), while the obtained variation was 21% for Age Zero.

Some issues should be mentioned in the tests performed. For one of the tests in Age Zero, one of the LVDT targets fell from the sample during the test, making it impossible to obtain mean LVDT displacements, because only three LVDT measurements were taken. When that happens using four LVDT measurements, opposed LVDT measurements can be eliminated in order to obtain the average LVDT displacement. For the place of coalescence of macrocraks in the tension-compression fatigue tests with unaged material, all nine tests presented failure within LVDT measurements. An analysis of the place of coalescence of cracks is found in Appendix B of this thesis. For the aged states, the main issue was related to variation between samples with respect to damage results. It was expected more variation for the test results, because one random process (aging in oven) was added to the preparation procedures. For Age 2, 85ºC, in the tests using the target initial strain amplitude (ISA) of 350μ, two of the three samples failed at their top. For the ISA of 500μ, one of the three tests was stopped because of a failure in the glue, i.e., the material did not actually fail. For Age 2, 135ºC, when testing at ISA of 500μ, one sample failed at the top and the other at the bottom. One sample was excluded from Age 45, 85ºC results, because it presented a damage curve almost equal to Age Zero results, and very different from the mean Age 45, 85ºC damage characteristic curve. Despite that variation with fatigue test results, the obtained Dynamic Modulus Ratios (DMR) was considered satisfactory: mean of 0.93 with coefficient of variation (CV) of 8.4% for Age Zero; 0.93 with CV of 7.3% for Age 2, 85ºC; 0.88 with CV of 7.3% for Age 2, 135ºC; and 0.91 with CV of 11% for Age 45, 85ºC.

Another important property which is an input for the damage characterization and for damage modeling is the damage parameter α, obtained from the linear viscoelastic material properties as presented in the Literature Review ($\alpha = 1 + 1/m$, where m denotes the maximum absolute log-log derivative of the relaxation modulus). It is obtained from the

Prony series fitted to the experimental storage modulus values for each aging state. Table 6 presents the results obtained for the aging states tested in this research.

Table 6 – Damage parameter α for the tested materials

	Age Zero	Age 2, 85ºC	Age 2, 135ºC	Age 45, 85ºC
α	2.993	3.089	3.101	3.126

It can be observed that, as aging progresses, the damage parameter increases. This occurs because the maximum absolute log-log derivative of the relaxation modulus decreases, i.e., the maximum relaxation rate of the material decreases due to aging. This was expected, because of the trend for stiffer and more elastic (lower phase angles) material previously observed in the linear viscoelastic characterization.

The last result for the damage characterization is the definition of the failure criteria as proposed by Sabouri and Kim (2014), and presented in the Literature Review. Although good agreement between the model proposed by Sabouri and Kim (2014) to relate energy dissipation and fatigue life showed very good agreement (R^2 higher than 0.93) for early ages, for the Age 45, 85ºC that agreement was less evident (R^2 equals to 0.82), probably because of the dispersion in results for all material properties. In addition, with the obtained results, no clear trend for the G_R vs N_f curve could be observed. Results are summarized in Figure 27.

Figure 27 – G_R vs N_f curves obtained in this work
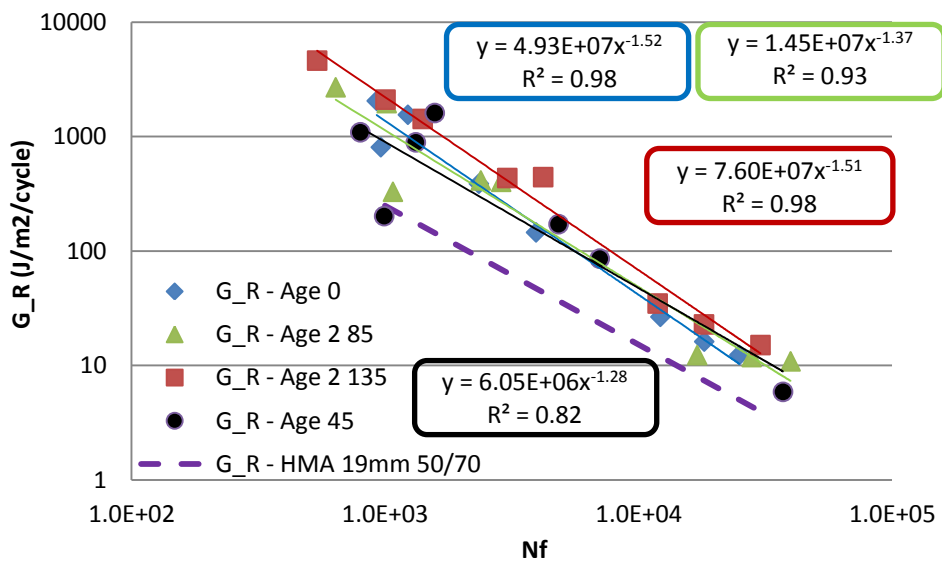
With the calibrated damage models, some simulations of fatigue behavior for the unaged and the aged states can be performed. This can be accomplished by using Equation 43 for constant strain amplitude solicitation and Equation 45 for constant stress amplitude solicitation. As an example, a comparison between the results for Age Zero and Age 45, 85°C considering constant strain amplitude solicitation is presented here. Simulation results were provided by Petrobras/Cenpes applying the procedure described by Nascimento et al., 2014 that considers the fatigue failure energy criterion proposed by Sabouri and Kim (2014) and evaluated in the present research.

Mixture behavior from both aging states was simulated at three different temperatures, in order to highlight the model capability of capturing temperature dependency of the fatigue behavior. As three different temperatures are simulated, results are obtained for three different values of dynamic modulus for each mixture. For each simulation, five different strain levels were selected, chosen to achieve 120,200, 60,200, 20,000, 5,000 and 1,000 loading cycles. Those strain levels were used in the plotted data in Figures 28 to 30. The obtained data relate the number of cycles to failure with the strain level and the dynamic modulus, making it possible to fit models for use in mechanistic-empirical design methods. The so-called transfer functions such as the one presented in Equation 60 can be fitted. That kind of equation is the most important one for the future application of the Brazilian mechanistic-empirical design method for asphalt pavements with respect to fatigue. The obtained parameters from the fitting for Age Zero and Age 45, 85°C are presented in Table 7.

$$N_f = K_1 . \left(\frac{1}{\varepsilon_t}\right)^{K_2} . |E^*|^{K_3} \tag{60}$$

Table 7 – Mechanistic-empirical model parameters obtained from fitting using simulations from S-VECD model

	Age Zero	Age 45, 85°C
K_1	2.95×10^{10}	1.50×10^{8}
K_2	4.44	6.25
K_3	-3.14	-3.66

Using the model results from Table 7, other simulation of Whöler curves for constant strain amplitude simulated tests at 15, 20 and 25°C are presented in Figures 28 to 30. They are analytically straight lines in log-log space (therefore $R^2 = 1$).

Figure 28 – Simulation of constant strain amplitude fatigue tests for Age Zero and Age 45, 85ºC at 15ºC
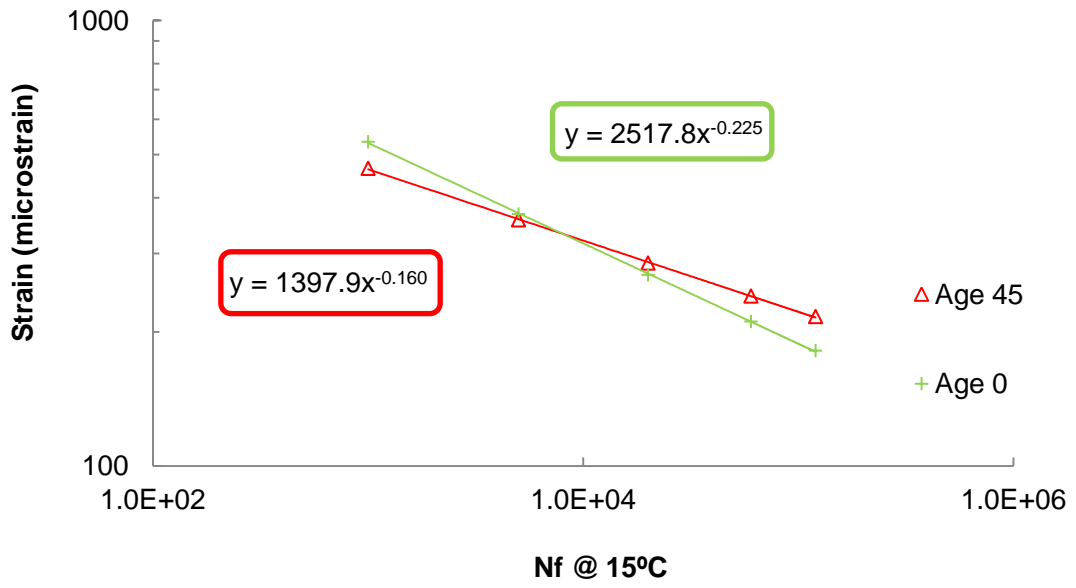

Figure 29 – Simulation of constant strain amplitude fatigue tests for Age Zero and Age 45, 85ºC at 20ºC
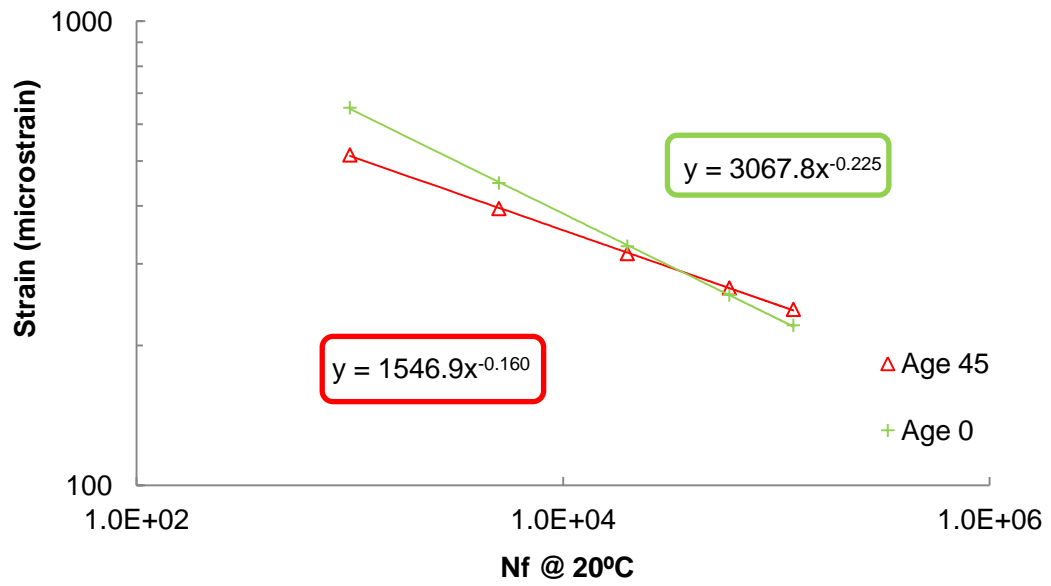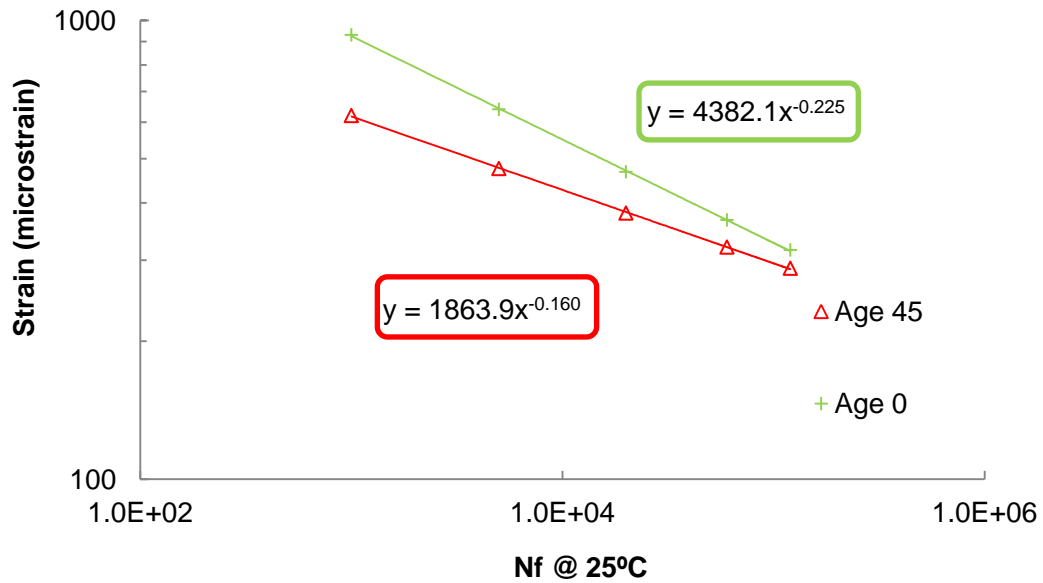
Figure 30 – Simulation of constant strain amplitude fatigue tests for Age Zero and Age 45, 85ºC at 25ºC

It can be inferred from manipulation of Equation 60 and observation of results in Figures 28 to 30 that the influence of temperature in fatigue behavior is accounted for by the stiffness term. The powers of the x-variable did not change for the different simulations, i.e., the slopes in the log-log space do not change with temperature, because they depend only on the value of $1/K_2$. It is actually the position of the Whöler curves in the y-axis that is changed by temperature, and this change is driven by dynamic modulus variation with temperature (from time-temperature superposition principle) and the model parameters K_2 and K_3 in Equation 60. It can be shown that the change in the position of the Whöler curves in the y-axis is driven by the factor $(K_3/K_2).\log|E^*|$.

For the results at 15ºC, within the simulated strain levels (from 210 to 470μ), unaged and aged mixture presented very similar results, with maximum difference between the predicted number of cycles to failure of approximately 30% at extension strain around 210μ, which is a relatively low difference for fatigue results. Most differences appeared at the temperature of 25ºC. At that temperature and within the simulated strain levels (from 316 to 620μ), the maximum difference between number of cycles to failure was approximately from 6,000 (for Age Zero) to 1000 (for Age 45, 85ºC) cycles, i.e., a reduction in more than 80% in the fatigue life, and occurred for strain levels of around 620μ. For strain levels around 320μ, the change was of approximately 120,000 to 60,000, representing a loss of 50% in fatigue life.

Although those mixture fatigue simulation results are indeed important to compare, one should not forget that the layers geometry (thicknesses) and stiffness play an important role for fatigue life of the mixture applied in the pavement. These characteristics, along with the stiffness of the asphaltic layer itself, drive the extension strain level at the bottom of the asphalt layers. So, depending on how the increase in stiffness due to aging induces a decrease in the strain level at the aged pavement, the difference in cycles can be less important.

Finally, for verification purposes, an example is presented comparing test result (exp.) and simulation (mod.) assuming the mean mixture damage parameters (damage characteristic curve - C *vs* S). Simulated results are obtained using the strain history (measured mean LVDT strain amplitude for each cycle obtained in the test) as input for the damage simulation. One of the samples results tested at a target initial strain amplitude of 350μ was used. The DMR value for that particular sample was 1.04. Results for the evolution of C for the loading cycles are presented in Figure 31 and the experimental result is presented in the same graph.

Figure 31 – Damage model verification (example with one of the tests for Age Zero)
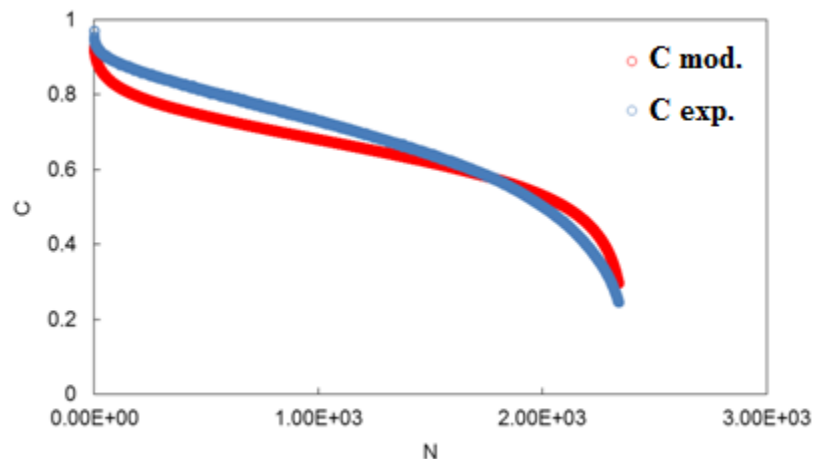
From Figure 31, it can be seen that the evolution of material integrity can be satisfactorily modeled using the damage model and the strain history as input. Using the same test results, it was investigated if the simulated failure criterion (G_R at failure) is compatible with the actually obtained failure criterion. The results are presented in Figure 32.

Figure 32 – Comparison between simulated each cycle and the experimental averaged released pseudo strain energy at failure
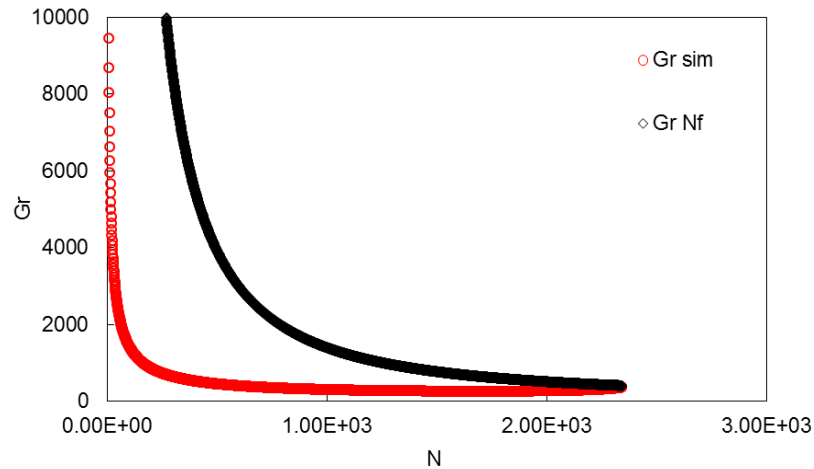

Figure 32 presents the simulated G_R curve (in red) and the mean G_R vs N_f curve obtained from regression of the experimental results (in black). The black curve is the same curve as the one in Figure 27 for Age Zero, but in natural scale, and therefore not a straight line as in the previous graph which is log-log. This experimental curve (black) represents somewhat of a limiting energy dissipated curve, similarly to what a yield surface represents in plasticity theory. Any simulated result below this limit curve means that the material has not yet failed. The simulated curve in Figure 32 (red) relates G_R and the actual number of cycles in the simulated test. The results in this figure are a verification of the model proposed by Sabouri and Kim (2014) for the combined phase angle drop and energy failure criteria. When the red curve touches the black curve, this is an indication that sample has failed. Actually, it is to be noticed that the black curve is obtained by curve fitting of failure points from different experimental red curves. It can be observed that, when considering the simulated red curve and the curve fitted G_R vs N_f curve for the studied material, the curves cross approximately at the estimated averaged released pseudo strain energy and number of cycles to failure. The example presented in Figure 32 is from Age Zero, at the target initial strain amplitude of 350μ. That sample failed at 2,342 cycles, with $G_R = 387.4$ at failure.

4.4   Conventional Characterization Results

Conventional asphalt mixture mechanical characterization in Brazil consists of tensile strength (TS), resilient modulus (RM) and controlled force indirect tensile fatigue tests. In the present research, three Marshall samples were tested for TS and RM, while nine

were tested for fatigue, all tests conducted at 25ºC. RM tests were performed using a load of 0.05MPa (approximately corresponding to 5% of the tensile strength of the material). Usually, a percentage of the TS is used (10% for example), but as the same samples were used for both tests, and TS is a destructive test, a load was guessed, targeting 5% of the TS for the unaged mixture. For the fatigue results, Whöler curves were constructed. Full characterization is presented for Age Zero and Age 2, 85ºC. For Age 2, 135ºC, only TS and RM are available. Results are summarized in Table 8, except for fatigue, which is presented subsequently. It is acknowledged the fact that three samples do not allow a proper statistical representation of the CV. Nevertheless, the number of samples tested in this thesis is typical in Brazil, and the CV value is included as a first approximation of the variation in the conventional tests performed. Lopes (2012) provided a thorough study on testing variability with asphalt mixtures in Ceará and how it compares to other states in the Northeast region of Brazil.

Table 8 – Results for mean and coefficient of variation of TS and RM at three different aging states

	Age Zero		Age 2, 85ºC		Age 2, 135ºC	
	TS (MPa)	RM (MPa)	TS (MPa)	RM (MPa)	TS (MPa)	RM (MPa)
Mean	1.21	3,570	1.04	3,789	1.60	5,215
CV (%)	3	4	5	23	27	31

Results from Table 8 present the general trend of increase in RM with aging, which was already expected. Also, the variation of test results for the aging states considerably increased. This was also expected as an additional procedure (aging) is included, and this may very well impact variability. The unexpected result was the TS for Age 2, 85ºC. As only three samples are tested, randomness can have led to results of TS lower for this aging state than for Age Zero. However, the expectation that tensile strength grows with aging is more clear when comparing results from Age 2, 135ºC and Age Zero. With respect to these results, it needs to be observed that conclusions drawn from them are only valid for the very specific observed loading conditions. Due to the viscoelastic properties of asphalt mixtures, it is not possible to reliably use those observations to estimate behavior under different loading conditions. Next, in Figure 33, the Whöler curves for failure as obtained for the controlled force indirect tensile fatigue tests for Age Zero and Age 2, 85ºC are presented and compared.

Figure 33 – Whöler curves for failure as obtained for the controlled force indirect tensile fatigue tests for Age Zero and Age 2, 85°C
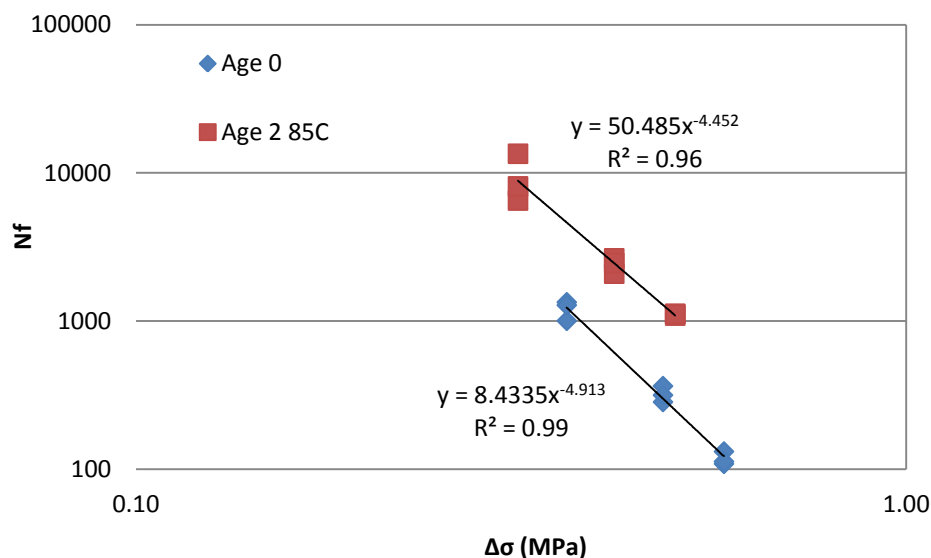
From that figure, one could infer that aged mixtures behave much better than unaged mixture ($\log N_f$ for Age 2, 85°C approximately 0.8 greater than $\log N_f$ for Age Zero, which is the earlier aged state studied in this research). This means that, depending on loading conditions, the number of cycles to failure for the aged mixture can be approximately six times greater than for Age Zero. In addition, Age 2, 85°C is the earlier aged state studied in this work.

That kind of conclusion can be caused by many factors, such as the use of controlled force mode. The only controlled variable in this mode is the value of the stress at the beginning of the test (when none or very low damage has occurred). When damage occurs, after some loading cycles, the same force used in the beginning to produce a certain strain leads to higher strain levels and higher effective stresses, because the undamaged cross sectional area is lower after the damage, and consequently apparent stiffness is also decreased. This happens even faster as damage evolves, until the material fails. As this can be strongly affected by initial material stiffness, samples tested at the same controlled force can actually face solicitation of completely different loading paths. For stiffer mixtures (as the aged mixture) and the same applied force, lower values of initial strain amplitude are applied and the test tends to require more cycle repetitions to cause failure.

A second reason is that, when the material fails, it is impossible to know if it failed because of fatigue or because of accumulation of creep flow. As the force is always

applied in the same direction, deformation accumulates, because the material is viscoelastic and flows. When high strains are accumulated, damage evolves. Consequently, a part of the damage in the sample is accumulated from cyclic solicitation and the other from creep. So, the number of cycles to failure obtained from this test is not for fatigue failure only. In addition, as material ages, it was shown in this thesis that it becomes more elastic (lower phase angle) above frequencies of the order of 10^{-2}Hz. This means that for almost all practical (in field) frequencies of load application the mixture tends to be more elastic after aging. So, the aged materials will flow more slowly than unaged materials. This can partially explain the trends of overestimating fatigue life for aged materials using controlled force indirect tensile tests.

From the presented results, it is already possible to observe how controlled force indirect tensile fatigue tests may lead to the clear conclusion that aged mixtures perform much better than unaged mixtures. It is to be noticed that such conclusion not only is temerarious when it comes to pavement analysis, but also it is not in agreement with mechanistic based characterization results and simulation presented before.

4.5   Mechanical Models with Coupled Aging Results

Using the value of the aging state variable obtained by optimization for the tested aging states, and the fitting of the aging model, it should be possible to explain variations in the viscoplastic and in the fatigue behavior of the mixture due to aging. This section presents some attempts to couple dynamic creep (FN and $\min\frac{d\varepsilon_p}{dN}$) and fatigue results.

Firstly, evolution laws analogous to Equations 59 used for linear viscoelastic parameters were tried for fitting dynamic creep results (FN and $\min\frac{d\varepsilon_p}{dN}$). The referred equations did not provide a good fit for the permanent deformation parameters. It was noticed that the power associated to $(1 - A)$ to predict the viscoplastic response was dependent on the very value of the aging state variable. Equations of the form $(Viscoplastic\ parameter)_{Aged} = (1 - A)^{-\alpha.A}.(Viscoplastic\ parameter)_{Unaged}$ were then tried and the results obtained were considered satisfactory. In the proposed evolution law for viscoplastic parameters, α represents the aging susceptibility of the evaluated parameter (FN or $\min\frac{d\varepsilon_p}{dN}$) with respect to aging. Fitting results (comparison between experimental and modeled results) are presented in Figures 34a and 34b.

Figure 34 – Flow Number (a) and (b) Minimum Strain Rate coupled to the aging model
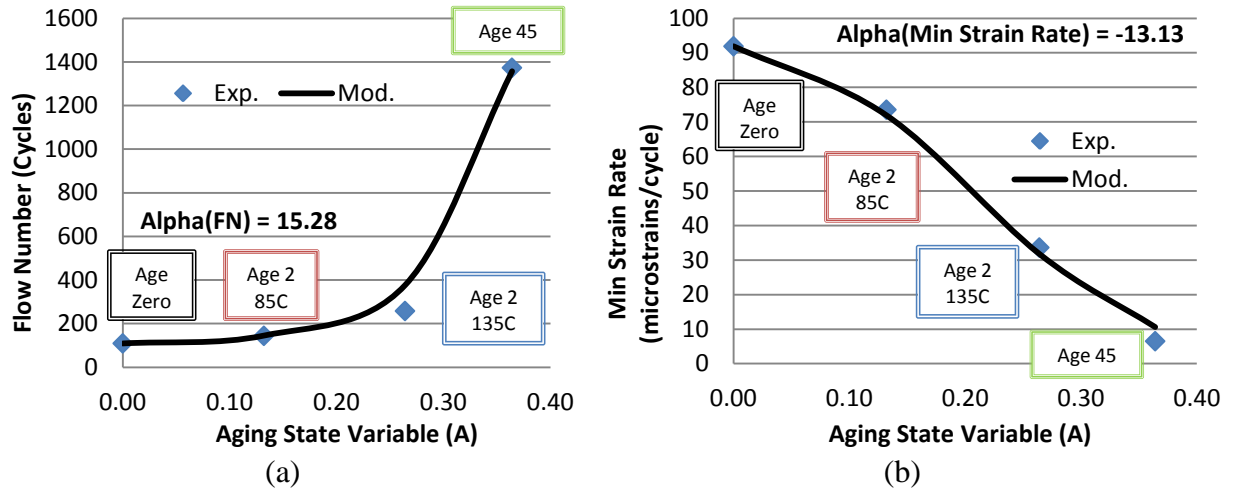
Those results show that resistance to permanent deformation grows very rapidly with the aging state of the material. The Flow Number of the mixture increases while the minimum strain rate decreases. Those results were expected, as it is commonly accepted that resistance to permanent deformation increases with aging, partly because the mixture becomes stiffer.

For the fatigue tests, it was more difficult to identify clear trends in the results with respect to the model parameters (C *vs* S Power law curve parameters C_{11} and C_{12} and G_R *vs* N_f log-log slope and intercept parameters). Figure 35 presents the relation between C_{11} and the value of the aging state variable. Figure 36 presents the relation between C_{12} and the value of the aging state variable. Figure 37 presents the relation between log-log slope of G_R *vs* N_f and the value of the aging state variable. Finally, Figure 38 presents the relation between log-log intercept of G_R *vs* N_f and the value of the aging state variable

Figure 35 – Obtained relation between C_{11} and the value of the aging state variable
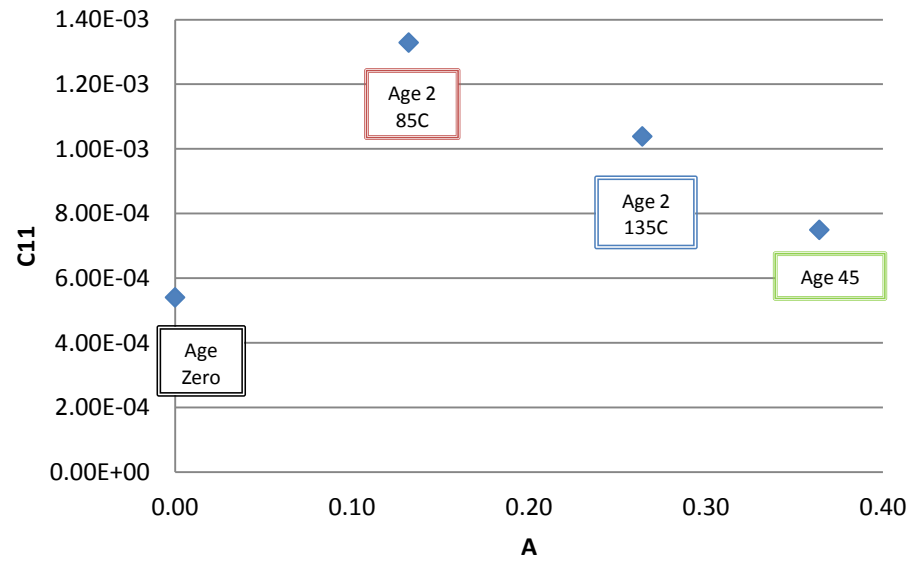
Figure 36 – Obtained relation between C_{12} and the value of the aging state variable
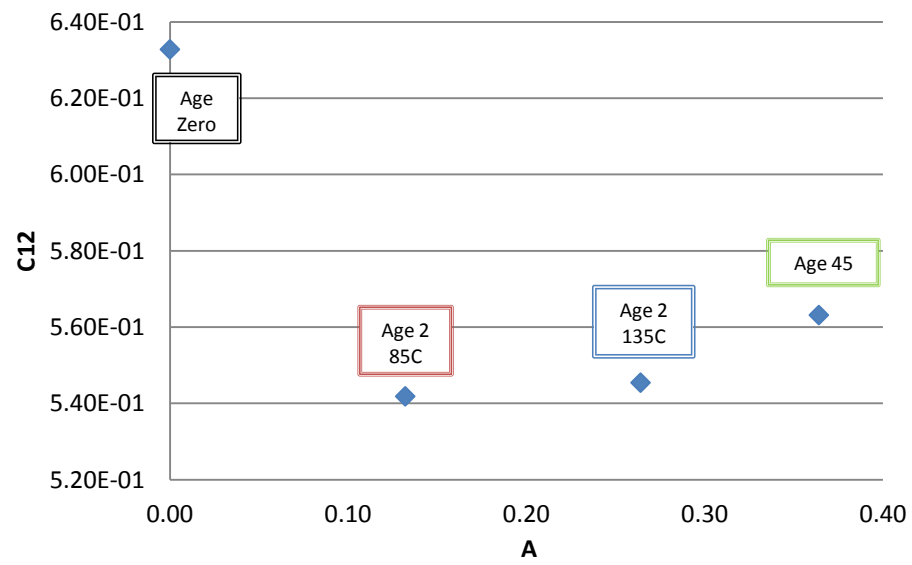
Figure 37 – Obtained relation between log-log slope of G_R vs N_f and the value of the aging state variable
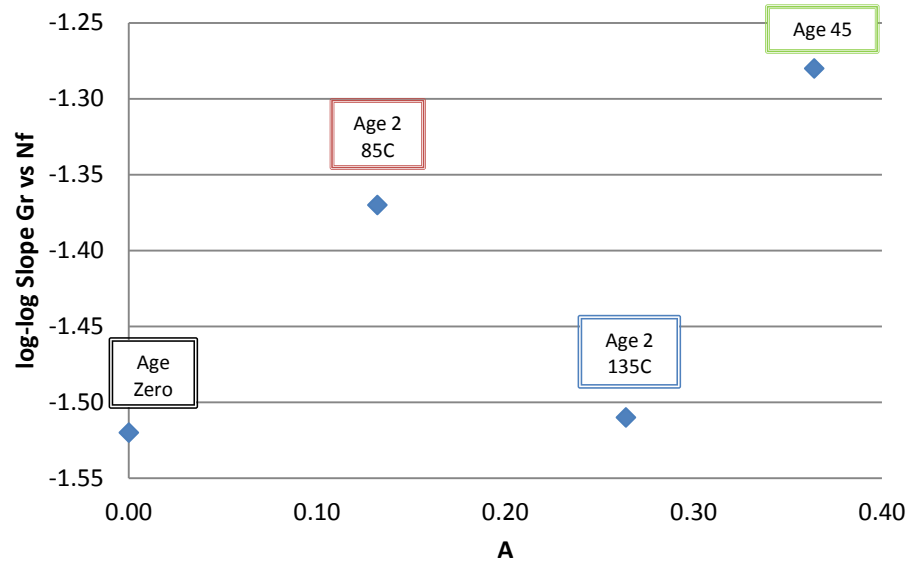
Figure 38 – Obtained relation between log-log intercept of G_R vs N_f and the value of the aging state variable
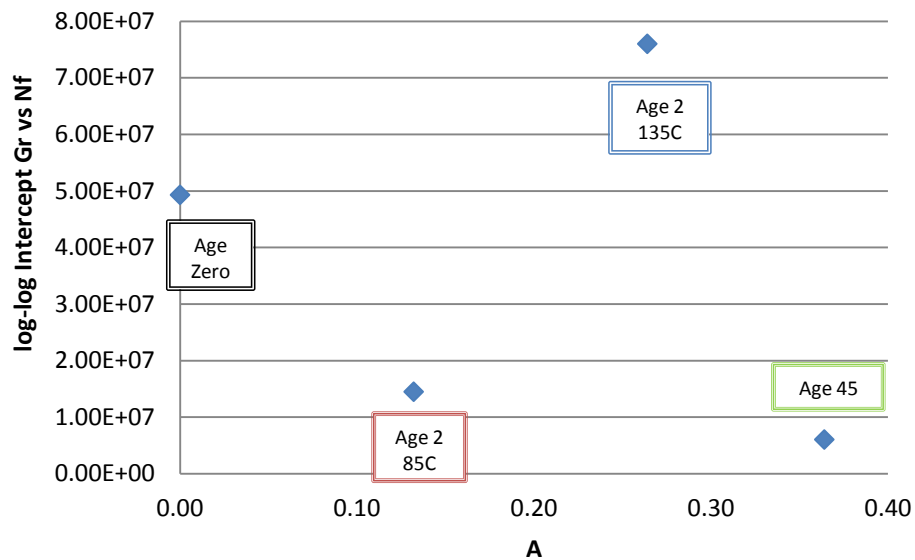

The presented fatigue experimental data showed how the damage characteristic curve changes with aging (increase in the values of material integrity for the same values of damage accumulation). However, it was not possible to obtain a clear trend of the damage characteristic curve parameters, probably because of the use of two parameters to represent the damage curve (C_{11} and C_{12}). One part of the effect of aging is showing in a parameter and the other part in another parameter, and this may have blurred the observation of a clear trend for those parameters with respect to aging. It is, however, possible to state that the damage characteristic curves present a clear trend of having higher values of material integrity for the same values of damage accumulation as damage accumulates. This could mislead to the

conclusion that the material is more resistant, as it has more material integrity, but, actually, it needs to be observed that the damage accumulation will evolve differently (and faster) in the aged material, because of the changes in the damage characteristic curve and because the material is stiffer in the aging state. In addition, the values of material integrity at failure were lower as the aging state has grown, i.e., the material is actually less damage tolerant. This also contributes for a decrease in the fatigue life of the material. However, in a pavement structure, the fact that the material is stiffened can cause sufficient decrease in the strains to which the material is subjected. This decrease may be such that fatigue life is not compromised because of aging. This will depend on layers geometry (thicknesses) and on the aging impact on material properties.

4.6   Simulation of Mixture Behavior

This section presents some simulations of stiffness changes with growing aging, adopting the fitted aging model coupled to the linear viscoelastic models. In the simulations, the percent change in the Dynamic Modulus is presented as time passes during aging at a constant temperature. From Equation 57, the change in a stiffness constant can be calculated as $\frac{(E_i)_A - E_i}{E_i} = (1 - A)^{-\alpha_2} - 1$. As α_2 was considered to be the same regardless of the relaxation time, that equation represents the overall mean change in the elastic constants. Neglecting the contribution of the change in the long-term modulus, which presents a lower order of magnitude when compared to some of the other stiffness constants, the proposed equation represents the mean change (vertical shift) in the dynamic modulus master curve. Different aging temperatures were evaluated, from 40 to 150°C. Results are summarized in Figure 39.

Figure 39 – Aging Simulation at Constant Aging Temperatures: 40, 60, 85, 135, 150ºC
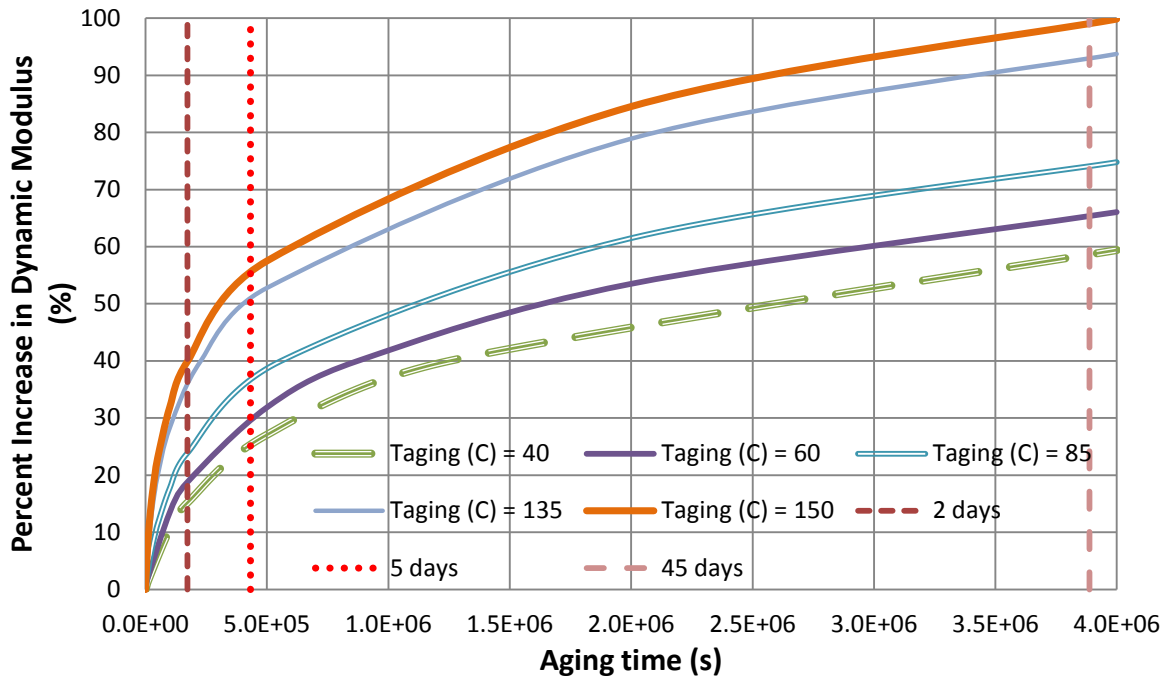
It can be seen that the fitted model predicts that a 40% increase in $|E^*|$ occurs at approximately 1.25×10^6, 8.74×10^5, 5.58×10^5, 2.27×10^5 and 1.74×10^5s, for 40, 60, 85, 135 and 150°C, respectively. This corresponds to the following aging times, in days: 14.5, 10.1, 6.5, 2.6 and 2.0 days. For a given aging time, for example, 2 days, the predicted percent increases in $|E^*|$ are approximately 15, 19, 24, 27 and 36%. In other words, it can be said that, based on some observations of the consequences of aging (change in moduli master curves in the case of this work) at few aging states, a phenomenological aging model based on an internal state variable can associate aging time and aging temperature. The aging model predicts the value of the aging internal state variable (A) and it is then coupled to the aging consequences using the susceptibility parameters (α_i's). This gives the aging model the ability to predict the evolution of the mechanical properties, such as the Storage and the Loss Moduli, of asphalt mixtures.

5   **CONCLUSIONS AND RECOMMENDATIONS FOR FUTURE WORK**

This work uses an existing aging phenomenological model to explain changes in HMA mechanical properties due to aging. The referred aging model utilizes an internal state variable and four material parameters. A developed aging experimental procedure inspired by a RILEM protocol is presented as part of a broader research effort under development in Brazil related to the country's new mechanistic-empirical pavement design method to be launched in 2016. The used procedure consisted of maintaining loose mixture in oven at a controlled temperature (85ºC and 135ºC) for determined aging periods (Zero, 2 and 45 days). Different aging temperatures allowed to identify the mixture aging sensitivity with respect to aging temperature, which constitutes a contribution with respect to the results originally presented by Al-Rub et al. (2013), in which aging temperature dependency was not evaluated.

Concerning the aging model fitted in this work, the material constants were obtained by minimizing square errors of the model compared to dynamic modulus experimental results at different aging states. A well-established procedure was used to fit the curves (Prony series) directly to experimental results (linear viscoelastic model), without pre-smoothing the data. The same relaxation times (ρ_i) were used for fitting all storage moduli (E') - aged an unaged mixtures - varying only the stiffness coefficients (E_i's). Combining the aging and the linear viscoelastic models, storage and loss moduli results at two different aging states were satisfactorily predicted. However, a single value for the aging susceptibility parameter for the relaxation moduli, independent of the associated relaxation times appears to be insufficient, because dynamic modulus master curve is not only vertically shifted but also reclined after aging. That observation was interpreted using the relaxation discrete spectra obtained at different aging states.

A simulation of the change in dynamic modulus with time (aging) was performed to show the potential of the coupled modeling approach. Although the inclination of the dynamic modulus master curve is not being represented using the model as it was fitted in this work, the simulation of dynamic modulus change appears to be reasonable with respect to the experimental results for aging at 85 and 135ºC. However, further work is necessary to obtain a model fitted to results from aging at higher temperatures (i.e., aging results obtained in lower laboratory aging periods) capable of realistically representing aging at moderate temperatures. In other words, further work in lower rate aging laboratory procedures should

be done, in order to verify whether modeling results obtained from aging experiments at 85 and 135ºC may realistically represent the results for aging at moderate temperatures. For example, it would be interesting to observe if the aging model calibrated for results of aging at 85ºC and 135ºC would predict results of aging for lower temperatures (40ºC and 60ºC for example).

It is possible to state that aging considerably increases HMA resistance to permanent deformation. Data presented in this work and results from the attempt to couple aging to viscoplasticity pointed that Flow Number increased as a power of the aging state, using $(Viscoplastic\ parameter)_{Aged} = (1 - A)^{-\alpha.A}.(Viscoplastic\ parameter)_{Unaged}$.

The presented fatigue experimental data showed how the damage characteristic curve changes with aging. It was possible to observe a clear trend for the damage characteristic curves of having higher values of material integrity for the same values of damage accumulation as damage accumulates. The same had been observed by Baek et al. (2012). That could mislead to the conclusion that a more resistant material was obtained after aging, as it presented a higher material integrity. However, it needs to be observed that the damage accumulation will evolve differently (and faster) in the aged material, because of the changes in the damage characteristic curve and because the material is stiffer in the aged state. In addition, the values of material integrity at failure were higher as aging evolved, i.e., aging produced less damage tolerant materials. This contributes for a decrease in the fatigue life of the material. Unfortunately, when it comes to the coupling between the damage model and the aging model, it was not possible to obtain a clear trend of the damage characteristic curve parameters (C_{11} and C_{12}) with aging. That made it difficult to mathematically couple aging to damage in this work.

It can then be concluded that aging does not necessarily affect negatively fatigue life in asphalt pavements, while certainly increasing its resistance to permanent deformation. The only way of accessing information about how pavement behavior changes with aging is conducting experiments as proposed in this research, coupling aging to the mechanical behavior of the asphalt mixtures, preferring to use mechanistic-based models that allow simulation of the pavement structure.

For the fatigue characterization in Brazil, from a modeling point of view, it is necessary to progressively change from the controlled force indirect tensile fatigue test, which does not necessarily lead to failure of samples due to fatigue only (it may be a creep failure combined to fatigue), towards more mechanistic characterization procedures. The way the test is performed, mean (with respect to time) force applied to the sample during the test is different from zero, i.e., the material is flowing in a creep like loading during the test. Results from the state-of-the-practice test can mislead the judgment of analysts and therefore produce false conclusions for fatigue simulations. This can be one of the reasons that lead laboratory-to-field factor of the order of 10^4 observed in Brazil using controlled force indirect tensile fatigue tests.

When aged mixtures are evaluated, as in this work, the referred tests can lead to the conclusion that pavement behaves, with respect to fatigue life, more than six times better after some aging, depending on the layer thicknesses. On the other hand, as a more mechanistic procedure for analysis of fatigue behavior is adopted, less difference is observed between results from aged and unaged mixtures. Actually, the consequence of aging can be either positive or negative depending on loading conditions, layers geometry and mixture properties. However, in this study mainly effects of isolated aging were studied. Properties linked to the adhesion and cohesion of mixture and how those properties change in the presence of water may be more affected by aging in a negative way than isolated aging as studied in this thesis. It is possible that aging affects more directly the interaction between aggregates, binder and water, significantly changing the material mechanical behavior.

Several recommendations for future research can be made after the work performed for this thesis, as listed below:

- To identify possible relations between the aging state variable and chemical properties of the binders recovered from the aged mixtures. This can lead to the identification of the chemical meaning of the aging variable;
- To include other mixtures in the analysis, with different binder content and type, aggregate source and distribution, in order to identify how aging model parameters relate to mixture constituents;

- To initiate the construction of a database for mechanistic fatigue characterization of asphalt mixtures. That was already started by the Petrobras Research Center (Cenpes), but the universities and research centers in Brazil still do not have testing and analysis procedures for tension-compression fatigue characterization using viscoelastic continuum damage mechanics models (this thesis is a start for LMP/UFC). Having that database together with information from field performance is key for changing towards mechanistic procedures for asphalt mixtures characterization in the future;

- To investigate how cohesion, adhesion and moisture damage resistance properties of mixtures change after aging. A key to understand how aging may negatively affect mixture behavior relies on those properties changes.

It is expected that this thesis has contributed to the Brazilian scenario of HMA characterization procedures, especially for fatigue. Also, contributions for aging modeling were proposed to the research community.

REFERENCES

Alavi, M. Z.; Hajj, E. Y.; Morian, N. E. (2013) **Approach for quantifying the effect of binder oxidative aging on the viscoelastic properties of asphalt mixtures**. Transportation Research Record: Journal of the Transportation Research Board, No. 2373, Transportation Research Board of the National Academies, Washington, D.C., 2013, pp. 109–120.

Al-Rub, R. K. A.; Darabi, M. K. (2012) **A thermodynamic framework for constitutive modeling of time- and rate-dependent materials. Part I: Theory**. International Journal of Plasticity. Vol. 34, pp. 61-92.

Al-Rub, R. K. A.; Darabi, M. K.; Kim, S-M.; Little, D. N.; Glover, C. J. (2013) **Mechanistic-based constitutive modeling of oxidative aging in aging-susceptible materials and its effect on the damage potential of asphalt concrete**. Construction and Building Materials. 41, pp. 439–454.

AASHTO R 30 (2002) **Standard practice for mixture conditioning of hot mix asphalt (HMA)**. American Association of State Highway and Transportation Officials, Washington, D.C.

AASHTO PP2 (1994) **Standard practice for short and long term aging of hot mix asphalt**, AASHTO Provisional standards. American Association of State Highway and Transportation Officials. Washington, D.C.

AASHTO TP 31 (1994) **Standard test method for determination of the resilient modulus of bituminous mixtures by indirect tension**. American Association of State Highway and Transportation Officials, Washington, D.C.

AASHTO TP 62-03 (2005) **Standard method of test for determining dynamic modulus of hot mix asphalt (HMA)**, American Association of State Highway and Transportation Officials, Washington, D.C.

AASHTO T 342 (2011) **Standard method of test for determining dynamic modulus of hot-mix asphalt concrete mixtures**, American Association of State Highway and Transportation Officials, Washington, D.C.

AASHTO TP 107 (2014) **Determining the damage characteristic curve of asphalt concrete from direct tension cyclic fatigue tests**. Provisional standard. American Association of State Highway and Transportation Officials, Washington, D.C.

AASHTO T-321-03 (2003). **Determining the fatigue life of compacted hot-mix asphalt (HMA) subjected to repeated flexural bending**. American Association of State Highway and Transportation Officials, Washington, D.C.

ABNT NBR 16018:2011 (2011) **Misturas asfálticas – Determinação da rigidez por compressão diametral sob carga repetida**. Associação Brasileira de Normas Técnicas. Rio de Janeiro.

ASTM D3497-79 (2003) **Standard test method for dynamic modulus of asphalt mixtures**. American Society for Testing and Materials.

Babadopulos, L. F. A. L.; Bodin, D.; Chailleux, E.; Dreessen, S. (2010) **Prony series fitting method to creep experimental data with different numbers of elements**. XXIV Congresso da Associação Nacional de Ensino e Pesquisa em Transportes (ANPET). Salvador, Bahia, Brazil.

Babadopulos, L. F. A. L. (2013) **Avaliação do modelo viscoelástico linear aplicado a misturas asfálticas utilizadas em revestimentos de pavimentos no brasil**. Projeto de Graduação. Curso de Engenharia Civil da Universidade Federal do Ceará. Fortaleza. In Portuguese.

Babadopulos, L. F. A. L.; Soares, J. B.; Castelo Branco, V. T. F. (2014) **Aging and constitutive modeling of asphalt mixtures: research developments in Brazil**.

Conference of the International Society for Asphalt Pavements (ISAP). Raleigh, North Carolina, USA.

Baek, C.; Underwood, B. S.; Kim, Y. R. (2012) **Effects of oxidative aging on asphalt mixture properties**. Transportation Research Record: Journal of the Transportation Research Board, No. 2296, Transportation Research Board of the National Academies, Washington, D.C., pp. 77–85.

Bari, J; Witczak, M. W. (2006) **Development of a new revised version of the Witczak E* Predictive Model for hot mix asphalt mixtures**. Journal of Asphalt Paving Technologists, Proceedings of the Annual Meeting, Association of Asphalt Paving Technologists, Vol. 75, pp. 381-424.

Boltzmann, L. (1874) **Zur theorie der elastischen nachwirkung**. Pogg. Ann. Physik, Vol. 70, pp. 275-306.

Borges, R. L. (2014) **Utilização do shift model para análise viscoplástica de deformação permanente em misturas asfálticas**. M.Sc. Thesis, Programa de Pós-Graduação em Engenharia de Transportes, Centro de Tecnologia, Universidade Federal do Ceará, Fortaleza, Brazil. In Portuguese.

Chehab, G. R. (2002) **Characterization of asphalt concrete in tension using a viscoelastoplastic model**. PhD Thesis, North Carolina State University, Raleigh, North Carolina, USA.

Choi, Y-T.; Subramanian, V.; Guddati, M. N.; Kim, Y. R. (2012) **Incremental model for prediction of permanent deformation of asphalt concrete in compression**. Vol. 2296 Asphalt Materials and Mixtures 2012, Vol. 4, pp. 24-35.

Choi, Y-T (2013) **Development of a mechanistic prediction model and test protocol for the permanent deformation of asphalt concrete**. Ph.D. Dissertation. North Carolina State University.

Christensen, R. M. (1982) **Theory of viscoelasticity** (2ª ed.). Academic Press, New York.

Christensen Jr., D. W.; Pellinen, T.; Bonaquist, R. F. (2003) **Hirsch model for estimating the modulus of asphalt concrete**. Journal of Asphalt Paving Technologists, Proceedings of the Annual Meeting, Association of Asphalt Paving Technologists, Vol. 72, pp. 97-121.

Coutinho, R. P.; Babadopulos, L. F. A. L.; Freire, R. A.; Castelo Branco, V. T. F.; Soares, J. B. (2014) **The use of stress sweep tests for asphalt mixtures nonlinear viscoelastic and fatigue damage responses identification**. Materials and Structures. Vol. 47 (5), pp. 895-909.

Clyne, T. R.; Li, X.; Marasteanu, M. O.; and Skok, E. L. (2003) **Dynamic and resilient modulus of MN/DOT asphalt mixtures**. MN/RC-2003-09. Minnesota Department of Transportation, Minneapolis.

Daniel, J. S.; Kim, Y. R.; J. Lee (1998) **Effects of aging on viscoelastic properties of asphalt-aggregate mixtures**. Transportation Research Record, Nº 1630, pp. 21-27.

Daniel, J. S.; Kim, Y. R. (2002) **Development of a simplified fatigue test and analysis procedure using a viscoelastic, continuum damage model**. J. Assn. Asphalt Paving Technologists, Vol. 71, pp. 619-650.

Darabi, M. K. (2011) **Thermo-viscoelastic-viscoplastic-viscodamage-healing modeling of bituminous materials: theory and computation**. Ph.D. Dissertation. Texas A&M University, College Station, Texas.

Darabi, M. K.; Al-Rub, R. K. A.; Masad, E. A.; Huang, C-W; Little, D. N. (2011) **A thermo-viscoelastic–viscoplastic–viscodamage constitutive model for asphaltic materials**. International Journal of Solids and Structures. Vol. 48, pp. 191-207.

Darabi, M. K.; Al-Rub, R. K. A.; Little, D. N. (2012a) **A continuum damage mechanics framework for modeling micro-damage healing**. International Journal of Solids and Structures. Vol. 49, pp. 492-513.

Darabi, M. K.; Al-Rub, R. K. A.; Masad, E. A.; Little, D. N. (2012b) **A thermodynamic framework for constitutive modeling of time- and rate-dependent materials. Part II: Numerical aspects and application to asphalt concrete**. International Journal of Plasticity. Vol. 35, pp. 67-99.

DNER-ME 133 (1994) **Misturas betuminosas – determinação do módulo de resiliência**, Departamento Nacional de Estradas de Rodagem – Método de Ensaio, Rio de Janeiro, RJ, Brasil. In Portuguese.

Di Benedetto, H.; Olard F.; Sauzéat, C.; Delaporte, B. (2004) **Linear viscoelastic behaviour of bituminous materials: from binders to mixes**. International Journal of Road Materials and Pavement Design, 5 (SI), pp. 163–202.

Di Benedetto, H.; Mondher, N.; Sauzéat, C.; Olard, F. (2007a) **Three-dimensional thermo-viscoplastic behaviour of bituminous materials: the DBN model**. International Journal of Road Materials and Pavement Design. 8(2), pp. 285-315.

Di Benedetto, H., Delaporte, B., Sauzéat, C. (2007b) **Three-dimensional linear behavior of bituminous materials: Experiments and modeling**. International Journal of Geomechanics, Vol. 7, pp. 149-157.

Di Benedetto, H.; Nguyen, Q. T.; Sauzéat, C. (2011) **Nonlinearity, heating, fatigue and thixotropy during cyclic loading of asphalt mixtures**. Road Materials and Pavements Design, Vol 12, Issue 1, pp. 129-158.

Ferry, J. D. (1980) **Viscoelastic properties of polymers**, John Wiley & Sons Inc.

Flintsch, G. W.; Al-Qadi, I. L.; Loulizi, A.; Mokarem, D. (2005) **Laboratory tests for hot-mix asphalt characterization in Virginia**. VTRC 05-CR22. Virginia Transportation Research Council, Charlottesville.

Flintsch, G. W.; Loulizi, A.; S. D. Diefenderfer; Galal, K. A.; Diefenderfer, B. (2007) **Asphalt materials characterization in support of implementation of the proposed mechanistic-empirical pavement design guide**. VTRC 07-CR10. Virginia Transportation Research Council, Charlottesville.

Gavin, H. P. (2013) **The Levenberg-Marquardt method for nonlinear least squares curve-fitting problems**. Available at the internet link *http://people.duke.edu/~hpgavin/ce281/lm.pdf*. Accessed in April 2014.

Ghuzlan, K. (2001). **Fatigue damage analysis in asphalt concrete mixtures based upon dissipated energy concepts**. PhD Dissertation. University of Illinois at Urbana-Champaign, EUA, 282 pg.

Glover, C. J.; Davison, R. R.; Domke, C. H.; Ruan, Y.; Juristyarini, P.; Knorr, D. B.; Jung, H. S. (2005) **Development of a new method for assessing asphalt binder durability with field validation**. Report FHWA/TX-03/1872-2, Texas Transportation Institute, College Station, Texas.

Glover, C. J.; Martin, A. E.; Chowdhury, A.; Han, R.; Prapaitrakul, N; Jin, X.; Lawrence, J. (2008) **Evaluation of binder aging and its influence in aging of hot mix asphalt concrete: literature review and experimental design**. Report No. FHWA/TX-08/0-6009-1.

Herrington, P. R.; Ball, G. F. A. (1996) **Temperature dependence of asphalt oxidation mechanism**. Fuel. Vol. 75, Issue 9, pp. 1129–1131.

Huet, C (1963) **Etude par une méthode d'impédance du comportement viscoélastique des matériaux hydrocarbonés**. Ph.D. Dissertation. Faculté des Sciences de l'université de Paris, Paris. In French.

IUPAC (2014) **Compendium of chemical terminology – the Gold Book**, electronic version available at: http://goldbook.iupac.org/index.html. Accessed in May 18th 2014.

Kachanov, L. M. (1958) **On time to rupture in creep conditions** (in russian). Izviestia Akademii Nauk SSSR, Otdelenie Tekhnicheskikh Nauk, 8, pp. 26–31.

Kim, Y. R.; Little, D. N. (1990) **One-dimensional constitutive modeling of asphalt concrete**. Journal of Engineering Mechanics, Vol. 116, No.4, pp. 751-772.

Kim, Y. R.; Chehab, G. R. (2004) **Development of a viscoelatoplastic continuum damage model for asphalt-aggregate mixtures: final report as part of the tasks F and G in the NCHRP 9-19 Project**. National Cooperative Highway Research Program, National Research Council, Washington, D.C.

Kim, Y. R.; Guddati, M. N.; Underwood; B. S.; Yun, T. Y.; Subramanian; V.; Savadatti, S.; Thirunavukkarasu, S. (2008) **Development of a multiaxial VEPCD-FEP++**. Publication FHWA-HRT-08-073. FHWA, U.S. Department of Transportation.

Kim, Y. R. (2009) **Modeling of Asphalt Concrete**. 1st edition. McGraw-Hill Professional.

Krajcinovic, D. (1989). **Damage Mechanics**. Mechanics of Materials, Vol. 8, pp. 117-197.

Lau, C. K.; Lunsford, K. M. ; Glover, C. J.; Davison, R. R. ; Bullin, J. A. (1992) **Reaction rates and hardening susceptibilities as determined from POV aging of asphalts**. Transp. Res. Rec., 1342, pp. 50-57.

Lee, D. Y.; Huang, R. J. (1973) **Weathering of asphalts as characterized by infrared multiple internal reflection**. Journal of the Society for Applied Spectroscopy, Vol. 27 (6), pp. 435-440.

Lee, H. J.; Kim, Y. R. (1998a) **Viscoelastic constitutive model for asphalt concrete under cyclic loading**. Journal of Engineering Mechanics, Vol.124, No.1, pp. 32-40.

Lee, H. J.; Kim, Y. R. (1998b) **Viscoelastic continuum damage model of asphalt concrete with healing**. Journal of Engineering Mechanics, Vol.124, No.11, pp. 1224-1232.

Lemaitre, J.; Chaboche, J-L. (1990) **Mechanics of solid materials**. Cambridge University Press. UK.

Liu, M.; Lunsford, K. M.; Davison, R. R.; Glover, C. J.; Bullin, J. A. (1996) **The kinetics of carbonyl formation in asphalt.** Journal of the American Institute of Chemical Engineers, Vol. 42(4), pp. 1069-1076.

Liu, M.; Ferry, M. A.; Davison, R. R.; Glover, C. J.; Bullin. J. A. (1998) **Oxygen uptake as correlated to carbonyl growth in aged asphalts and asphalt Corbett fractions**. Ind. Eng. Chem. Res., Vol. 37, pp. 4669-4674.

Lopes, M. M. (2012) **Programa interlaboratorial de agregados e misturas asfálticas da rede asfalto N/NE**. M.Sc. Thesis, Programa de Pós-Graduação em Engenharia de Transportes, Centro de Tecnologia, Universidade Federal do Ceará, Fortaleza, Brazil. In Portuguese.

Lundström, R.; Isacsson, U. (2003a) **Asphalt fatigue modeling using viscoelastic continuum damage theory**. International Journal of Road Materials and Pavement Design, vol. 4, n. 1, pp. 51-75.

Lundström, R.; Isacsson, U. (2003b) **Characterization of asphalt concrete deterioration using monotonic and cyclic tests**. International Journal of Pavement Engineering. Vol. 4, n. 3, pp. 143-153.

Lundström, R.; Isacsson, U., Ekblad, J. (2003) **Investigations of stiffness and fatigue properties of asphalt mixtures**. Journal of Material Science, v. 38, pp 4941-4949.

Lundström, R.; Isacsson, U. (2004) **Linear viscoelastic and fatigue characteristics of SBS modified asphalt mixtures**. Journal of Materials in Civil Engineering, vol. 16, n.6, pp. 629–638.

Lundström, R.; Ekblad, J.; Isacsson, U. (2004) **Influence of hysteretic heating on asphalt fatigue characterization.** Journal of Testing and Evaluation, Vol. 32, n. 6, pp. 484-493.

Lundström, R; Ekblad, J (2006) **Fatigue characterization of asphalt concrete using Schapery´s Work Potential Model**. Annual Transactions of the Nordic Rheology Society, vol. 14.

Mangiafico, S. (2014) **Linear viscoelastic properties and fatigue of bituminous mixtures produced with Reclaimed Asphalt Pavement and corresponding binder blends**. Ph.D. Dissertation. École Nationale des Travaux Publics de l'État - Université de Lyon. Expected defense for June 23rd.

Martins, A. T. (2014) **Contribuição para a validação do ensaio de resistência ao dano por fadiga para ligantes asfálticos**. M.Sc. Thesis. Programa de Pós-graduação em Engenharia Civil, COPPE, Universidade Federal do Rio de Janeiro. In Portuguese.

Medeiros, M. S. (2006) **Estudo da interconversão entre o módulo complexo e a creep compliance na caracterização de misturas asfálticas**. M.Sc. Thesis. Programa de Pós-Graduação em Engenharia de Transportes, UFC. In Portuguese.

Mello, L. G. R. (2008) **A teoria do dano em meio contínuo no estudo da fadiga em misturas asfálticas**. Ph.D. Dissertation. Universidade de Brasília. Brasília - DF. In Portuguese.

Michalica, P.; Kazatchkov, I. B.; Stastna, J.; Zanzotto, L. (2008) **Relationship between chemical and rheological properties of two asphalts of different origins**, Fuel, 87, pp. 3247-3253.

Nascimento, L. A. H.; Rocha, S. M. N.; Nascimento, C. E. H.; Kim, Y. R.; Chacur, M.; Martins, A. T. (2014) **Uso da mecânica do dano contínuo na caracterização de misturas asfálticas brasileiras**. Anais do 21° Encontro de Asfalto do Instituto Brasileiro de Petróleo, Gás e Biocombustíveis - IBP. Rio de Janeiro. In Portuguese.

NCHRP 1-28 (1996) **Proposed test protocol for determination of resilient modulus of bituminous mixtures by indirect tension**. National Cooperative Highway Research Program (NCHRP).

NCHRP 1-28A (2003) **Recommended standard test method for determination of the resilient modulus of bituminous mixtures by indirect tension**. National Cooperative Highway Research Program (NCHRP).

Nunes, F. R. G. (2006) **Caracterização mecânica de misturas asfálticas confeccionadas com agregados sintéticos de argila calcinada quanto a deformação permanente**. 189 f. M.Sc. Thesis, Programa de Pós-Graduação em Engenharia de Transportes, Centro de Tecnologia, Universidade Federal do Ceará, Fortaleza, Brazil. In Portuguese.

Papazian, H. S. (1962) **The response of linear viscoelastic materials in the frequency domain with emphasis on asphaltic concrete**. In: International Conference on the Structural Design of Asphalt Pavements, Michigan, USA. pp. 454-63.

Park, S. W.; Kim, Y. R.; Schapery, R. A. (1996) **Viscoelastic continuum damage model and its application to uniaxial behavior of asphalt concrete**. Mechanics of Materials, Vol.24, No.4, pp. 241-255.

Park, S. W.; Kim, Y. R. (1998) **Analysis of layered viscoelastic system with transient temperatures**. Journal of Engineering Mechanics, Vol. 124, n° 2, pp. 223-231.

Park, S. K.; Kim, Y. R. (2001) **Fitting Prony series viscoelastic models with power-law presmoothing**. Journal of Materials in Civil Engineering. Vol. 13 n° 1, pp. 26–32.

Park, S. W.; Schapery, R. A. (1997) **A viscoelastic constitutive model for particulate composites with growing damage**. International Journal of Solids and Structures. Vol. 34, n° 8, 931-947.

Park, S. W.; Schapery, R. A. (1999) **Methods of interconversion between linear viscoelastic material functions. Part I – a numerical method based on Prony series**. International Journal of Solids and Structures, 36, pp. 1653–1675.

Partl, M. N.; Bahia, H. U.; Canestrari, F.; de la Roche, C.; Di Benedetto, H.; Piber, H.; Sybilski, D. (Eds.) (2012) **Advances in interlaboratory testing and evaluation of bituminous materials**. Report STAR 206-ATB. Unedited version of State-of-the-Art Report of the RILEM Technical Committee 206-ATB.

Petersen, J. C.; Branthaver, J. F.; Robertson, R. E.; Harnsberger, P. M.; Duvall, J. J.; Ensley, E.K. (1993) **Effects of physicochemical factors on asphalt oxidation kinetics**. Transp. Res. Rec., 1391, pp. 1-10.

Pronk, A. C. (1997) **Fatigue lives of asphalt beams in 2 and 4 point dynamic bending tests based on a "new" fatigue life definition using the dissipated energy concept**. Road and Hydraulic Engineering Division, Rijkswaterstaat, The Netherlands, 23 p.

Pronk, A. C. (2003) **The variable dashpot**. Ministry of water and transport, Rijkswaterstaat: Delft, Netherlands.

Pronk, A. C. (2006) **The Huet-Sayegh Model: a simple and excellent rheological model for master curves of asphaltic mixes**. Geotechnical Special Publications of the American Society of Civil Engineers (ASCE). Asphalt Concrete: Simulation, Modeling and Characterization. Proceedings of the R. Lytton Symposium on Mechanics of Flexible Pavements in June 2005, Baton Rouge, Louisiana, USA.

Pronk, A. C.; Hopman, P. C. (1990) **Energy dissipation: the leading factor of fatigue**. Proceedings of United States Strategic Highway Research Program – Sharing the Benefits, London.

Qin, Q.; Schabron, J. F.; Boysen, R. B.; Farrar, M. J. (2014) **Field aging effect on chemistry and rheology of asphalt binders and rheological predictions for field aging**. Fuel Vol. 121 pp. 86–94.

Reese, R. (1997) **Properties of aged asphalt binder related to asphalt concrete fatigue life**. Proceedings of the Association of Asphalt Paving Technologists, Vol. 66, pp. 604-632.

Sabouri, M.; Kim, Y. R. (2014) **Development of a failure criterion for asphalt mixtures under different modes of fatigue loading**. TRB Annual Meeting. Washington, D.C., United States.

Sayegh, G. (1965) **Variation des modules de quelques bitumes purs et bétons bitumineux**. Ph.D. Dissertation. Faculté des Sciences de l'université de Paris, Paris. In French.

Schapery, R. A. (1962) **Irreversible thermodynamics and variational principles with applications to viscoelasticity**. Ph.D. Dissertation. California Institute of Technology, Pasadena, California.

Schapery, R. A. (1975) **A theory of crack initiation and growth in viscoelastic media, Part l: Theoretical development, Part II: Approximate methods of analysis, Part III: Analysis of continuous growth**, International Journal Fracture, Vol. 11, pp. 141-159, pp. 369-388, pp. 549-562.

Schapery, R. A. (1984) **Correspondence principles and a generalized J integral for large deformation and fracture analysis of viscoelastic media**. International Journal of Fracture, Vol.25, No.3, pp. 195-223.

Schapery, R. A. (1990a) **A theory of mechanical behavior of elastic media with growing damage and other changes in structure**. J. Mech. Phys. Solids, Vol. 38, pp. 215-253.

Schapery, R. A. (1990b) **Simplifications in the behavior of viscoelastic composites with growing damage**. Symposium on Inelastic Deformation of Composite Materials. Troy, New York. Springer, New York-Wien, pp. 193-214.

Silva, H. N.; Sousa, P. C.; De Holanda, A. S.; Soares, J. B. (2008) **Computer program for linear viscoelastic characterization using Prony Series**. XXIX CILAMCE – Congresso Ibero-Latinoamericano de Métodos Computacionais em Engenharia. Maceió, Brasil.

Silva, H. N. (2009) **Caracterização viscoelástica linear de misturas asfálticas: Operacionalização Computacional e Análise pelo Método dos Elementos Finitos**. M.Sc. Thesis, Programa de Pós-Graduação em Engenharia de Transportes, Centro de Tecnologia, Universidade Federal do Ceará, Fortaleza, Brazil. In Portuguese.

Soares, J. B.; Souza, F. V. (2002) **Verificação do comportamento viscoelástico linear em misturas asfálticas**. In: 16º Encontro de Asfalto, IBP, Rio de Janeiro. In Portuguese.

Soares, J. B.; Souza, F. V. (2003) **Considerações sobre módulo resiliente e módulo dinâmico em misturas asfálticas com base na teoria da viscoelasticidade**. XII Congresso Ibero-Latinoamericano do Asfalto, Quito. In Portuguese.

Sousa, P. C. ; Silva, H. N. ; Soares, J. B. (2007) **Método da colocação para obtenção de séries de Prony usadas na caracterização viscoélastica de materiais asfálticos**. XXI Congresso de Pesquisa e Ensino em Transportes – ANPET. Rio de Janeiro, Brasil. In Portuguese.

Souza, F. V. (2012) **Proposta de modelo constitutivo viscoelástico não-linear para materiais asfálticos em regime de grandes deformações**. Revista Transportes, v. 20, n 3. pp. 54-61. In Portuguese.

Subramanian, V. (2011) **A Viscoplastic model with rate-dependent hardening for asphalt concrete in compression**. Ph.D. Dissertation. North Carolina State University.

Tashman, L. (2003) **Microstructural Viscoplastic Continuum Model for Asphalt Concrete**. PhD Dissertation, Civil Engineering, Texas A&M University.

Theisen, K.M.; Nuñez, W.P.; Bittencourt E. (2007) **Modelagem do ensaio de módulo dinâmico e de compressão diametral de cargas cíclicas através de curva de fluência e do princípio da correspondência elasto-viscoelástica**. XXI Congresso de Pesquisa e Ensino em Transportes – ANPET. Rio de Janeiro, Brasil. In Portuguese.

Teixeira, V.F.; Sousa, F.V.; Soares J.B. (2007) **Modelagem da vida de fadiga e do acúmulo de deformações permanentes em pavimentos asfálticos por meio de um modelo de dano contínuo**. Revista Transportes. Vol. XV, No 2. In Portuguese.

Underwood, B.S.; Y. Kim, Y. R.; Savadatti, S.; Thirunavukkarasu, S.; Guddati, M. (2009) **Response and fatigue performance modeling of ALF pavements using 3-D finite element analysis and a simplified viscoelastic continuum damage model**. Asphalt Paving Technology, AAPT, Vol. 78, pp. 829-868.

Underwood, B. S.; Kim, Y. R.; Guddati; M. N. (2010) **Improved calculation method of damage parameter in viscoelastic continuum damage model**. International Journal of Pavement Engineering, Vol. 11, No. 6, pp. 459-476.

Underwood, B. S.; Baek, C.; Kim, Y. R. (2012) **Simplified viscoelastic continuum damage model as platform for asphalt concrete fatigue analysis**. Transportation Research Record: Journal of the Transportation Research Board, 2296(-1), pp. 36-45.

Underwood, B. S.; Kim, Y. R. (2013) **Nonlinear viscoelastic behavior of asphalt concrete and its implication for fatigue modeling**. Transportation Research Record: Journal of the Transportation Research Board, No. 2373, Transportation Research Board of the National Academies, Washington, D.C., pp. 100-108.

Walubita, L. F. (2006) **Comparison of fatigue analysis approaches for predicting fatigue lives of hot mix asphalt concrete mixtures (HMA)**. Ph.D. Dissertation, Texas A&M University, College Station, TX.

Witczak, M. W.; Fonseca, O. A. (1996) **Revised predictive model for dynamic (complex) modulus of asphalt mixtures**. Transportation Research Record, 1540, pp. 15-23.

Williams, M. L.; Landel, R. F.; Ferry, J. D. (1955) **The temperature dependence relaxation mechanism in amorphous polymers and other glass forming liquids**. Journal of the American Chemical Society, 77 (14), pp 3701-3707.

Williams, M. L. (1964) **Structural analysis of viscoelastic materials**. American Institute of Aeronautics and Astronautics (AIAA) Journal. Vol. 2(5). pp. 785-808.

Woldekidan, M. F. (2011) **Response modelling of bitumen, bituminous mastic and mortar**. Ph.D. Dissertation. Delft University of Technology, Delft, Netherlands.

Wright, J. R. (1965) **Weathering: Theoretical and Practical Aspects of Asphalt Durability**. Ch. 8 In *Bituminous Materials: Asphalts, Tars and Pitches, Vol. II* (A. J. Hoiberg, ed.), Interscience Publishers, New York, pp. 249-306.

Yun, T.; Kim, Y. R. (2011) **A viscoplastic constitutive model for hot mix asphalt in compression at high confining pressure**. Construction and Building Materials, Vol. 25, Issue 5, pp. 2733–2740.

Zhang, Y.; Luo, R.; Lytton, R. L. (2012) **Characterizing permanent deformation and fracture of asphalt mixtures by using compressive dynamic modulus tests**. Journal of Materials in Civil Engineering, 24(7), pp. 898-906.

Zhang, J.; Sabouri, M.; Kim, Y. R.; Guddati, M. N. (2013) **Development of a failure criterion for asphalt mixtures under fatigue loading**. In: Road Materials and Pavement Design, Vol. 14, Supplement 2, pp.1-15.

APPENDIX A - Summary of Results

Age 0

Permanent Deformation

Figure A1 – Results for unconfined dynamic creep tests for Age Zero mixture
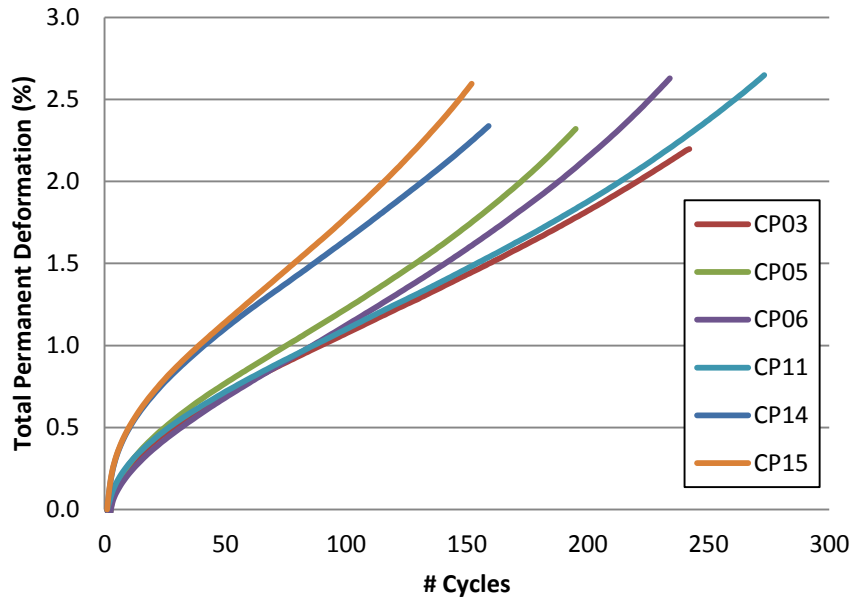
Fatigue

Figure A2 – Results for material integrity *vs* reduced test time for tension-compression fatigue tests with Age Zero mixture
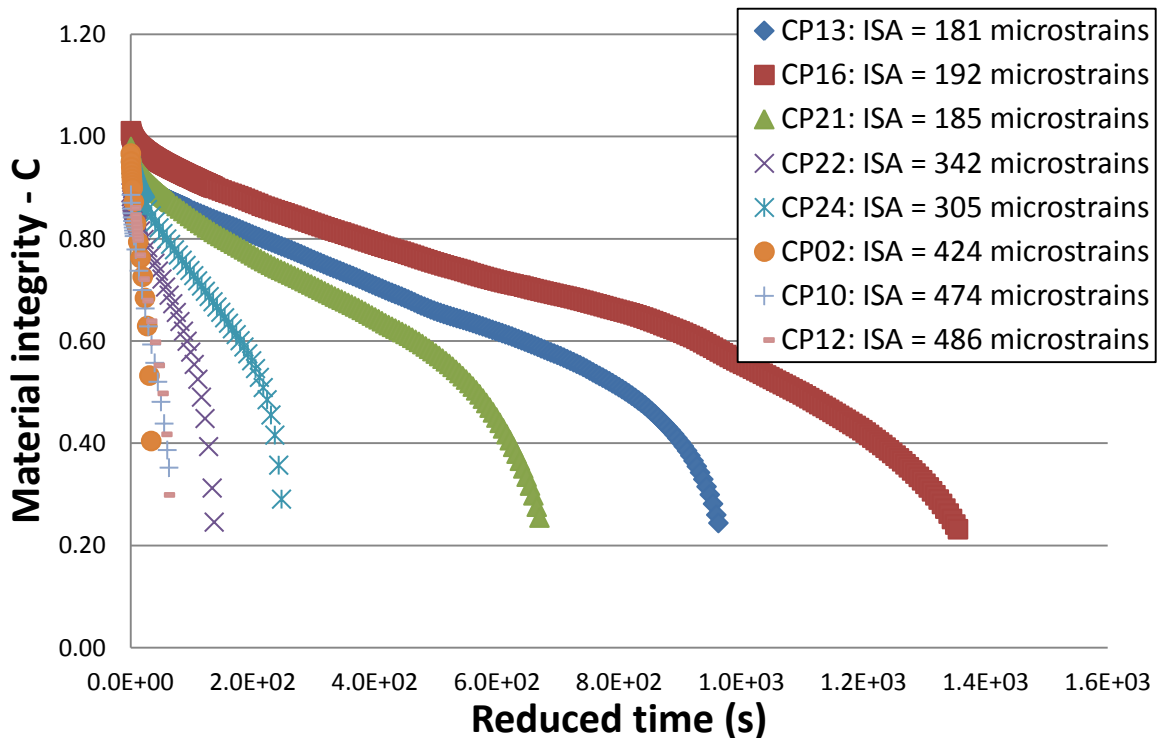
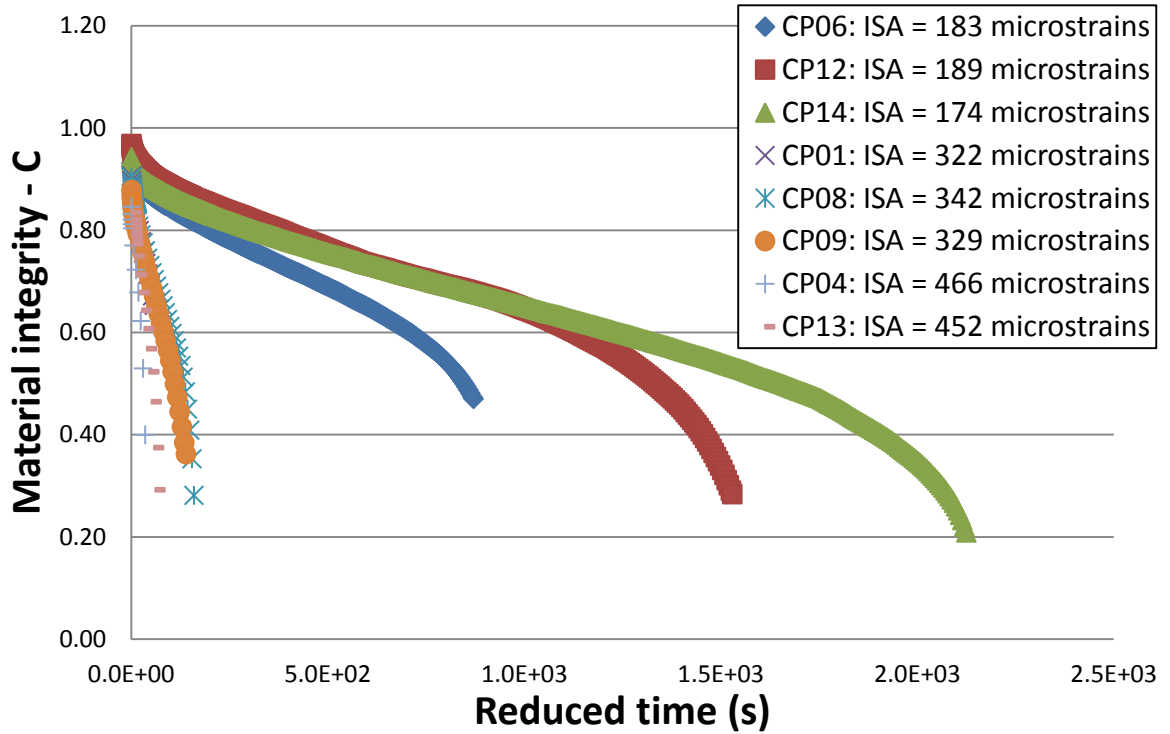Figure A3 – Results for damage accumulation *vs* reduced test time for tension-compression fatigue tests with Age Zero mixture
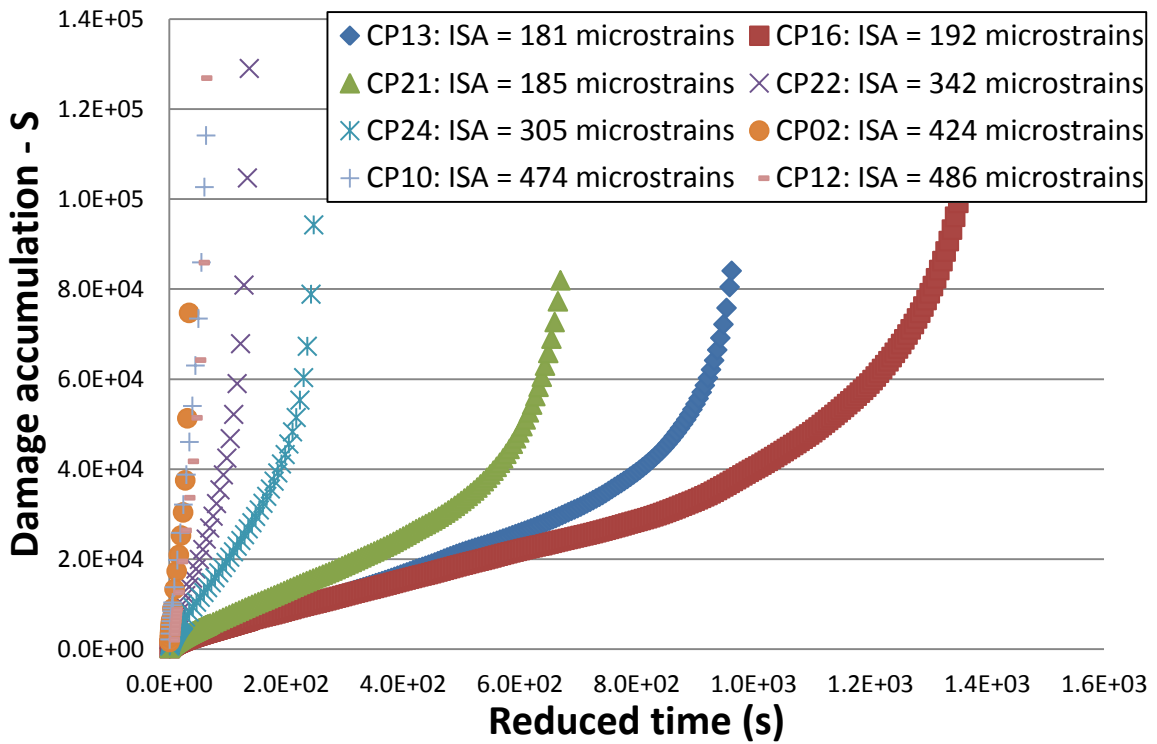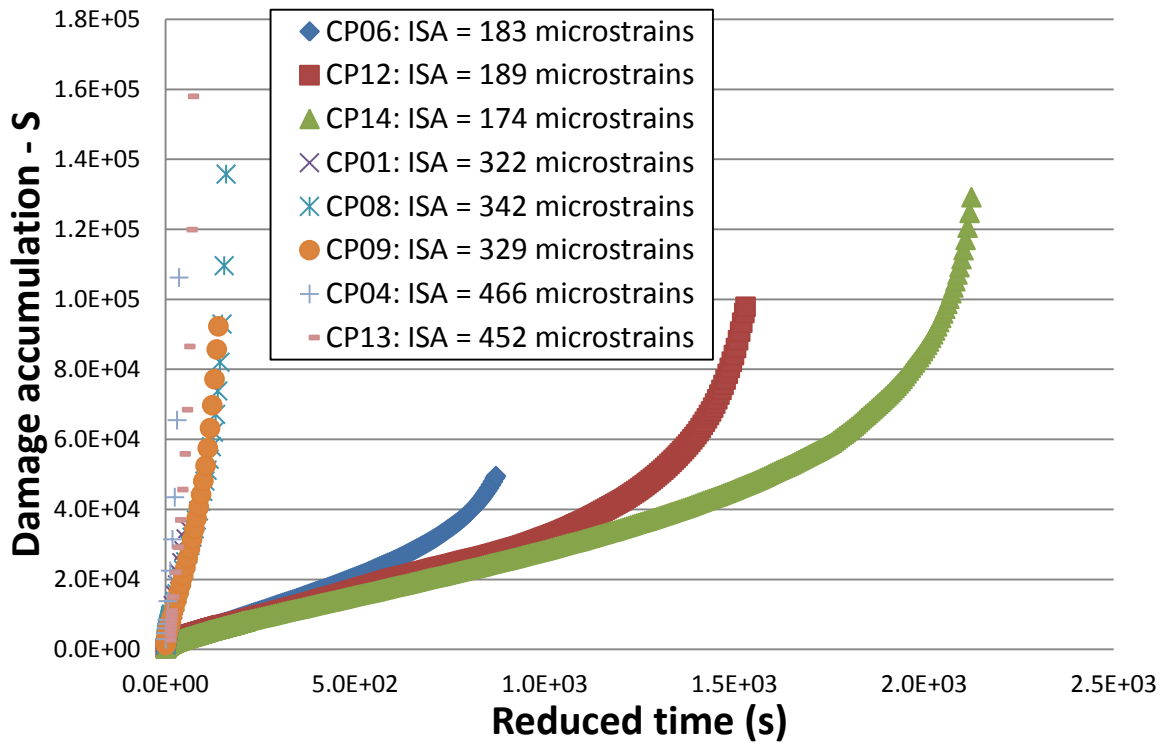

Figure A4 – Results for material integrity *vs* damage accumulation (experimental and curve fitting) for tension-compression fatigue tests with Age Zero mixture
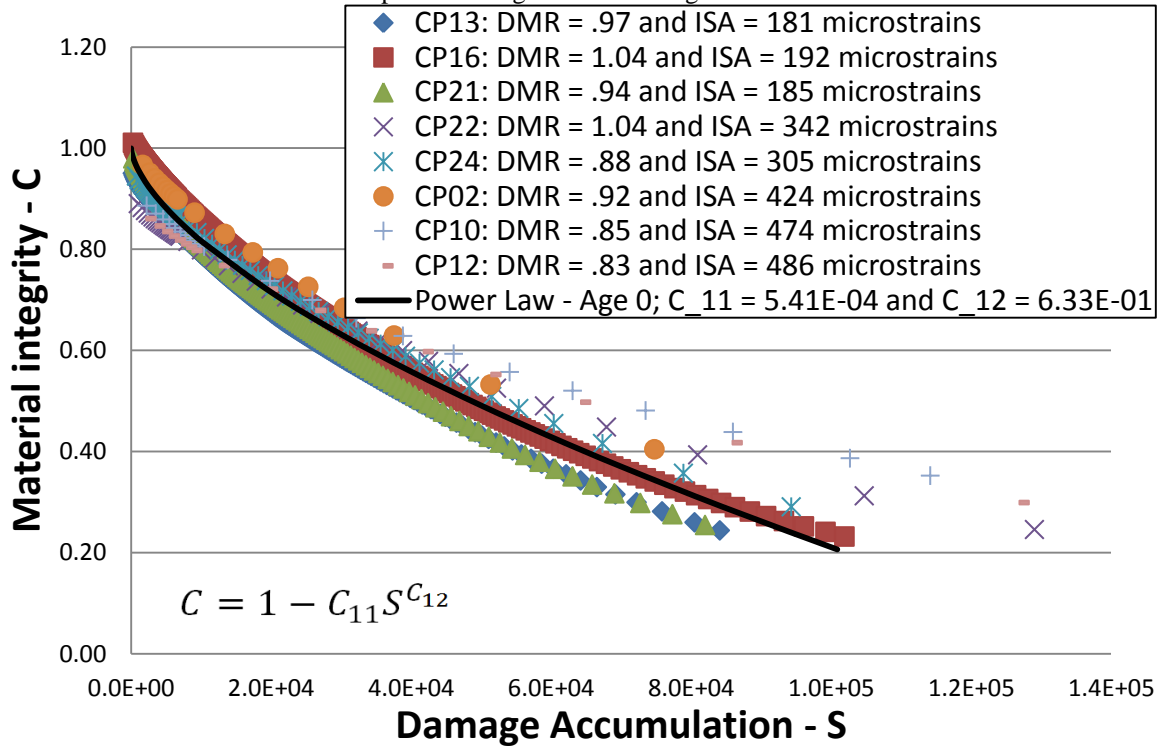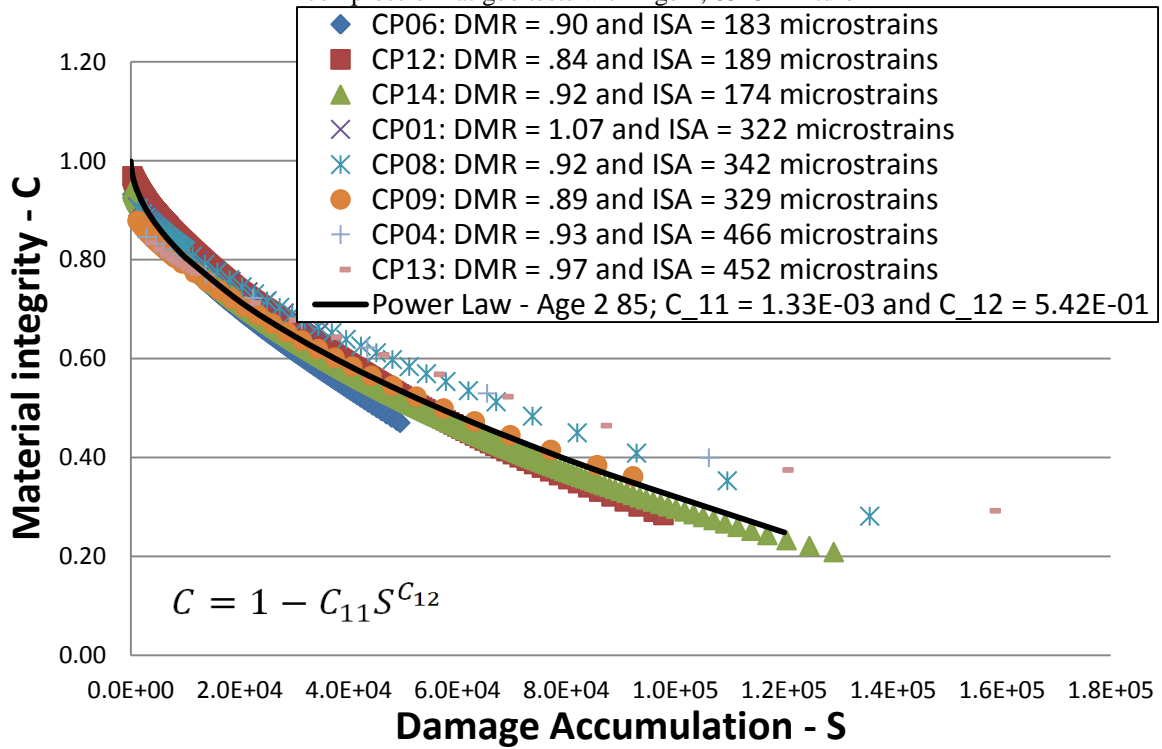
Figure A5 – Results for averaged released pseudo strain energy *vs* number of cycles to failure (experimental and curve fitting) for tension-compression fatigue tests with Age Zero mixture
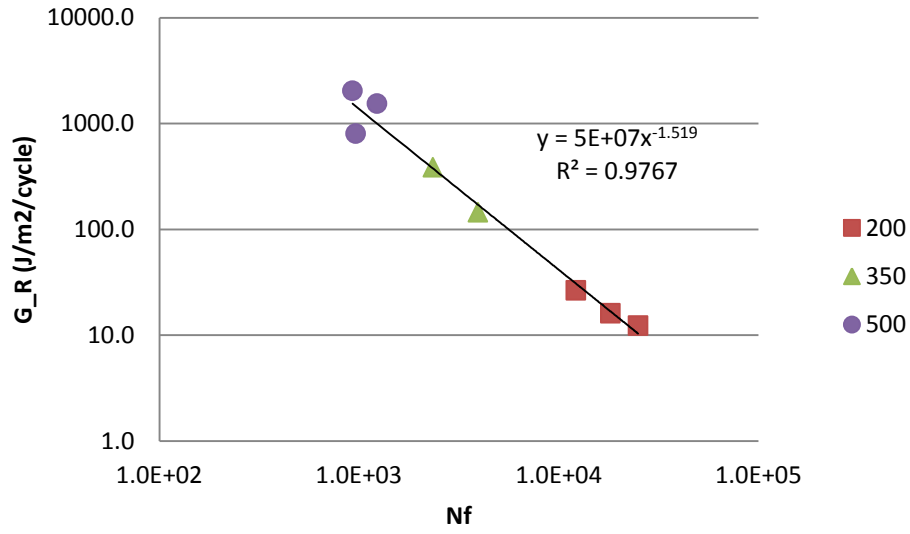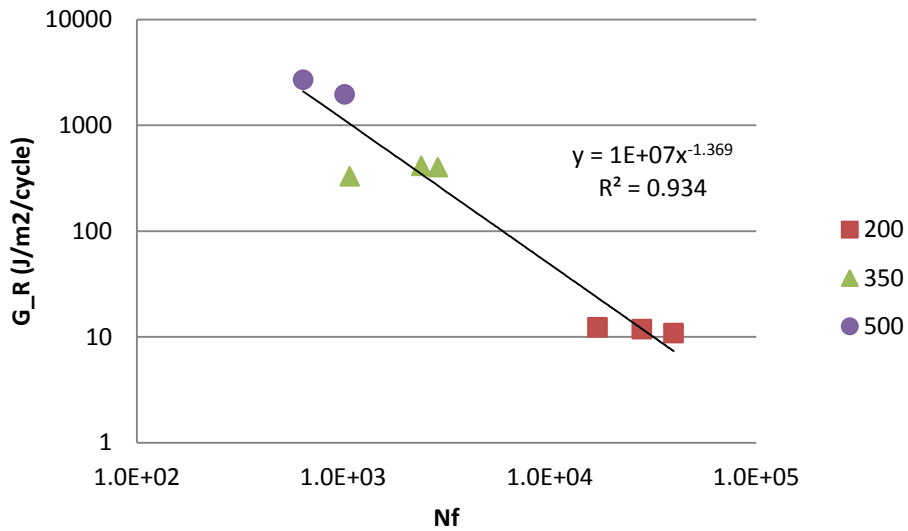

Figure A6 – Results for material integrity at failure *vs* initial strain amplitude for tension-compression fatigue tests with Age Zero mixture
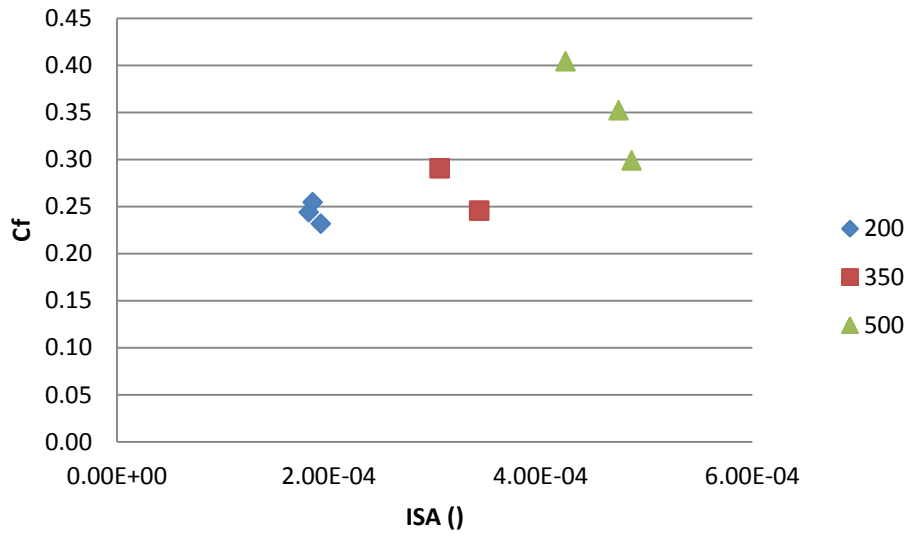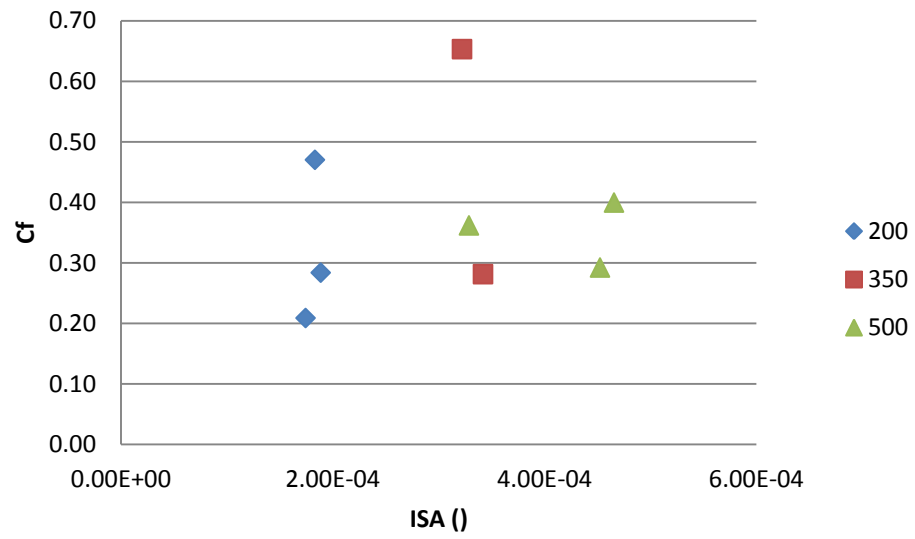
Figure A7 – Results for damage accumulation at failure *vs* initial strain amplitude for tension-compression fatigue tests with Age Zero mixture
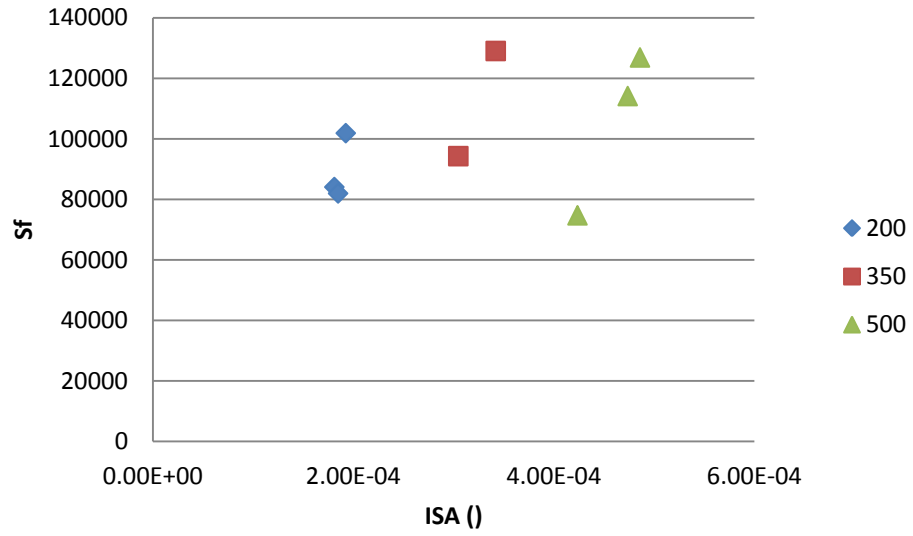
Age 2, 85ºC

Permanent Deformation

Figure A8 – Results for unconfined dynamic creep tests for Age 2, 85ºC mixture
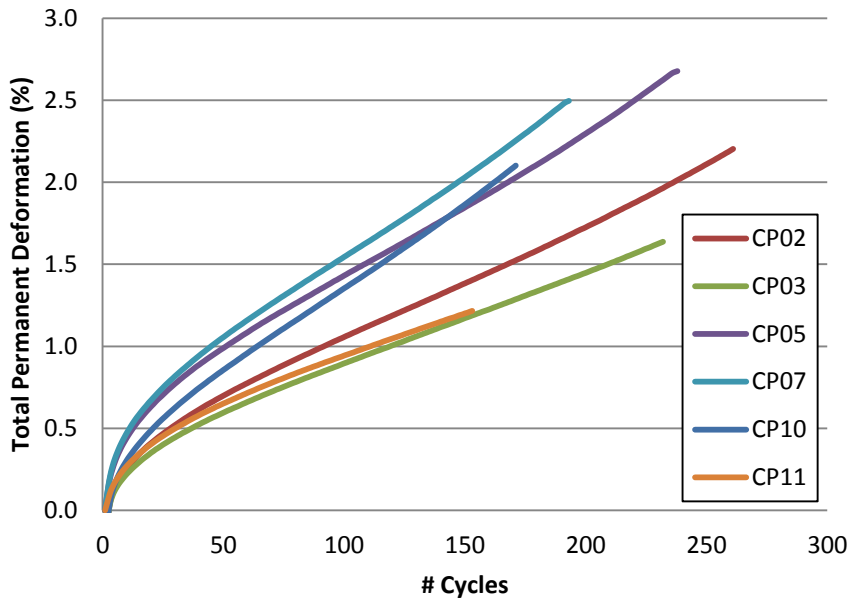
Fatigue

Figure A9 – Results for material integrity *vs* reduced test time for tension-compression fatigue tests with Age 2, 85ºC mixture
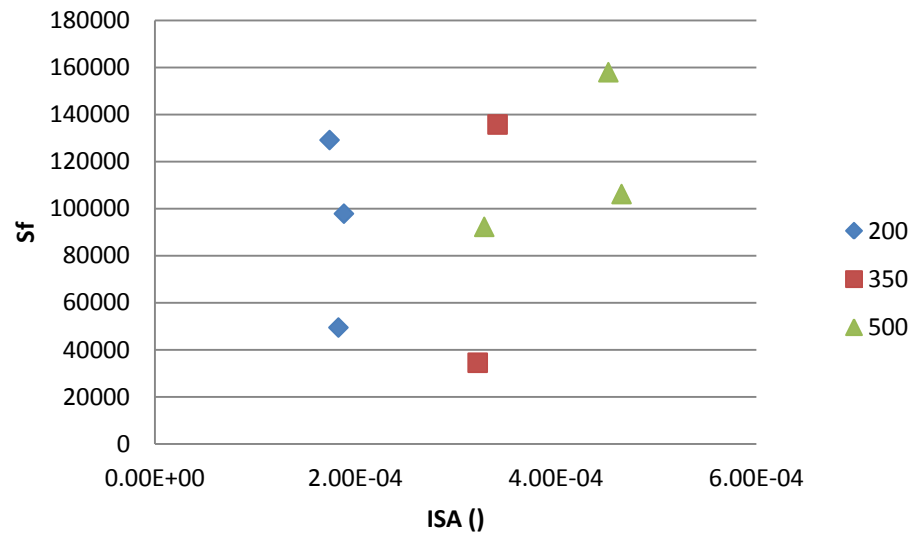

Figure A10 – Results for damage accumulation *vs* reduced test time for tension-compression fatigue tests with Age 2, 85ºC mixture
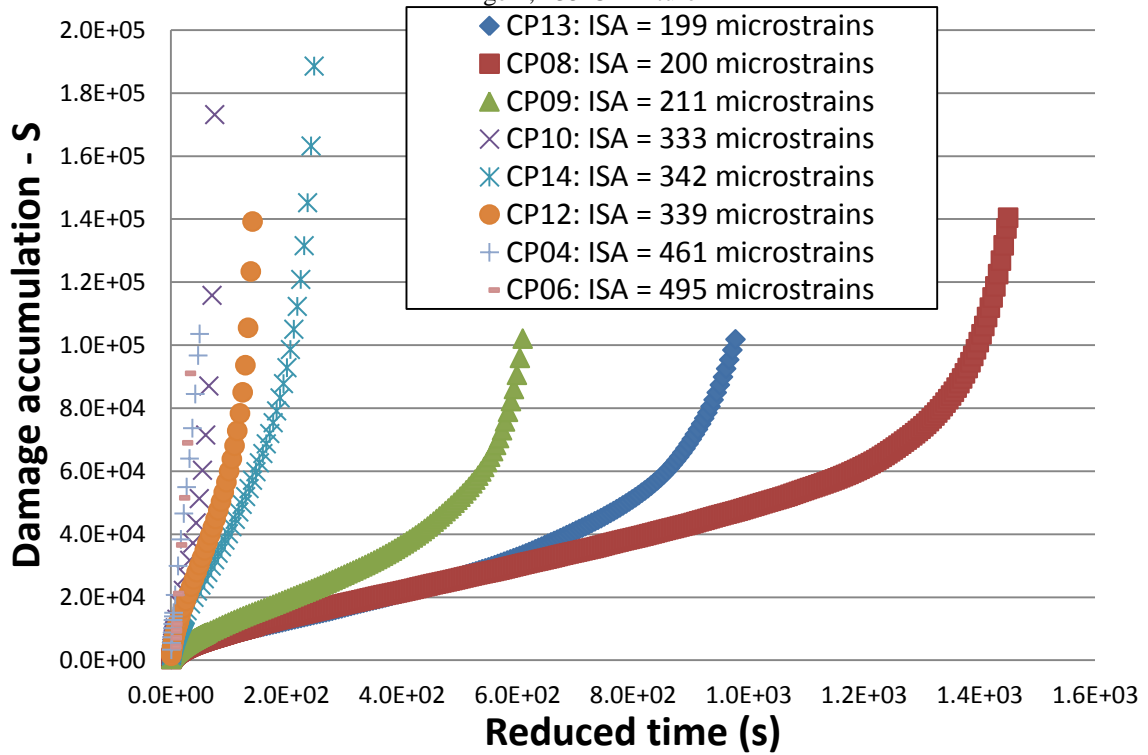
Figure A11 – Results for material integrity *vs* damage accumulation (experimental and curve fitting) for tension-compression fatigue tests with Age 2, 85ºC mixture
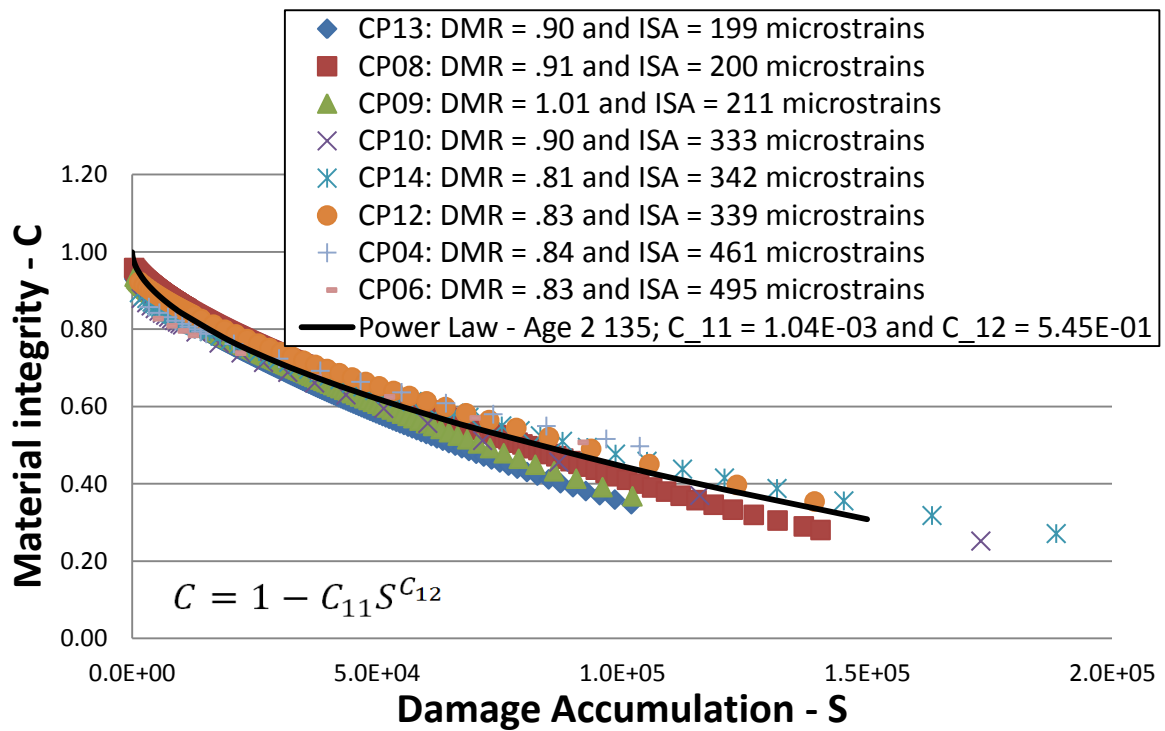

$$C = 1 - C_{11}S^{C_{12}}$$

Figure A12 – Results for averaged released pseudo strain energy *vs* number of cycles to failure (experimental and curve fitting) for tension-compression fatigue tests with Age 2, 85ºC mixture
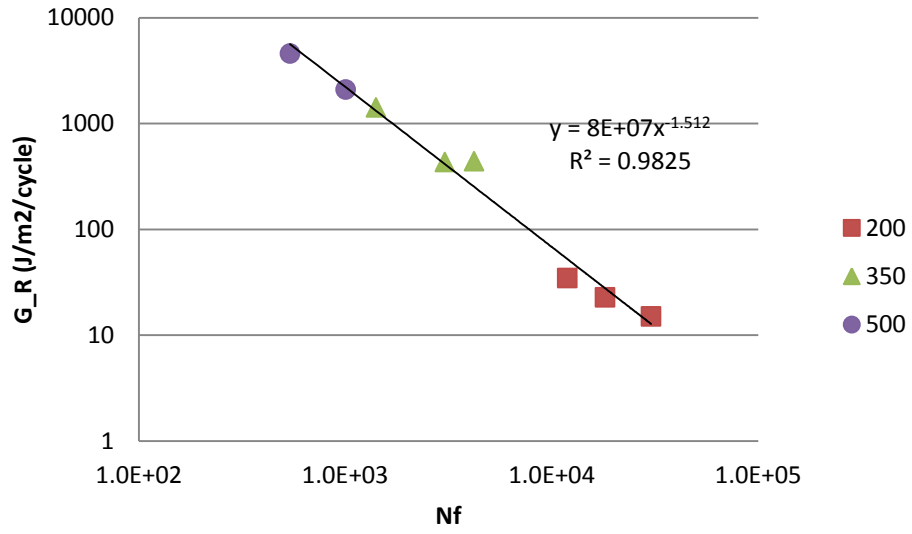
Figure A13 – Results for material integrity at failure *vs* initial strain amplitude for tension-compression fatigue tests with Age 2, 85ºC mixture

Figure A14 – Results for damage accumulation at failure *vs* initial strain amplitude for tension-compression fatigue tests with Age 2, 85ºC mixture

Age 2, 135ºC

Permanent Deformation

Figure A15 – Results for unconfined dynamic creep tests for Age 2, 135ºC mixture

Fatigue

Figure A16 – Results for material integrity *vs* reduced test time for tension-compression fatigue tests with Age 2, 135ºC mixture

Figure A17 – Results for damage accumulation *vs* reduced test time for tension-compression fatigue tests with Age 2, 135ºC mixture

Figure A18 – Results for material integrity *vs* damage accumulation (experimental and curve fitting) for tension-compression fatigue tests with Age 2, 135ºC mixture

$$C = 1 - C_{11}S^{C_{12}}$$

Figure A19 – Results for averaged released pseudo strain energy *vs* number of cycles to failure (experimental and curve fitting) for tension-compression fatigue tests with Age 2, 135ºC mixture

Figure A20 – Results for material integrity at failure *vs* initial strain amplitude for tension-compression fatigue tests with Age 2, 135ºC mixture
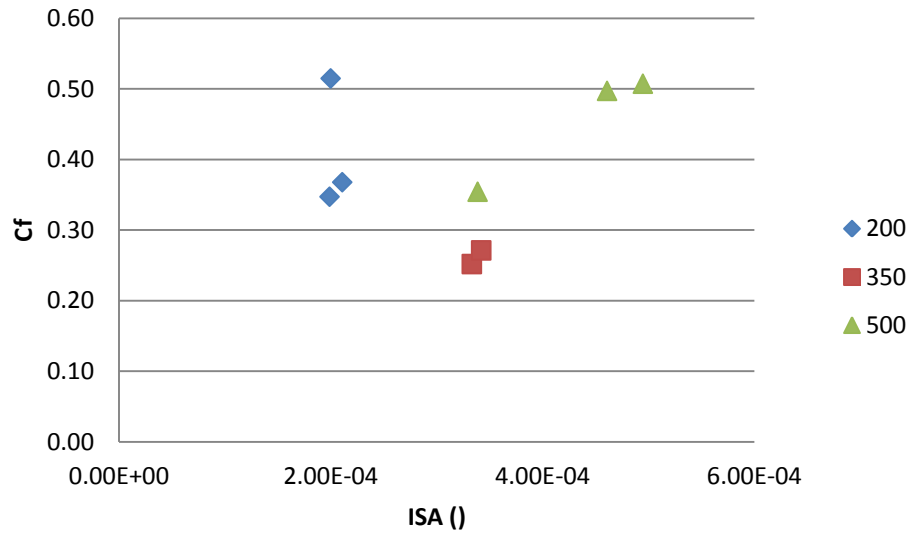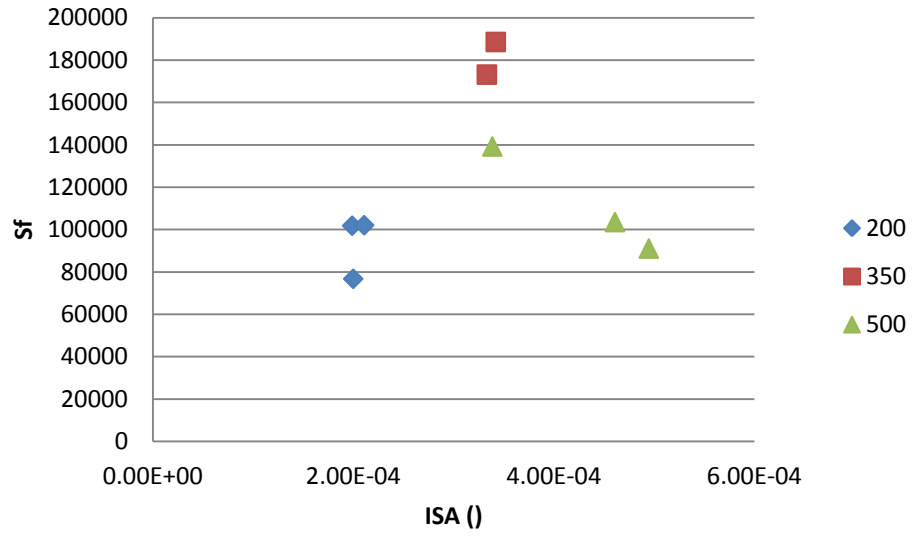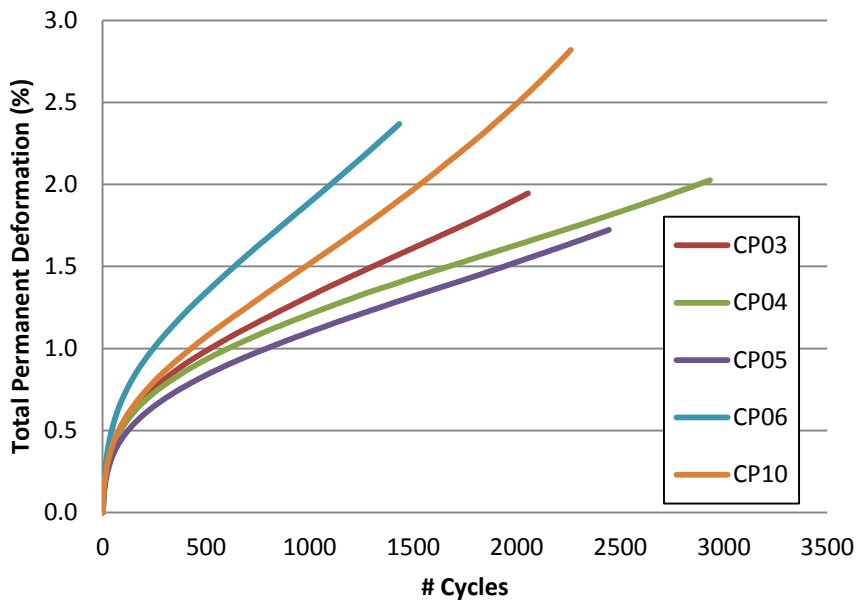
Figure A21 – Results for damage accumulation at failure *vs* initial strain amplitude for tension-compression fatigue tests with Age 2, 135ºC mixture

Age 45, 85ºC

Permanent Deformation

Figure A22 – Results for unconfined dynamic creep tests for Age 45, 85ºC mixture

Fatigue

Figure A23 – Results for material integrity *vs* reduced test time for tension-compression fatigue tests with Age 45, 85ºC mixture
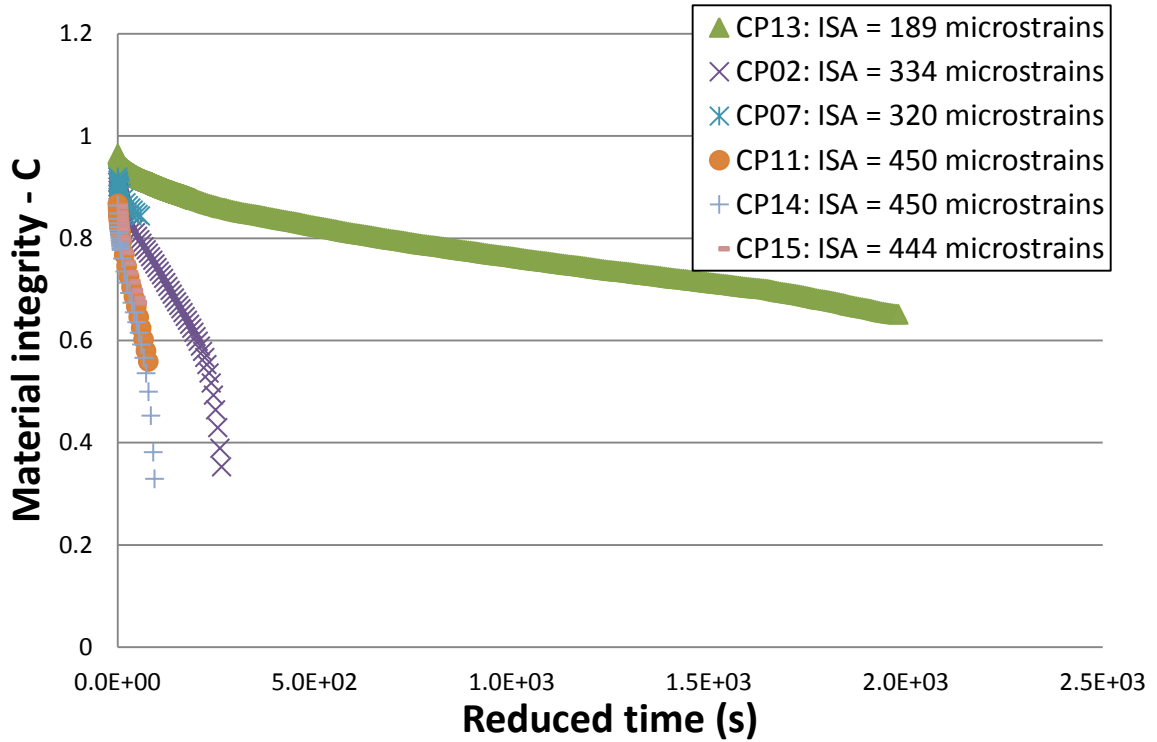

Figure A24 – Results for damage accumulation *vs* reduced test time for tension-compression fatigue tests with Age 45, 85ºC mixture
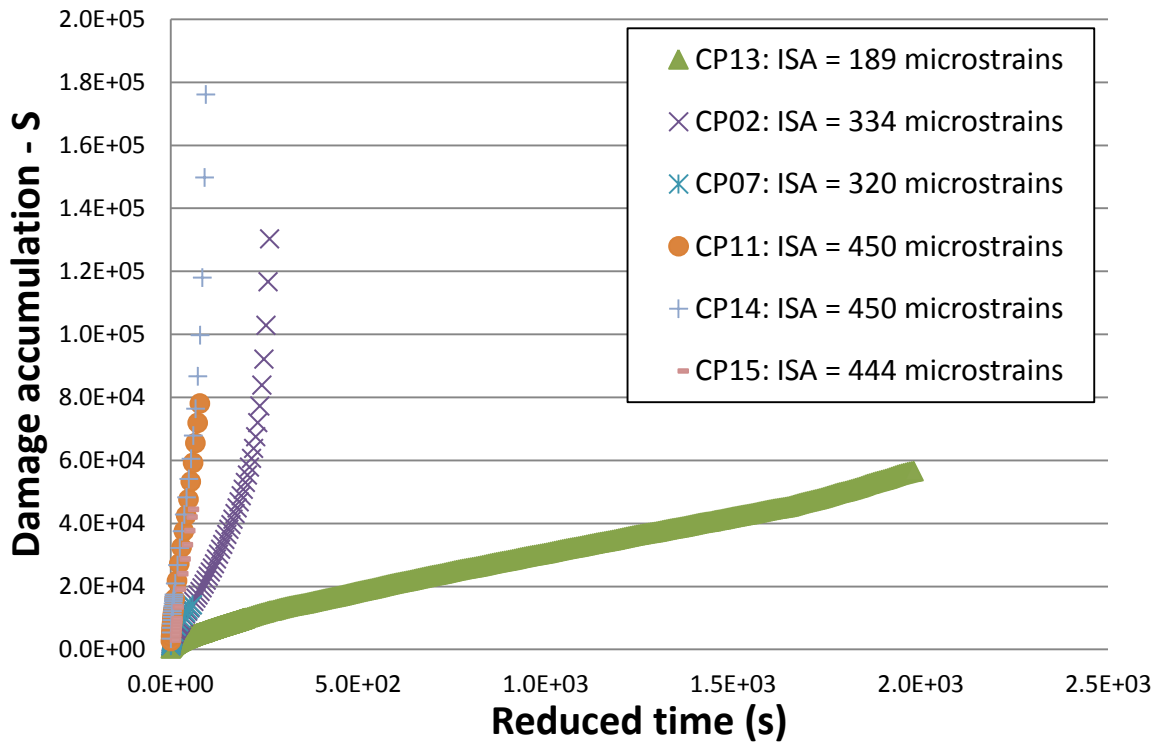
Figure A25 – Results for material integrity *vs* damage accumulation (experimental and curve fitting) for tension-compression fatigue tests with Age 45, 85ºC mixture

$$C = 1 - C_{11}S^{C_{12}}$$

- ▲ CP13: DMR = .93 and ISA = 189 microstrains
- ✕ CP02: DMR = .97 and ISA = 334 microstrains
- ✳ CP07: DMR = 1.01 and ISA = 320 microstrains
- ● CP11: DMR = .89 and ISA = 450 microstrains
- + CP14: DMR = .77 and ISA = 450 microstrains
- – CP15: DMR = .87 and ISA = 444 microstrains
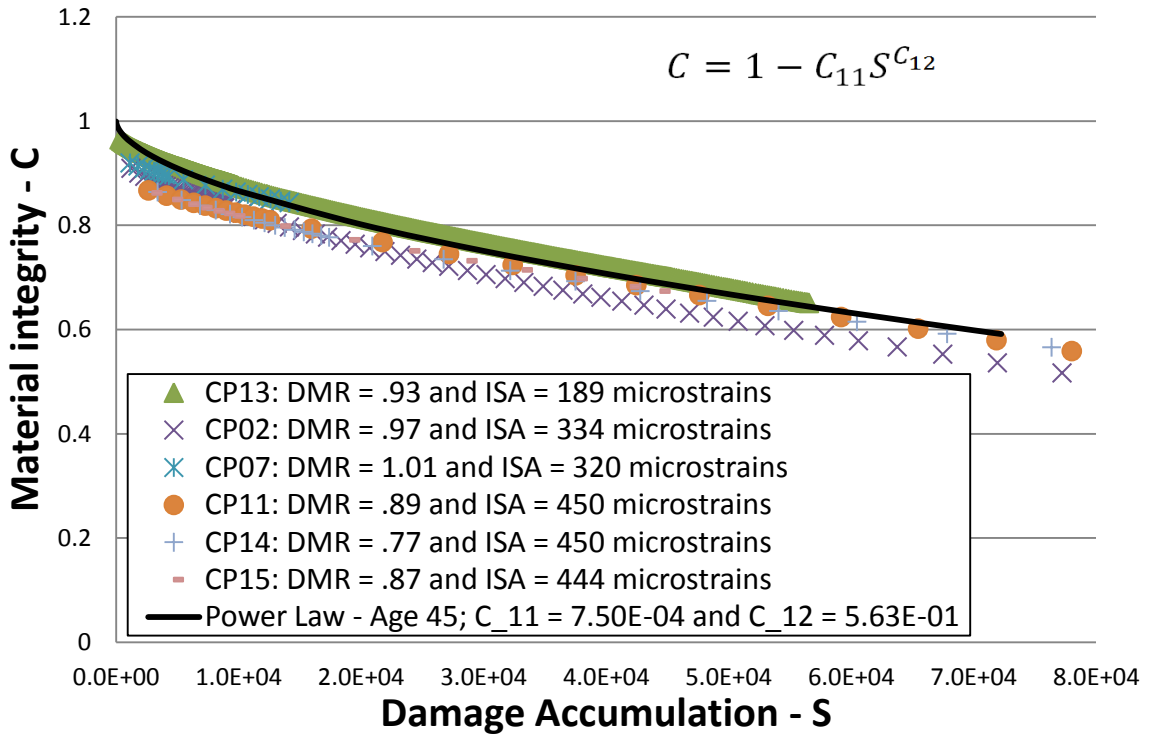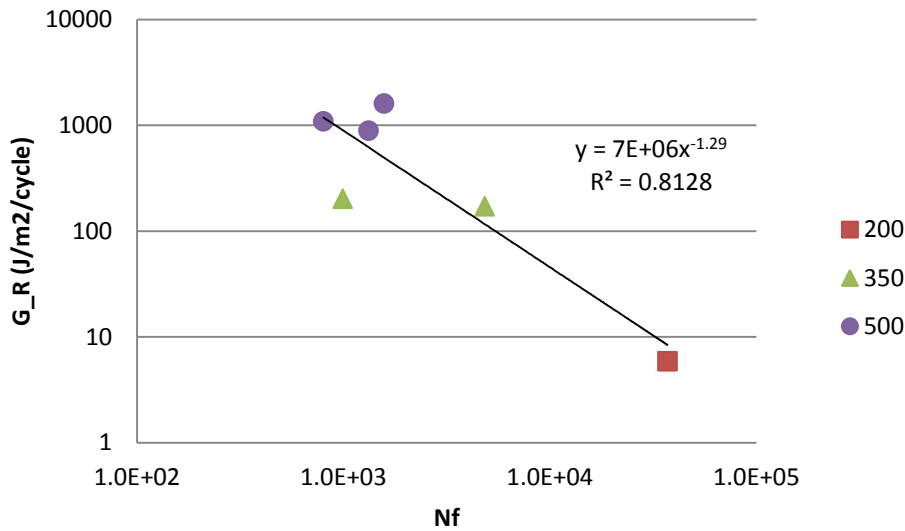- — Power Law - Age 45; C_11 = 7.50E-04 and C_12 = 5.63E-01

Figure A26 – Results for averaged released pseudo strain energy *vs* number of cycles to failure (experimental and curve fitting) for tension-compression fatigue tests with Age 45, 85ºC mixture

$y = 7E+06x^{-1.29}$
$R^2 = 0.8128$

- ■ 200
- ▲ 350
- ● 500

135

Figure A27 – Results for averaged released pseudo strain energy *vs* number of cycles to failure (experimental and curve fitting) for tension-compression fatigue tests with Age 45, 85ºC mixture
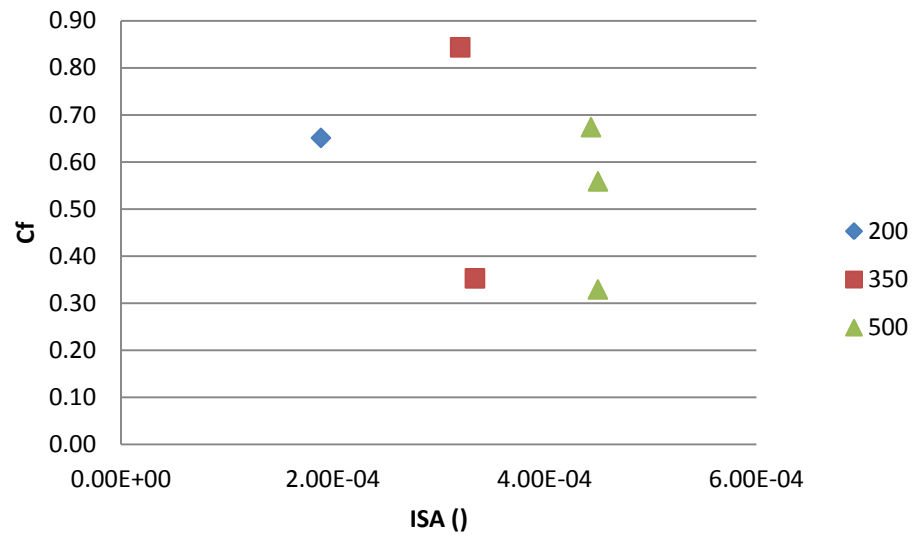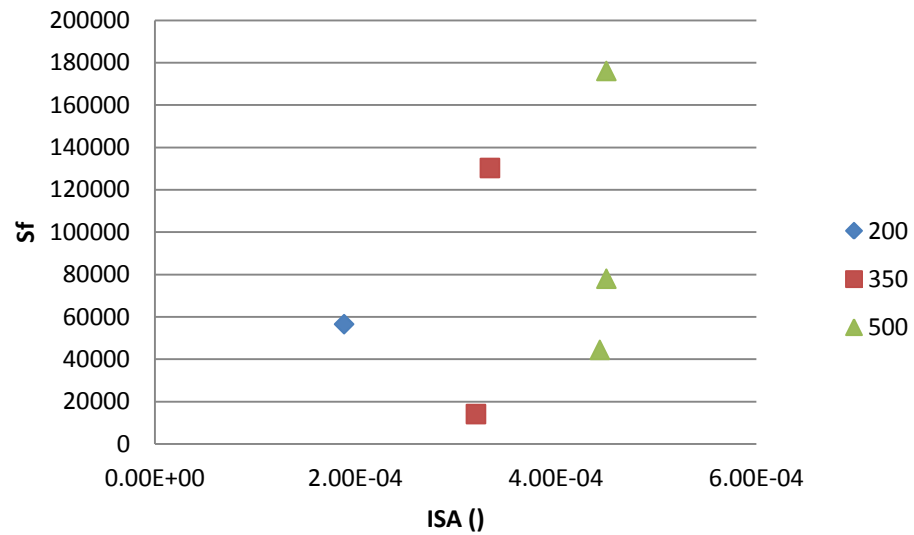

Figure A28 – Results for damage accumulation at failure *vs* initial strain amplitude for tension-compression fatigue tests with Age 45, 85ºC mixture

APPENDIX B - Failure Position and Distribution of Voids in Superpave Samples

In this Appendix, it is presented a discussion about where failure is more likely to happen in tension-compression fatigue tests. This is important because if failure, i.e. localization of cracks, does not occur within LVDT measurements, the phase angle drop is not clear and it is more difficult to determine accurately the number of cycles to failure (see Figure 9 and comments).

In order to evaluate the localization of cracks within the samples, the following terminology is used henceforth: top failure when failure is localized in the top of the specimen (above LVDT measurements), mid failure when the macrocrack appeared within LVDT measurements, and bottom failure when failure occurred below LVDT measurements. All samples were glued to the endplates in the same position as they were compacted, i.e., the top face (when compacted) of the specimen was glued to the top endplate, i.e., compaction position corresponds to fatigue test position. Failure in the glue is also possible or even unsticking of the glue from the endplate. The described possibilities of crack localization are illustrated in the next figures. It is observed that usually samples are not torn apart after the fatigue tests. In order to track the crack localization, after failure, samples are marked with an "X" at the place of failure when still being loaded, in order to identify the position of the crack.

Figure B1 – Unsticking of the glue from the endplate (sample at the left) and failure in the mixture (sample at the right)

Figure B2 – Failure in the glue

Figure B3 – (a) Bottom failure; (b) Mid failure; (c) Top failure

(a)   (b)   (c)

In ideal conditions, i.e., if the tested material is perfectly homogeneous and endplates and sample are concentric and perfectly aligned, the stress in a cross section perpendicular to the sample axis is of pure compression or pure tension. Except for cross sections near the glued endplates, where Saint Venant's principle does not apply, the stress is approximately constant within the sample (homogeneous state of stress). One could then expect failure to happen with equal probability for most of the points along the axis of the cylinder. However, mixture is not homogeneous. Mainly because of the compaction process, air voids do not distribute uniformly along the cylinder axis. One of the ways of accessing information about air voids distribution is by tomographies of the samples. Petrobras/Cenpes provided tomography results for a typical asphalt concrete mixture, compacted with different geometries (diameter by height): 100×178mm for Sample 15; 100×150mm for Sample 07 (used in this research); 100×160mm for Sample 18; and 150×178mm for Sample 10. Results represent the average air voids for a given cross section of the sample.

Figure B4 – Voids distribution in different Superpave compaction dimensions (data from Petrobras/Cenpes)
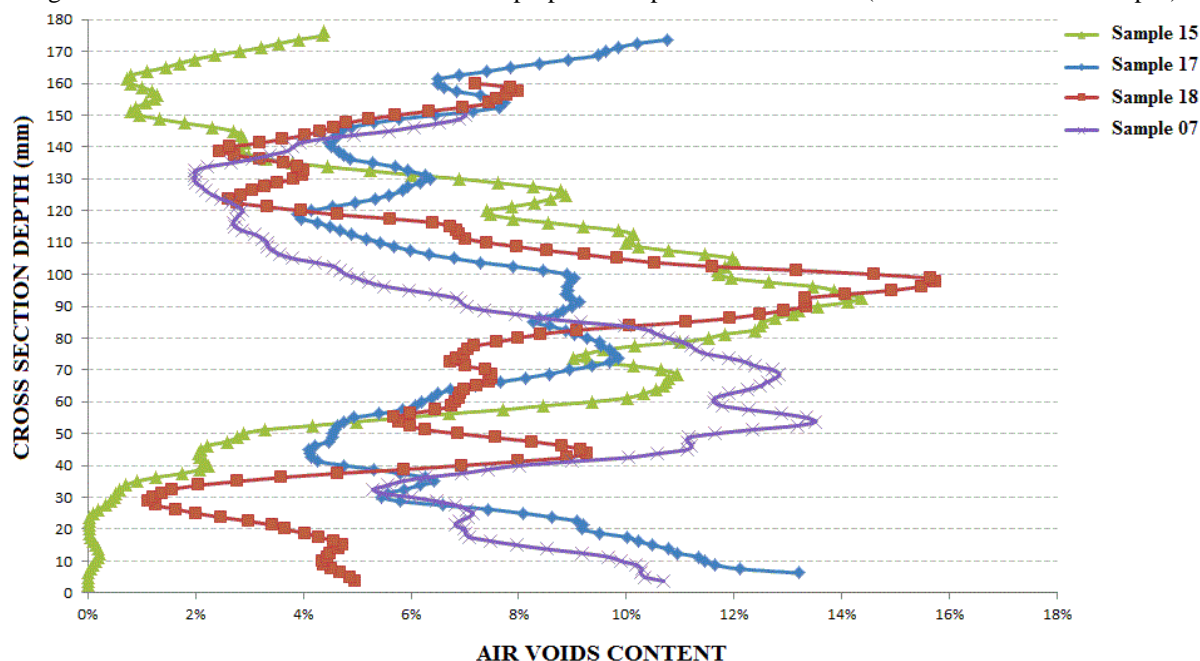
It is possible to observe that relatively high void concentration occurs in the extremities and approximately in the middle of the sample. The exact position of maximum voids concentration can vary from sample to sample. In addition, it is to be observed that in the gluing process, a part of the air voids at the top and at the bottom of the samples are filled with glue.

For 100×150mm samples (as Sample 07 and the samples compacted for this research), maximum air voids concentration is most likely to occur in the center of the sample. For the result presented in the figure, approximately 8% air voids was observed at the top, 11% at the bottom and 14% at the center of the sample. For that sample, for example, fatigue crack concentration in a tension-compression test would be more likely to occur around 55mm from the bottom of the sample, i.e., within LVDT measurements (mean displacement obtained between 37.5 and 112.5mm from the bottom of the sample). This could explain the fact that 100% of the nine tested samples for Age Zero mixture failed between LVDT measurements.

As aging increases variability in the results for all tested properties in this work, it is reasonable to assume that the position where maximum air voids concentration occur is also more variable for aged specimens. Furthermore, local defects are most likely to occur due to

possible non homogeneities created by the aging process. Both factors – increased variability and local defects – combined can produce samples that fail in more variable positions, i.e., the crack localization position is more random. This was observed in this work as indicated in Table B1. It is noted that failure outside LVDT measurements tends to occur with more frequency for aged materials, even for loose asphalt mixture aging procedures as used in this thesis.

Table B1 – Distribution of failure position for the tested samples

	Top	Center	Bottom	Glue	Total
Age Zero	0	9	0	0	9
Age 2, 85ºC	2 (for 350μ)	6	0	1 (for 500μ)	9
Age 2, 135ºC	1 (for 500μ)	6	1 (for 500μ)	0	8
Age 45, 85ºC	1 (for 500μ)	4	4 (1 for 200μ; 2 for 350μ and 1 for 500μ)	0	9